**Non-Ideal Thermodynamic Models of Cryobiological Solutions and the Intracellular Space**

by

Michał Wojciech Zielinski

A thesis submitted in partial fulfillment of the requirements for the degree of

Doctor of Philosophy

in

Materials Engineering and Medical Sciences

Departments of Chemical and Materials Engineering and Laboratory Medicine and Pathology

University of Alberta

## Abstract

**Non-Ideal Thermodynamic Models of Cryobiological Solutions and the Intracellular Space**

Mathematical models of cryopreservation processes are an important tool in the development of cryopreservation protocols that successfully avoid cryoinjury. Theoretical models of solution thermodynamic behaviour, known as solution theories, lie at the core of many cryopreservation models, including those that simulate the cellular osmotic response. However, to provide accurate predictions of solution behaviour, these solution theories must be able to account for the inherent thermodynamic non-ideality of cryobiological solutions. They must also be able to provide predictions in the complex multi-solute solutions that are characteristic of cryobiology—*i.e.*, aqueous solutions potentially containing an extremely wide range of solutes—and, ideally, they should be able to do so without requiring an overwhelming number of experimentally-obtained characteristic coefficients or fitting parameters. One recently-developed solution theory which meets these requirements, and which has been demonstrated to provide accurate predictions of solution behaviour in cryobiologically-relevant solutions, is the Elliott *et al.* form of the multi-solute osmotic virial equation. However, this solution theory was not yet complete, with some key pieces requiring further work. Accordingly, the overall objective of this thesis was to further develop the Elliott *et al.* model and to incorporate it into models of cellular osmotic response in order to advance understanding of cell behaviour during cryopreservation.

The work contained in this thesis presents a complete and thermodynamically consistent molality-based form of the Elliott *et al*. model, capable of modeling all of the solution behaviour required by higher-level cryopreservation models in the complex, non-ideal, multi-solute solutions that occur during cryopreservation. The work herein also conclusively shows that with this solution theory, a grouped intracellular solute approach can be used to represent the cytoplasm without

affecting model predictions; thus, this model can be used to provide accurate predictions of non-ideal solution behaviour inside of cells even where—as is generally the case—the composition of the cytoplasm is unknown. Finally, this thesis describes methods for obtaining all of the thermodynamic coefficients required to use the molality-based form of the Elliott *et al*. model, including those corresponding to a grouped intracellular solute, and provides values of these coefficients for several cryobiologically-relevant solutes and for the grouped intracellular solute of human umbilical vein endothelial cells (HUVECs).

Overall, this thesis advances our understanding of the solution thermodynamics of cryobiology, and—in particular—cellular cryobiology, allowing for more accurate predictions of cryobiological solution behaviour. These advancements will in turn enable greater accuracy in the prediction of cryopreservation processes, thus ultimately aiding in the development of successful cryopreservation protocols.

## Preface

Chapter 2 of this thesis, along with Appendices A and B, has been published as M.W. Zielinski, L.E. McGann, J.A. Nychka, J.A.W. Elliott, Comparison of non-ideal solution theories for multi-solute solutions in cryobiology and tabulation of required coefficients, Cryobiology 69 (2014) 305–317. This work is available at http://dx.doi.org/10.1016/j.cryobiol.2014.08.005.

Chapter 3 of this thesis, along with Appendices C and D, has been published as M.W. Zielinski, L.E. McGann, J.A. Nychka, J.A.W. Elliott, A Non-Ideal Solute Chemical Potential Equation and the Validity of the Grouped Solute Approach for Intracellular Solution Thermodynamics, J. Phys. Chem. B. 121 (2017) 10443–10456. This work is available at http://pubs.acs.org/articlesonrequest/AOR-38xihDTThrSv82dTdyFp.

Chapter 4 of this thesis, with modifications, is being prepared for submission as M.W. Zielinski, L.E. McGann, J.A. Nychka, J.A.W. Elliott, Measurement of grouped intracellular solute osmotic virial coefficients.

## Acknowledgements

I would like to express my sincere appreciation and gratitude to the following individuals, without whom this thesis would not have been possible.

To my supervisors, Drs. Janet Elliott, John Nychka, and Locksley McGann. Thank you for your encouragement, support, and wisdom, and for always helping me see the big picture when I got bogged down in the details.

To my supervisory committee members, Drs. Jason Acker and John Shaw. Thank you for your time, advice, and support.

To Drs. Mehmet Toner and Vinay Prasad, my examiners. Thank you for your insight and feedback.

To members of the McGann/Elliott Cryolab, the Mati Group, and the Acker Cryolab, past and present, including Nicole Lee Robertson, Anthony Reardon, Billal Sultani, Lisa Ross-Rodriguez, and Leah Marquez-Curtis. Thank you for your friendship, advice, and support.

To my parents, Piotr and Joanna, and my brother Arthur. Thank you for your love and support.

To my wife, Katherine. Thank you for your unconditional love, extensively-tested patience, and for always believing in me.

## Table of Contents Page:

## List of Tables

**Page:**

## List of Figures

**Page:**

# Chapter 1. Introduction

## 1.1. The principle of cryopreservation

Cryobiology is the study of biological systems at low—generally, below freezing—temperatures. A major focus of cryobiologists is the development of cryopreservation protocols. Cryopreservation refers to the process by which biological materials such as cells or tissues are cooled to low subfreezing temperatures and stored for extended periods of time before being returned to ambient temperatures when needed. The storage of cells and tissues in this way has a number of clinical and research applications, including transplantation [98], stem cell therapies in cancer treatment [38], and the maintenance of human and animal cell lines [131]. However, while successful cryopreservation has been achieved for some types of cells in suspension [74,101,130,133], many cell types and most tissues cannot be cryopreserved with an acceptable number of viable cells [63,98,147].

The primary obstacle to the development of successful cryopreservation protocols is the damage that occurs in cells and tissues during cooling, warming, and the addition and removal of cryobiological solutions. As part of an interdisciplinary effort to study and understand the nature of this damage, mathematical models have been developed to simulate the biophysical processes that occur during cryopreservation [1,12–14,23,27,53–55,62,65,66,81,115,116,129,139,153]. Although many of these models are quite advanced, there do remain areas where additional work is required. One such area—and the focus of this thesis—is the thermodynamic modeling of cryobiological solutions and of the intracellular space (*i.e.*, the cytoplasm). In this work, this topic will be studied in the context of the cryopreservation of individual cells in suspension.

### 1.2. Cellular cryopreservation and the osmotic response

A principle consideration in the cryopreservation of individual cells is the plasma membrane. The plasma membrane is the outermost boundary of a cell, separating the intra- and extracellular environments [80]. These two environments consist of distinct aqueous solutions containing salts, proteins, carbohydrates, and other solutes. The functionality of a cell depends on the ability of the plasma membrane to maintain the differences between the intra- and extracellular environments [80]. Due to the nature of its structure, the plasma membrane allows water and some solutes—*i.e.*, permeating solutes—to pass through, while preventing the passage of other solutes—*i.e.*, nonpermeating solutes. As such, it is generally considered to be semi-permeable [95].

Membrane transport may be passive or active. Due to the lower temperatures involved in cryopreservation, cryobiologists are mainly concerned with passive transport. While the semi-permeability of a cell determines whether or not a given chemical species can move into or out of the cell by passive transport, whether or not that species will actually move is governed by thermodynamics. More specifically, transport across the cell membrane is primarily governed by a thermodynamic property called chemical potential [95]. The chemical potential of a given species in a given phase can be defined as a measure of the tendency of that species to leave that phase [40]. By this definition, a species will tend to move from a phase where it has high chemical potential to one where it has low chemical potential [40]. Thus, for water or a permeating solute, the driving force for transport across the cell membrane is the difference between the intra- and extracellular chemical potentials—at equilibrium, the two chemical potentials are the same and there is no net movement across the membrane [95]. It is important to note that while chemical potential is dependent on concentration—generally, all else held constant, the higher the concentration, the higher the chemical potential—the two properties are not the same.

Although liquid water is generally a good solvent, the solid phase of water—ice—has effectively no solubility for most solutes [124]. Thus, when ice crystals form in an aqueous solution, any solutes present will be excluded into the remaining liquid fraction. The equilibrium freezing point of an aqueous solution is subject to freezing point depression—*i.e.*, the freezing point of the solution decreases with increasing solute concentration [95]. As a result, the extent of ice formation in aqueous solutions is a function of temperature: when ice forms at a given temperature, it concentrates the liquid solution, depressing the solution freezing point and preventing additional ice formation until the temperature is dropped further [95].

During the cryopreservation of cells in suspension, it has been observed that under conditions of slow (*i.e.*, near-equilibrium) cooling, the nucleation and growth of ice occur almost exclusively extracellularly [81]. The lack of intracellular ice formation under these conditions can be attributed to two factors: first, there appear to be "no efficient ice nucleating agents in cells"; and second, it is believed to be thermodynamically unfavourable for ice crystals to penetrate the hydrophobic cell membrane when cooling is sufficiently slow [81].

As a cell in suspension is cooled in the presence of extracellular ice, the progressive growth of the ice with decreasing temperature and the accompanying increase in the extracellular solute concentration result in an imbalance of water chemical potential across the cell membrane [95]. Specifically, the increased solute concentration outside the cell decreases the extracellular water chemical potential. In response, water will move out of the cell, thus decreasing the cell volume, increasing the intracellular solute concentration, and—correspondingly—decreasing the intracellular water chemical potential. At the same time, any permeating solutes present in the solution will also move across the membrane according to their respective chemical potential gradients. The movement of water and permeating solutes will continue until equilibrium is

established. In general, changes in cell volume and intracellular composition as a result of changing extracellular conditions are collectively referred to as the osmotic response of the cell [95].

### 1.3. Cellular cryoinjury and cryoprotectants

According to Mazur *et al.*'s "two-factor hypothesis" [83], there are two distinct mechanisms responsible for the damage that occurs to cells during cryopreservation: intracellular ice formation and solution effects injury. Each of these mechanisms is described briefly below. The cumulative effect of both damage mechanisms will be referred to as cryoinjury.

Intracellular ice formation occurs under conditions of rapid cooling. As noted above, at least initially, ice tends to nucleate and grow outside of the cell on cooling [81]. Thus, the solutes that are excluded out of the liquid solution on freezing will directly enter the extracellular solution. The osmotic response of a cell is a kinetic (*i.e.*, time-dependent) process. If cooling is too rapid, water (as well as any permeating solutes) will not have time to equilibrate across the cell membrane as the system temperature drops, extracellular ice forms, and the extracellular solution becomes progressively more concentrated. As a result, the intracellular solution will become increasingly dilute relative to the extracellular environment, and, accordingly, the equilibrium freezing point of the intracellular solution will fall further and further behind the overall system temperature as it drops—*i.e.*, the intracellular solution will become increasingly supercooled. This intracellular supercooling increases with cooling rate, as higher cooling rates give even less time for water equilibration across the cell membrane. For any liquid aqueous solution, the probability of ice nucleation increases with the extent of supercooling [81]. Therefore, the higher the cooling rate, the greater the degree of intracellular supercooling, and thus the greater the probability of

intracellular ice formation [83]. While it is not entirely understood how intracellular ice formation causes damage to a cell, it is generally agreed upon that "with rare reported exceptions, intracellular ice appears to be uniformly destructive" [91].

Solution effects injury occurs under conditions of slow cooling. Here, intracellular ice formation is usually unlikely, as the cell should have time to equilibrate at all temperatures. However, when cooling is slow, the cell is spending extended periods of time in increasingly concentrated solutions at relatively high (as compared to the final storage temperature) subfreezing temperatures. Although the exact mechanisms are not fully understood, these conditions appear to give rise to cell damage, and it is this damage that is termed solution effects injury [91]. As the damage appears to increase with both exposure time and solution concentration, it can be concluded that the lower the cooling rate, the greater the extent of solution effects injury [83,91].

Cellular cryoinjury can be at least somewhat attenuated through the use of chemicals called cryoprotectants [26,85,90]. Cryoprotectants are generally categorized by their ability to cross the cell membrane—*i.e.*, permeating versus non-permeating [85,90]. Permeating cryoprotectants include dimethyl sulphoxide, ethylene glycol, and glycerol; non-permeating cryoprotectants include hydroxyethyl starch, polyvinylpyrolidone, and sucrose [90].

The mechanisms by which the two types of cryoprotectants prevent damage on freezing and thawing have been found to differ [85]. Permeating cryoprotectants act by depressing the freezing point of the solution [85,95]. Freezing point depression has the effect of decreasing the amount of ice formed—and thus the concentration of salts present—in the solution at any given temperature, which in turn decreases the extent of solution effects injury on slow cooling [85,95]. Non-permeating cryoprotectants act by decreasing the extracellular chemical potential of water, thus causing cells to become dehydrated [85,95]. As a result, the intracellular contents become

more concentrated and hence less susceptible to supercooling and intracellular ice formation on rapid cooling. An important distinction should be noted here: permeating cryoprotectants appear to protect against damage on slow cooling but not against damage on rapid cooling, whereas nonpermeating cryoprotectants appear to protect against damage on rapid cooling but not against damage on slow cooling [95].

While cryoprotectants can be used to reduce cryoinjury, they do have two major drawbacks which limit the amount of protection that they can offer. First, cryoprotectants are often toxic to the very cells that they are meant to protect [12,13,28,33,34]. This toxicity increases with increasing temperature, cryoprotectant concentration, and exposure time. Second, the addition and removal of permeating cryoprotectants generally causes changes in cell volume (*i.e.*, shrinking or swelling), which can lead to osmotic damage [12,13,39,52,64]. Osmotic damage occurs where the cell volume deviates too far from its isotonic—*i.e.*, normal physiological—value, exceeding the limits of what the cell can tolerate. With respect to cryoprotectant addition and removal, the likelihood of such excessive volume excursion increases with the rate of addition/removal.

### 1.4. The role of mathematical modeling and solution thermodynamics in cryopreservation

A successful cryopreservation protocol can be defined as one that can take cells down to the target storage temperature and then back up to physiological conditions—including the addition and subsequent removal of any cryoprotectants—without causing excessive and/or irreversible damage to the cell population as a whole; generally, this means that the cells must survive and remain functional. Developing a successful protocol is a complex challenge. As described above, there are at least four potential sources of cell damage that must be considered when developing cryopreservation protocols: intracellular ice formation, solution effects injury,

cryoprotectant toxicity, and osmotic damage. Simultaneously avoiding all of them becomes a balancing act. Cooling too rapidly leads to intracellular ice formation, whereas cooling too slowly exacerbates solution effects injury. Survival can be increased by adding cryoprotectants, but while higher concentrations may reduce cryoinjury, they also increase the likelihood of fatal toxicity and osmotic damage. Further, the rate of cryoprotectant addition and removal must be considered: higher rates correspond to lower exposure times and thus lower risk of toxic effects, but they also correspond to greater excursions in cell volume and thus greater risk of osmotic damage. Survival can also be improved by using non-linear cooling protocols such as interrupted cooling, where cells are held at an intermediate temperature before cooling is allowed to continue [36,117]. Finally, all of these factors—from optimal cooling rates [91] to cell reactions to cryoprotectants [20,33]—are cell type-specific and must thus be determined independently for each type of cell to be cryopreserved. In short, given the number of factors that must be accounted for, it is not feasible to develop cryopreservation protocols exclusively by trial-and-error. For this reason, kinetic and thermodynamic mathematical models which simulate the biophysical processes occurring during the various stages of cryopreservation have become important tools in the development of cryopreservation protocols [1,12–14,23,27,53–55,62,65,66,81,115,116,129,139,153].

Most mathematical models of cryopreservation processes rely on thermodynamic solution theories to predict the behaviour of the solutions inside and outside of cells, as this information is needed to simulate larger-scale behaviour (*e.g.*, the cellular osmotic response) [1,12–14,23,27,53–55,62,65,66,81,115,116,129,139,153]. However, many of these models use ideal dilute solution theories that fail to account for the inherently non-thermodynamically ideal nature of the majority of cryobiological solutions [12,13,39,53,54,60,61,64–66,81,129,137]. The distinction between ideal and non-ideal solutions is important. An ideal solution can most generally be defined as a

solution for which the enthalpy of mixing—*i.e.*, the enthalpy change associated with the mixing of the solution's components—is zero [41]. Any solution for which the enthalpy of mixing is not zero is considered non-ideal. A notable feature of ideal solution theories is that they assume that there are no interactions between solute molecules in solution [105]. While this assumption may hold at low solute concentrations where the solute molecules are few and far apart, it becomes less accurate as concentration increases. Under most circumstances relevant to cryopreservation, cryobiological solutions tend to be very highly concentrated, due to either the formation of ice (and corresponding rejection of solutes into the liquid fraction), the addition of cryoprotectants, or both. As such, the ideal dilute approach is not appropriate for cryobiological modeling.

Recently, a novel non-ideal solution theory—referred to herein as the Elliott *et al.* form of the multi-solute osmotic virial equation—has been developed for use with cryobiological solutions and has been shown to accurately predict non-ideal solution behaviour in these solutions [11,24,27,105,106]. This solution theory is particularly applicable to cryobiology (and to biological solutions in general) because it relies solely on *solute*-specific thermodynamic coefficients to account for non-ideality, as opposed to the *solution*-specific coefficients that are used by many other non-ideal models [5,32,96,97,100,146]. Such coefficients are typically obtained by curve-fitting to experimental measurements in the solution of interest: single-solute (*i.e.*, binary) solutions for solute-specific coefficients [24,105,106], and solutions containing the exact combination of solutes for solution-specific coefficients [5,32,96,97,100,146]. For the Elliott *et al.* model, the solute-specific coefficients are osmotic virial coefficients [24,105,106]. The Elliott *et al.* model's use of these solute-specific coefficients means that it can make predictions in multi-solute solutions using only single-solute solution data, thus drastically reducing the number

of experimental measurements that must be made in order to model the wide variety of solutions that are relevant in cryobiology.

However, despite the demonstrated applicability of the Elliott *et al.* form of the multi-solute osmotic virial equation to cryopreservation modeling, further development of this model is still required. Notably, the model is not complete in terms of all units of concentration measurement used in cryobiology. Complete modeling of cryopreservation processes such as the osmotic response requires the ability to calculate the chemical potentials of both water and permeating solutes (*e.g.*, cryoprotectants). While the model at present does provide a complete set of equations for both water and solute chemical potential in terms of concentration in mole fraction [24,27], it did not prior to this thesis work include a solute chemical potential equation in terms of concentration in molality, a commonly-used measure in cryobiology. In addition, a complication arises when the model is applied to predict chemical potentials inside the cell—*i.e.*, in the cytoplasm. In order to make predictions in a given solution, the Elliott *et al.* model requires as inputs the exact concentrations of every solute in that solution. The problem is that, in general, the exact composition of the cytoplasm is unknown, thus precluding the use of the model without making assumptions about the intracellular contents. One way around this limitation is to use a "grouped intracellular solute" approach, where—for the purpose of thermodynamic modeling—all of the non-permeating solutes inside the cell are treated as a single non-permeating solute. Such a grouped solute approach has been applied in practice with the Elliott *et al.* form of the multi-solute osmotic virial equation [118], but it has never been shown that this approach is actually equivalent to modeling the cytoplasm with the exact concentrations of all solutes known—*i.e.*, that using the grouped solute approach does not change model predictions. Furthermore, even if the grouped solute approach is so equivalent, in order to apply it with the Elliott *et al.* model, the

osmotic virial coefficients of the grouped intracellular solute must be known. These coefficients cannot be obtained for the grouped intracellular solute with the same methods as they would be for other solutes—*i.e.*, from measurements of single-solute solution data—because the grouped intracellular solute cannot be isolated in a single-solute solution, given that it is a purely theoretical construct that exists solely within the cell, rather than an actual physical solute. A method has been developed for measuring grouped intracellular solute osmotic virial coefficients [118], but this technique lacks precision. This limitation is a problematic one, as models of the cellular osmotic response can be highly sensitive to the values of grouped intracellular solute osmotic virial coefficients when permeating solutes are present (see Chapter 4).

### 1.5. Thesis objectives

The overall goal of this thesis is to advance understanding of cell behaviour during cryopreservation by further developing the Elliott *et al.* form of the multi-solute osmotic virial equation and incorporating this solution model into models of cellular osmotic response.

The specific objectives of this thesis are:

1) To evaluate and compare the performance of leading ideal and non-ideal solution theories in cryobiology for predicting water chemical potential (Chapter 2).
2) To derive a non-ideal molality-based solute chemical potential equation that is thermodynamically consistent with the existing third-order molality-based water chemical potential equation of the Elliott *et al.* model (Chapter 3).
3) To use a thermodynamic proof to show that when calculating intracellular chemical potentials with the molality-based Elliott *et al.* form of the multi-solute osmotic virial equation, modeling the cytoplasm using a grouped intracellular solute approach is

mathematically equivalent to treating the cytoplasm as if the concentrations of all non-permeating intracellular solutes are known (Chapter 3).

4) To develop and apply a novel high-precision method that incorporates thermodynamic theory and biological experiments to measure grouped intracellular solute osmotic virial coefficients (Chapter 4).

# Chapter 2. Comparison of non-ideal solution theories for multi-solute solutions in cryobiology and tabulation of required coefficients[1]

**Chapter Summary:** Thermodynamic solution theories allow the prediction of chemical potentials in solutions of known composition. In cryobiology, such models are a critical component of many mathematical models that are used to simulate the biophysical processes occurring in cells and tissues during cryopreservation. A number of solution theories, both thermodynamically ideal and non-ideal, have been proposed for use with cryobiological solutions. In this work, we have evaluated two non-ideal solution theories for predicting water chemical potential (*i.e.*, osmolality) in multi-solute solutions relevant to cryobiology: the Elliott *et al.* form of the multi-solute osmotic virial equation, and the Kleinhans and Mazur freezing point summation model. These two solution theories require fitting to only single-solute data, although they can make predictions in multi-solute solutions. The predictions of these non-ideal solution theories were compared to predictions made using ideal dilute assumptions and to available literature multi-solute experimental osmometric data. A single, consistent set of literature single-solute solution data was used to fit for the required solute-specific coefficients for each of the non-ideal models. Our results indicate that the two non-ideal solution theories have similar overall performance, and both give more accurate predictions than ideal models. These results can be used to select between the non-ideal models for a specific multi-solute solution, and the updated coefficients provided in this work can be used to make the desired predictions.

[1] This chapter, along with Appendices A and B, has been published as M.W. Zielinski, L.E. McGann, J.A. Nychka, J.A.W. Elliott, Comparison of non-ideal solution theories for multi-solute solutions in cryobiology and tabulation of required coefficients, Cryobiology 69 (2014) 305–317. This work is available at http://dx.doi.org/10.1016/j.cryobiol.2014.08.005.

## 2.1. Introduction

Many of the mathematical models that are used to simulate cryopreservation protocols [1,2,27,53,54,60,65,66,81,104,115,116,137] rely on the ability to accurately predict thermodynamic solution behaviour, since important processes such as water and solute transport and ice formation are ultimately dictated by differences in chemical potential. As a consequence, it is important to give some thought to the choice of the solution theories that are used to calculate these chemical potentials. This article examines and evaluates some of the available theories for predicting water (*i.e.* solvent) chemical potential, in particular those that do not depend on multi-solute solution data.

In cryobiology, water chemical potential is often expressed in terms of its composition dependence, osmolality [5,19,24,27,47,105,106,144], or in terms of the related properties freezing point depression [5,24,27,32,47,69,96,97,100,105,144–146] and osmotic pressure [68,81,105,143]. Freezing point depression and osmotic pressure are physically measurable solution properties, and the relationships between them and osmolality (described below in Equations 2.2 and 2.3 and in Equation 2.4, respectively) allow one to experimentally obtain values for the osmolality of a solution. Solution osmolality can also be related to other measurable properties, including vapour pressure [50,132] and, for polymers, light scattering (based on index of refraction) [48,57,58,67,110]. Such relationships form the basis of osmometry, and allow one to measure the osmolality of any solution of interest. However, for the purposes of modeling cryopreservation processes, measuring the osmolality of every solution of interest is not feasible (*e.g.* solution compositions change constantly as ice forms, or when cryoprotectants are added), nor is it always possible (*e.g.*, intracellular solutions are not accessible for instantaneous

measurement). As such, the ability to accurately predict the solution osmolality is essential for cryobiological models where this property is an input.

By their nature, cryobiological solutions contain diverse solutes ranging from salts and cryoprotectants to proteins and other macromolecules, often at high concentrations—even those solutions that are relatively dilute at room temperature become highly concentrated when frozen. As a result, cryobiological solutions are generally thermodynamically non-ideal. Although this non-ideality can be ignored and an ideal dilute solution theory can be used to model the solution behaviour [39,53,54,60,61,64–66,81,137], doing so can introduce significant errors in the predictions of chemical potential [24,105,106]. Accordingly, there are a number of solution theories available in the literature which account for solution non-ideality and have been demonstrated to accurately model the osmolality of multi-solute solutions of cryobiological interest [5,11,24,32,69,96,97,100,105,106,146]. However, the majority of these solution theories depend on fitting to multi-solute data, meaning that every solution system (*i.e.*, combination of solutes) of interest must be fit independently prior to being modeled [5,32,96,97,100,146]. Considering the vast range of possible solution systems that are relevant in cryobiology (*e.g.* cytoplasm, plasma and interstitial fluids, multi-cryoprotectant vitrification cocktails [35,56,88]) and the challenges inherent to the measurement of multi-solute phase diagrams (*e.g.*, the number of measurements required for a given compositional resolution increases exponentially with the number of solutes present in solution) [69], this type of approach is not practical for general modeling applications. Alternatively, there are at least two solution theories available which allow the prediction of osmolality in non-ideal multi-solute solutions using only single-solute (*i.e.*, binary solution) data: the form of the multi-solute osmotic virial equation developed by Elliott *et al.* [11,24,27,105,106], and the freezing point summation model of Kleinhans and Mazur [69]. The

primary aim of this work is to compare predictions of multi-solute solution osmolality made with these two non-ideal solution theories to available experimental data, to one another, and to ideal dilute model predictions. This work expands upon earlier comparisons [24,105], employing a larger set of literature data, and addressing statistical and thermodynamic issues in the previous studies.

## 2.2. Multi-solute solution theories used in cryobiology

### *2.2.1. Solution thermodynamic properties*

As mentioned above, osmolality, freezing point depression, and osmotic pressure are all related to one another and, ultimately, to water chemical potential. As these properties will be used interchangeably throughout this paper, we have summarized the relationships between them here. Osmolality, $\pi$, is mathematically defined as [24]

$$\pi = -\frac{\mu_1 - \mu_1^o}{RTM_1}, \tag{2.1}$$

where $\mu_1$ is the chemical potential of water, $\mu_1^o$ is the chemical potential of pure water, $R$ is the universal gas constant, $T$ is absolute temperature (in Kelvin), and $M_1$ is the molar mass of water (note that the subscript "1" is typically reserved for the solvent—in this case, water). Freezing point depression, $\Delta T_m$, and osmolality are related by [105]

$$\Delta T_m = T_m^o - T_m = \frac{RT_m^o \pi \left[M_1/\overline{\Delta s_{f1}^o}\right]}{1 + R\pi\left[M_1/\overline{\Delta s_{f1}^o}\right]}, \tag{2.2}$$

or, equivalently

$$\pi = \frac{\Delta T_m}{RT_m\left[M_1/\overline{\Delta s_{f1}^o}\right]} = \frac{T_m^o - T_m}{RT_m\left[M_1/\overline{\Delta s_{f1}^o}\right]}, \tag{2.3}$$

where $T_m$ is the absolute freezing point of the solution, $T_m^\circ$ is the absolute freezing point of pure water, and $\overline{\Delta s_{f1}^o}$ is the standard molar entropy change of fusion of water. Equation 2.3 is commonly

linearized as $\pi = 1.86\Delta T_m$; however, this linearization introduces considerable error [105] and will not be used here. Osmotic pressure, $\Pi$, is related to osmolality by [105]

$$\Pi = RT\rho_1\pi\,, \tag{2.4}$$

where $\rho_1$ is the density of water. The values and units of the constants in Equations 2.1, 2.2, 2.3, and 2.4 are contained in Table 2.1.

*2.2.2. Elliott et al. multi-solute osmotic virial equation*

The Elliott *et al.* multi-solute osmotic virial equation is based on the osmotic virial equation of McMillan and Mayer [87], an equation of state in which the osmolality is represented as a polynomial in terms of solute concentration. Depending on the underlying theoretical assumptions, different units of concentration can be used, giving two distinct thermodynamic models [24]. In terms of molal concentration or molality (*i.e.*, moles of solute per kg of solvent), following Landau and Lifshitz solution theory [73], the single-solute osmotic virial equation for a solute *i* is [24,87]

$$\pi = m_i + B_{ii}{m_i}^2 + C_{iii}{m_i}^3 + \cdots\,, \tag{2.5}$$

where $m_i$ is the molality of solute *i* (in moles of solute/kg of water), and $B_{ii}$ and $C_{iii}$ are the second and third molality-based osmotic virial coefficients of solute *i*, respectively (in [moles of solute/kg of water]$^{-1}$ and [moles of solute/kg of water]$^{-2}$, respectively). Alternatively, in terms of solute concentration in mole fraction (*i.e.*, moles of solute per total moles of all species), per regular solution theory [102], the single-solute osmotic virial equation for solute *i* is [87,105]

$$\tilde{\pi} = x_i + B_{ii}^{*}{x_i}^2 + C_{iii}^{*}{x_i}^3 + \cdots\,, \tag{2.6}$$

where $\tilde{\pi}$ is osmole fraction (unitless), $x_i$ is the mole fraction of solute *i*, and $B_{ii}^{*}$ and $C_{iii}^{*}$ are the second and third mole fraction-based osmotic virial coefficients of solute *i*, respectively (unitless). Osmole fraction is a rarely-used alternative form of osmolality, defined as [24]

$$\tilde{\pi} = -\frac{\mu_1 - \mu_1^o}{RT}. \tag{2.7}$$

Comparing Equations 2.1 and 2.7, osmolality and osmole fraction are related by

$$\tilde{\pi} = M_1 \pi . \tag{2.8}$$

The osmotic virial coefficients in Equations 2.5 and 2.6 account for increasing orders of interaction between molecules of solute *i*: the second osmotic virial coefficient represents interactions between two solute *i* molecules, the third osmotic virial coefficient represents interactions between three solute *i* molecules, and so forth. As such, these coefficients represent the non-ideality of the solute—if they are all zero, solute *i* is thermodynamically ideal. For electrolyte solutes, solute concentration must be multiplied by an additional parameter, the dissociation constant [106]

$$\pi = k_i m_i + B_{ii}(k_i m_i)^2 + C_{iii}(k_i m_i)^3 + \cdots , \tag{2.9}$$

$$\tilde{\pi} = k_i^* x_i + B_{ii}{}^*(k_i^* x_i)^2 + C_{iii}{}^*(k_i^* x_i)^3 + \cdots , \tag{2.10}$$

where $k_i$ is the molality-based dissociation constant of solute *i* and $k_i$* is the mole fraction-based dissociation constant of solute *i*. This dissociation constant empirically accounts for ionic dissociation, charge screening, and other additional complexities inherent to electrolytes [106]; for non-electrolyte solutes, its value is effectively 1. Through a simple, empirical demonstration, Prickett *et al.* [106] have shown that for applications of interest to cryobiology, this approach for electrolytes is as accurate as the more sophisticated Pitzer-Debye-Huckel approach. To obtain values of the osmotic virial coefficients and (if applicable) the dissociation constant for any solute of interest, Equations 2.5, 2.6, 2.9, or 2.10 can be curve-fit to osmometric (*i.e.*, concentration versus osmolality) data for a binary aqueous solution containing that single solute.

The osmotic virial equation can be extended to multi-solute solutions by introducing osmotic virial cross-coefficients, which represent interactions between molecules of different

solutes [24,87] – for example, for a solution containing ($r$ – 1) solutes, the molality-based osmotic virial equation (*i.e.* Equation 2.5) can be written as follows

$$\pi = \sum_{i=2}^{r} m_i + \sum_{i=2}^{r}\sum_{j=2}^{r} B_{ij} m_i m_j + \sum_{i=2}^{r}\sum_{j=2}^{r}\sum_{k=2}^{r} C_{ijk} m_i m_j m_k + \cdots , \tag{2.11}$$

where $B_{ij}$, $C_{iij}$, $C_{ijj}$, $C_{ijk}$, etc. are cross-coefficients (*e.g.*, $B_{ij}$ accounts for interactions between one molecule of solute $i$ and one of solute $j$). In order to fit for the values of the cross-coefficients in Equation 2.11, one must use multi-solute osmometric data. Alternatively, it is possible to develop combining rules to avoid this requirement. Thermodynamic combining rules are theoretical relations that predict the values of cross-coefficients using the values of individual solute coefficients. Elliott *et al.* [24,27] have proposed the following second and third order combining rules for the molality- and mole fraction-based osmotic virial equations

$$B_{ij} = \frac{B_{ii} + B_{jj}}{2}, \tag{2.12}$$

$$C_{ijk} = \left(C_{iii} C_{jjj} C_{kkk}\right)^{1/3}, \tag{2.13}$$

$$B_{ij}^{*} = \frac{B_{ii}^{*} + B_{jj}^{*}}{2}, \tag{2.14}$$

$$C_{ijk}^{*} = \left(C_{iii}^{*} C_{jjj}^{*} C_{kkk}^{*}\right)^{1/3}. \tag{2.15}$$

Applying these combining rules yields the molality- and mole fraction-based Elliott *et al.* multi-solute osmotic virial equations

$$\pi = \sum_{i=2}^{r} m_i + \sum_{i=2}^{r}\sum_{j=2}^{r}\left[\frac{\left(B_{ii} + B_{jj}\right)}{2} m_i m_j\right] + \sum_{i=2}^{r}\sum_{j=2}^{r}\sum_{k=2}^{r}\left[\left(C_{iii} C_{jjj} C_{kkk}\right)^{1/3} m_i m_j m_k\right] + \cdots , \tag{2.16}$$

$$\tilde{\pi} = \sum_{i=2}^{r} x_i + \sum_{i=2}^{r}\sum_{j=2}^{r}\left[\frac{\left({B_{ii}}^* + {B_{jj}}^*\right)}{2} x_i x_j\right] + \sum_{i=2}^{r}\sum_{j=2}^{r}\sum_{k=2}^{r}\left[\left({C_{iii}}^* {C_{jjj}}^* {C_{kkk}}^*\right)^{1/3} x_i x_j x_k\right] + \cdots, \tag{2.17}$$

or, in the presence of electrolytes

$$\pi = \sum_{i=2}^{r} k_i m_i + \sum_{i=2}^{r}\sum_{j=2}^{r}\left[\frac{\left(B_{ii} + B_{jj}\right)}{2} k_i m_i k_j m_j\right] + \sum_{i=2}^{r}\sum_{j=2}^{r}\sum_{k=2}^{r}\left[\left(C_{iii} C_{jjj} C_{kkk}\right)^{1/3} k_i m_i k_j m_j k_k m_k\right] + \cdots, \tag{2.18}$$

$$\tilde{\pi} = \sum_{i=2}^{r} k_i^* x_i + \sum_{i=2}^{r}\sum_{j=2}^{r}\left[\frac{\left({B_{ii}}^* + {B_{jj}}^*\right)}{2} k_i^* x_i k_j^* x_j\right] + \sum_{i=2}^{r}\sum_{j=2}^{r}\sum_{k=2}^{r}\left[\left({C_{iii}}^* {C_{jjj}}^* {C_{kkk}}^*\right)^{1/3} k_i^* x_i k_j^* x_j k_k^* x_k\right] + \cdots, \tag{2.19}$$

where *r* is the number of solutes present. These equations have been found to provide accurate predictions of osmolality in a wide variety of non-ideal multi-solute solutions [5,11,24,76,104–106]. It should, however, be noted that although Equations 2.16 (or 2.18) and 2.17 (or 2.19) are similar in form and were derived using similar methods, they were obtained using different starting assumptions (regarding concentration units *i.e.*, Landau and Lifshitz solution theory versus regular solution theory). They are not equivalent, will not necessarily yield the same predictions for a given solution, and it is not possible to directly convert the coefficients of one to those of the other. That is, Equations 2.16 and 2.17 are effectively separate and distinct solution theories.

*2.2.3. Kleinhans and Mazur freezing point summation model*

The Kleinhans and Mazur freezing point summation model is similar to the osmotic virial equation in that it also models the osmolality (or, in this case, freezing point depression directly)

as being a polynomial function in terms of solute concentration [69]. For a binary aqueous solution containing a single solute *i*, this model represents the freezing point depression as [69]

$$\Delta T_m = T_m^o - T_m = -(C_{1i}m_i + C_{2i}{m_i}^2 + C_{3i}{m_i}^3)\,, \tag{2.20}$$

where $C_{1i}$, $C_{2i}$, and $C_{3i}$ are empirical solute-specific coefficients. Like the osmotic virial coefficients, the coefficients in Equation 2.20 can be obtained by fitting to single-solute solution osmometric data. For multi-solute solutions, Kleinhans and Mazur proposed summing the freezing point depression equations of all solutes present, *i.e.* [69],

$$\Delta T_m = T_m^o - T_m = -\sum_{i=2}^{r}(C_{1i}m_i + C_{2i}{m_i}^2 + C_{3i}{m_i}^3)\,, \tag{2.21}$$

where the number of solutes present is ($r$ – 1). While this approach removes the need for multi-solute data, it does not account for interactions between different solutes – that is, it ignores cross-coefficients. Despite this assumption, Equation 2.21 has been found to provide accurate predictions of freezing point depression in a number of specific multi-solute solutions [5,47,69,145].

*2.2.4. Ideal dilute models*

Despite the non-ideal thermodynamic nature of the solutions involved, solution models incorporating an ideal dilute assumption are prevalent in cryobiology [15,16,19,20,39,59,60,65,68,70,117,122,123,125,126,136,137,139]. One commonly-used form of ideal model is to assume that the solution osmolality is equal to the total solute concentration [19,20,39,65,68,117,139]. This approach can be implemented with concentration expressed in terms of, for example, molality or mole fraction, *i.e.*, respectively

$$\pi = \sum_{i=2}^{r} m_i\,, \tag{2.22}$$

$$\tilde{\pi} = \sum_{i=2}^{r} x_i \, . \tag{2.23}$$

For electrolyte solutes in Equations 2.22 and 2.23, one can follow the approach of Prickett *et al.* [105,106] and use the dissociation constants obtained for the molality- and mole fraction-based osmotic virial equations, *i.e.*

$$\pi = \sum_{i=2}^{r} k_i m_i \, , \tag{2.24}$$

$$\tilde{\pi} = \sum_{i=2}^{r} k_i^* x_i \, . \tag{2.25}$$

For the purposes of this study, the above ideal models will be referred to as the molality- (Equations 2.22 and 2.24) and mole fraction- (Equations 2.23 and 2.25) based ideal dilute models.

Another ideal dilute approach often used in cryobiological models [15,16,59,60,70,122,123,125,126,136,137] is based on a direct implementation of Raoult's law (*i.e.* for an ideal dilute solution, chemical activity equals mole fraction) and, notably, assumes that electrolytes dissociate ideally in solution. In essence, this model, which will herein be referred to as the ideal dissociation model, assumes that ionic dissociation is the only property inherent to electrolytes that sets them apart from non-electrolyte solutes with regards to contributing to solution osmolality, and accounts for this dissociation with a stoichiometric coefficient reflecting the number of ions released per solute molecule. This approach is in direct contrast to the other models considered here, all of which use empirically-measured coefficients to account for *all* potential electrolyte effects. Consistent with the notation used in this work, the ideal dissociation model can be expressed as

$$\pi = \frac{1}{M_1} \ln\left(1 + \frac{1}{x_1} \sum_{i=2}^{r} \kappa_i x_i\right), \tag{2.26}$$

where $\kappa_i$ is the stoichiometric dissociation coefficient of solute $i$ (if applicable; *e.g.*, for NaCl or KCl, $\kappa_i = 2$) and $x_1$ is the mole fraction of water. It should be noted that a natural logarithm that has been linearized in the mole fraction-based ideal dilute model (Equations 2.23 and 2.25) has not been linearized in the ideal dissociation model (Equation 2.26). (Note also that this issue does not arise in the molality-based ideal dilute model (Equations 2.22 and 2.24), as no natural logarithm is obtained in the derivation of water chemical potential from Landau and Lifshitz solution theory.)

### 2.3. Comparison of multi-solute solution theories

Although both forms of the Elliott *et al.* multi-solute osmotic virial equation (*i.e.*, Equations 2.16 and 2.17) as well as the Kleinhans and Mazur freezing point summation model (*i.e.*, Equation 2.21) have been observed to accurately predict non-ideal solution behaviour in multi-solute solutions using only single-solute data, it would be useful to compare the accuracy of the predictions of these three models in as many multi-solute solutions of cryobiological interest as possible. Such information could be used to help choose the optimal model for working with a given solution system of interest. Limited comparisons between these solution theories have been made in the past [5,24,47,105], but these have been restricted to only a few of the multi-solute systems for which data are available in the literature, and none have directly compared the molality- and mole fraction-based forms of the multi-solute osmotic virial equation. There has yet to be a comprehensive quantitative study comparing the abilities of all three of these models to predict non-ideal multi-solute solution behaviour for the range of available cryobiologically-relevant multi-solute data in which the predictions of all three models are based on a single

consistent set of binary solution data. Such a study is the ultimate goal of this work; however, there are some issues that must first be addressed.

Solute-specific coefficients are available in the literature for a variety of solutes for both the multi-solute osmotic virial equation [105] and the freezing point summation model [69,145]. However, the binary solution data sets used to curve-fit for these coefficients are not consistent—*i.e.*, different data sets were used to obtain the osmotic virial coefficients than were used to obtain the freezing point summation coefficients, and, in fact, only half of the solutes which have had osmotic virial coefficients determined have had freezing point summation coefficients determined. As such, before comparing the predictions made by the three non-ideal models being studied here, solute-specific coefficients will need to be curve-fit for each model for all solutes of interest using a single consistent collection of binary solution data sets. Additionally, it should be noted that the mole fraction-based osmotic virial coefficients previously presented by Prickett *et al.* [105] were not curve-fit using Equation 2.8 to convert between osmolality and osmole fraction; rather, the following conversion equation was used

$$\tilde{\pi} = M_1 x_1 \pi \,. \tag{2.27}$$

Equation 2.27 arises from an *a priori* assumption that is true only under very specific conditions, namely, an ideal dilute solution if the relationship between osmole fraction and chemical potential is defined as in this paper and in reference [24] (the relationship is not given in reference [105]). Since the conversion between osmolality and osmole fraction is useful only in non-ideal circumstances and we have carefully defined all of the surrounding relationships in this work, we suggest that Equation 2.27 not be used. Accordingly, we have herein used Equation 2.8 to refit the available data to obtain updated mole fraction-based osmotic virial coefficients.

Finally, it is important to point out that while the Kleinhans and Mazur freezing point summation model defines the number of solute-specific coefficients to be used for each solute (three), the osmotic virial equation does not. In principle, it is possible to fit the osmotic virial equation to osmometric data with any number of osmotic virial coefficients, regardless of solute, and the fit should improve, even if only slightly, with each added coefficient. However, the model fit converges quickly (recall that the osmotic virial coefficients represent increasing orders of interactions between solute molecules), with each added coefficient contributing progressively less to the accuracy of the fit. Indeed, previous studies [24,105] have shown that for most solutes, the second osmotic virial coefficient is sufficient to accurately capture non-ideal solution behaviour, although some particularly non-ideal solutes such as proteins require a third osmotic virial coefficient [105]. Furthermore, as noted by Prausnitz *et al.* [102], excessive coefficients (*i.e.*, overfitting) may actually lead to a loss of accuracy when predicting the thermodynamic behaviour of more complex, multi-solute solutions, due to the corresponding need for a greater number of combining rules, each of which may have some uncertainty associated with it arising from assumptions made in its development. For these reasons, when curve-fitting the osmotic virial equation, the number of coefficients used (*i.e.*, the order of the fit) should be limited to the minimum that gives an adequate fit. Prickett *et al.* [105] defined and applied a criterion based on the adjusted $R^2$ statistic for determining the adequate order of fit for the osmotic virial equation. However, this criterion did not account for the fact that the osmotic virial equation must pass through the origin (*i.e.*, the osmolality of pure water is zero). Furthermore, there exist other criteria that are appropriate for establishing the order of fit. In this work, two criteria were applied to determine the number of osmotic virial coefficients required for both the molality- and mole

fraction-based osmotic virial equations: the adjusted $R^2$ statistic, taking into account regression through the origin, and confidence intervals on the osmotic virial coefficients.

In summary, the specific objectives of this work are threefold. First, to provide revised osmotic virial coefficients for the molality- and mole fraction-based multi-solute osmotic virial equations for solutes of interest to cryobiology, using the relationship between osmolality and osmole fraction defined through water chemical potential and an improved and extended set of criteria for selecting the order of fit. Second, to provide coefficients for the freezing point summation model for all the solutes considered in the first objective using the same data sets. And finally, using available literature experimental data, to quantitatively evaluate and compare the accuracy of multi-solute solution osmolality predictions made by these three non-ideal models, the ideal dissociation model, and the molality- and mole fraction-based ideal dilute models.

### 2.4. Statistical methods for fitting to single-solute (binary) solution data

Multiple linear regression was used to curve-fit the osmotic virial equation (Equations 2.5, 2.6, 2.9, and 2.10) and the freezing point summation model (Equation 2.20) to literature single-solute solution osmometric data in order to obtain the corresponding solute-specific coefficients. The regression was performed using an analytical matrix approach [93] (see Appendix A for details). Solutes considered included sodium chloride (NaCl) [142], potassium chloride (KCl) [142], dimethyl sulphoxide (DMSO) [8,24,51,109], glycerol [8,24,89,142], propylene glycol (PG) [8,89,142,145], ethylene glycol (EG) [89,142], ethanol [142], methanol [142,145], mannitol [142], sucrose [43,142], dextrose [142], trehalose [92], hemoglobin [17], bovine serum albumin (BSA) [140], and ovalbumin (OVL) [149]. All of the data sets used were obtained from the literature expressed in terms of either osmotic pressure versus solute concentration [17,140,149] or freezing

point depression versus solute concentration [8,24,43,51,89,92,109,142,145]. For fitting the osmotic virial equation, the data were converted to osmolality versus concentration using Equations 2.3 and 2.4, whereas for fitting the freezing point summation model, the data were converted to freezing point depression versus concentration using Equations 2.2 and 2.4.

*2.4.1. Determining order of fit for the osmotic virial equation*

For each solute, the order of fit for the osmotic virial equation (*i.e.*, the number of osmotic virial coefficients required) was determined using two criteria based on the adjusted $R^2$ statistic and on confidence intervals on the osmotic virial coefficients. These criteria are described in detail below. In each case, starting with a zero-order fit (no coefficients), the order of fit was increased until one or both of the criteria was no longer satisfied. The maximum order of fit that was not rejected by either criterion was chosen to represent the solute in question.

As the freezing point summation model has a fixed number of coefficients, calculations to determine order of fit were not required for this model. However, confidence intervals on the coefficients were calculated using Equation 2.30 (see below).

*2.4.2. Adjusted $R^2$ criterion*

The coefficient of determination, $R^2$, is commonly used to evaluate the fit of a model to data. In this work, in order to determine the order of fit for the osmotic virial equation, a regression-through-origin form of the adjusted $R^2$ was used

$$R^2_{adj,\mathrm{RTO}} = 1 - \frac{\sum\left(y_{(a)} - \hat{y}_{(a)}\right)^2/(n-p)}{\sum\left(y_{(a)}\right)^2/(n)}, \tag{2.28}$$

where $y_{(a)}$ is the value at the $a^{\text{th}}$ data point, $\hat{y}_{(a)}$ is the fitted model prediction of the $a^{\text{th}}$ data point, $n$ is the total number of data points, and $p$ is the number of parameters/coefficients in the model (see Appendix B for further details). Note that the subscript "RTO" here and elsewhere in this

work indicates that the value applies to regression through the origin. The specific criterion used to determine the order of fit was defined as follows: for the solute of interest, the order of the fit was progressively increased as long as the added osmotic virial coefficient increased $R^2_{adj,\mathrm{RTO}}$ by at least 0.005.

*2.4.3. Confidence interval criterion*

Another method of determining the order of fit for the osmotic virial equation is by using confidence intervals calculated on the osmotic virial coefficients (and if applicable, the dissociation constant) at a given significance level. Specifically, when considering an increase in the order of fit, it should be verified that in the higher-order model, the confidence interval of the added coefficient does not include zero—if it does, then the higher-order model is not appropriate and, therefore, the order of fit should not be increased. It should be noted that this criterion is mathematically equivalent to conducting a *t*-test to evaluate the hypothesis that the regression coefficient that would be added (in the higher-order model) is equal to zero.

For the $i^{\text{th}}$ regression coefficient $\beta_i$, a 100(1–$\alpha$)% confidence interval can be calculated using [93]

$$\hat{\beta}_i \pm t_{\alpha/2,n-p}\sigma_{\hat{\beta}_i}\,, \tag{2.29}$$

where $\sigma_{\hat{\beta}_i}$ is the standard error of $\hat{\beta}_i$ and $t_{\alpha/2,n-p}$ is the right-tailed ($\alpha$/2)% point of the Student's *t*-distribution with $n - p$ degrees of freedom. The standard error of $\hat{\beta}_i$ is given by

$$\sigma_{\hat{\beta}_i} = \sqrt{\hat{\sigma}^2 S_{ii}}\,, \tag{2.30}$$

where $S_{ii}$ is the $ii^{\text{th}}$ element of covariance matrix $\underline{S} = \left(\underline{F}^T\underline{F}\right)^{-1}$, $\underline{F}$ is the design matrix (see Appendix A), and $\hat{\sigma}^2$ is the estimated model variance, defined by

$$\hat{\sigma}^2 = \frac{\sum\left(y_{(a)} - \hat{y}_{(a)}\right)^2}{n - p}. \tag{2.31}$$

In this work, a criterion based on a 95% confidence interval (*i.e.*, $\alpha = 0.05$) was used.

It should be noted that for electrolyte solutes, which require a dissociation constant and thus use the forms of the osmotic virial equation in Equations 2.9 and 2.10, the regression coefficients do not equal the osmotic virial coefficients. As a consequence, the calculation of confidence intervals on the osmotic virial coefficients of electrolyte solutes requires the use of error propagation equations to obtain the corresponding standard errors (*e.g.*, see Bevington and Robinson [6]).

### 2.5. Statistical methods for evaluation of multi-solute (ternary and quaternary) solution osmolality predictions

Once all required coefficients had been obtained, the three non-ideal models (*i.e.*, the molality- and mole fraction-based multi-solute osmotic virial equations and the freezing point summation model) along with the ideal dissociation model and the molality- and mole fraction-based ideal dilute models were used to predict osmolalities in several multi-solute solution systems of cryobiological interest for which experimental data [5,24,43,47,51,100,128,145,150] were available in the literature. For the freezing point summation model (Equation 2.21), freezing point depression predictions were converted to osmolality predictions using Equation 2.3. For both mole fraction-based models (Equations 2.17 and 2.19 and Equations 2.23 and 2.25), osmole fraction predictions were converted to osmolality predictions using Equation 2.8.

The osmolality predictions of all six models were compared to the literature experimental osmolality measurements. All of the literature data were considered in the form of solution osmolality versus overall solute concentration (conversions were carried out where necessary),

with the data for each solution system organized into one or more isopleths. An isopleth is a set of osmolality measurements made at increasing overall solute concentrations with all solute mass ratios held constant. The number of isopleths available for the various solution systems considered varied from 1 to 100 (see Table 2.2 for details). For some of the solution systems [24,47,145,150], numerical data were directly available; for others [5,43,51,100,128], only graphical data were available. In the latter case, numerical data values were estimated by digitizing the published graphs. For all but one of these data sets, the graphical data contained individual data points for each composition of interest. The exception was the data for the glycerol + NaCl system [128], for which only plots (*i.e.*, curves) of the data were available. To analyse this data set, evenly-spaced (in terms of composition) points were chosen along each data curve, and those points were taken to represent the data for that curve. The number of "data points" obtained this way ranged from eight to thirteen, depending on the length of the curve. Special note should also be taken of the data for the EG + NaCl system [5]. In this case, Benson *et al.* took three experimental measurements at each composition of interest. However, the graphical data in that work does not always show the three measurements as distinct. In such instances, the measurements were assumed to overlay—*i.e.*, the one data point apparent was taken to represent three measurements.

The accuracy of the model predictions was evaluated using two quantitative measures. The first was the regression-through-origin (non-adjusted) $R^2$ statistic, $R_{\mathrm{RTO}}{}^2$, *i.e.*,

$$R_{\mathrm{RTO}}{}^2 = 1 - \frac{\sum\left(y_{(a)} - \hat{y}_{(a)}\right)^2}{\sum\left(y_{(a)}\right)^2}, \tag{2.32}$$

where $\hat{y}_{(a)}$ in this case refers to the multi-solute (as opposed to fitted single-solute) model prediction of the $a^{\mathrm{th}}$ data point. The second measure was the percent mean relative magnitude error (%*MRME*), defined as

$$\%MRME = \frac{1}{n}\sum_{a=1}^{n}\left|\frac{y_{(a)} - \hat{y}_{(a)}}{y_{(a)}}\right| \times 100\% \,. \tag{2.33}$$

For each of the six solution models, $R_{\mathrm{RTO}}^2$ and %*MRME* values were calculated for each isopleth in each solution system. The values of each measure were then averaged over all the isopleths within a given solution system. The resulting averages represent the overall accuracy of the corresponding model predictions in that solution system.

## 2.6. Results and discussion

The fitted molality- and mole fraction-based osmotic virial coefficients obtained from literature single-solute solution data are given in Tables 2.3 and 2.4, respectively. As done by Prickett *et al.* [105], the solutes here have been organized into groups by type of molecule: electrolytes, cryoprotectants, alcohols, sugars, and proteins. For both the molality- and mole fraction-based osmotic virial equations, the same twelve solutes (of fifteen considered) were found to require at least second order fits (*i.e.*, second osmotic virial coefficients $B_{ii}$). The exceptions in both cases were KCl, mannitol, and trehalose; these solutes did not require any osmotic virial coefficients and thus, by the criteria defined in this work, can be considered ideal when using the osmotic virial equation. Further, for the molality-based osmotic virial equation, three solutes—ethanol, and the proteins hemoglobin and BSA—required third-order fits, and for the mole fraction-based osmotic virial equation, four solutes—DMSO, ethanol, hemoglobin, and BSA—also required third-order fits. None of the solutes for either model were found to require fourth-order or higher fits. The molality-based coefficients obtained here are largely the same as those reported by Prickett *et al.* [105], with the exceptions of those for EG, ethanol, sucrose, and trehalose. For ethanol and trehalose, these differences reflect the updated criteria used for selecting

the order of fit; for sucrose, they reflect additional data [43] that were used; and for EG, they reflect both additional data [89] and the new criteria. Conversely, the mole fraction-based coefficients are almost entirely different from those of Prickett *et al.* (the exception here being the ideal non-electrolyte solute mannitol). The differences in this latter case primarily arise from the use of Equation 2.8 (instead of Equation 2.27) to define the relationship between osmolality and osmole fraction in this work.

The fitted coefficients for the Kleinhans and Mazur freezing point summation model are given in Table 2.5. Kleinhans and Mazur [69] have previously reported coefficients for NaCl, glycerol, DMSO, sucrose, and EG, and Weng *et al.* [145] have previously reported coefficients for methanol and PG. The coefficients obtained here for those solutes are, in all cases, at least slightly different. These differences likely have to do with the additional data used in this work, as well as the fact that Kleinhans and Mazur thinned the data that they used in order to minimize the weighting of data at lower concentrations [69]. In this work, all available data points from all cited sources were used. It should be noted that for many of the solutes considered (specifically: DMSO, PG, ethanol, mannitol, dextrose, trehalose, hemoglobin, BSA, and OVL), the 95% confidence intervals for one or more of the freezing point summation coefficients include zero (see bolded values in Table 2.5). These occurrences may indicate situations where the use of a third order fit with the freezing point summation model is not appropriate.

Using the corresponding coefficients in Tables 2.3, 2.4, and 2.5, the molality- and mole fraction-based Elliott *et al.* multi-solute osmotic virial equations (Equations 2.16 and 2.18 and 2.17 and 2.19, respectively), the Kleinhans and Mazur freezing point summation model (Equation 2.21), the ideal dissociation model (Equation 2.26), and the molality- and mole fraction-based ideal dilute models defined in Equations 2.22 and 2.24 and 2.23 and 2.25, respectively, were used to make

predictions of solution osmolality in each of the ten multi-solute solution systems listed in Table 2.2. Figures 2.1 to 2.10 show a representative isopleth and corresponding model predictions from each of the considered solution systems. Tables 2.6 and 2.7 give the average values of $R_{RTO}^2$ and %*MRME*, respectively, calculated over all isopleths within a given solution system for each of the six models considered. Each table also contains an overall (unweighted, *e.g.*, with respect to number of isopleths) average value of its corresponding measure calculated over all the solution systems for each model.

Before discussing the results in Tables 2.6 and 2.7, an important point should be made regarding one of the measures of model prediction accuracy used in this work, that is, $R_{RTO}^2$. As is discussed in greater detail in Appendix B, $R_{RTO}^2$ is not directly comparable to a "standard" $R^2$ statistic (*i.e.*, one with the total sum of squares calculated using Equation B.3 instead of Equation B.7). In fact, $R_{RTO}^2$ values for a given prediction or fit will always be higher than the corresponding $R^2$ values. Thus, for example, while a value of $R^2 = 0.9$ might represent a respectable prediction, $R_{RTO}^2 = 0.9$ does not.

From the results in Tables 2.6 and 2.7 and Figures 2.1 to 2.10, it is evident that the three non-ideal models perform considerably better than the three ideal models. However, none of the three non-ideal models is clearly superior to the others. Each non-ideal model has solution systems where it is noticeably—at least, in terms of *%MRME*—more accurate than the other two (*e.g.*, DMSO + glycerol for the molality-based multi-solute osmotic virial equation, EG + NaCl + sucrose for the mole fraction-based multi-solute osmotic virial equation, and NaCl + sucrose for the freezing point summation model), but overall the performance of all three non-ideal models is very close. In contrast to the non-ideal models, there is a distinct difference in the performance of one of the ideal models relative to the other two: the molality-based ideal dilute model and the

ideal dissociation model clearly provide more accurate predictions than the mole fraction-based ideal dilute model in almost all of the solution systems considered (the lone exception being BSA + OVL, where all three ideal models provide equally poor predictions). Given that the main difference between the molality- and mole fraction-based ideal dilute models is the way in which concentration is defined, the gap in their prediction accuracy highlights the importance of the choice of concentration units in thermodynamic modeling.

## 2.7. Conclusions

Our results indicate that the three non-ideal models provide superior multi-solute predictions as compared to the three ideal models. Furthermore, although in certain solution systems there was a clearly dominant model, all three non-ideal models exhibited similar performance overall (*i.e.*, when accounting for all considered solution systems). Based on these results, we strongly recommend the use of at least one of the three non-ideal models evaluated here when predicting solution osmolality (*e.g.*, when modeling osmotic responses). The results of the multi-solute solution analysis in this work can be used to aid in the choice of a particular model, depending on the composition of the solutions being modeled. Once a model has been chosen, the corresponding single-solute coefficients that have been determined here can be used to make the desired predictions.

Table 2.1. Values and units of the constants in Equations 2.1, 2.2, 2.3, and 2.4 [10].

| Constant | Value |
|---|---|
| $R$ | 8.314 J/(mol K) = 8.314 Pa $m^3$/(mol K) |
| $M_1$ | $1.802 \times 10^{-2}$ kg/mol |
| $T_m^o$ | 273.15 K |
| $\overline{\Delta s_{f1}^o}$ | 22.00 J/(mol K) |
| $\rho_1$ | 997 kg/$m^3$ |

Table 2.2. Number of isopleths available for each of the multi-solute solution systems considered in this work.

| Solution System | Number of Isopleths | Source |
|---|---|---|
| BSA + OVL | 1 | [150] |
| DMSO + Glycerol | 2 | [24] |
| DMSO + NaCl | 8 | [51] |
| EG + NaCl | 5 | [5] |
| Glycerol + NaCl | 7 | [128] |
| Methanol + NaCl | 3 | [145] |
| NaCl + PG | 3 | [145] |
| NaCl + Sucrose | 6 | [43] |
| EG + NaCl + Sucrose | 100 | [47] |
| Glycerol + NaCl + PG | 3 | [100] |

Table 2.3. Elliott *et al.* molality-based osmotic virial coefficients with corresponding 95% confidence intervals (CI), for use in Equation 2.16. The order-limiting criterion for each solute denotes which of the fitting criteria—adjusted $R^2$ ($R^2_{adj,\mathrm{RTO}}$), confidence interval (CI), or both—rejected further increases in the order of fit for that solute.

| **Solute [Source]** | **Maximum Molality (mol/kg)** | **$k_i$ [±95% CI]** | **$B_{ii}$ (molal$^{-1}$) [±95% CI]** | **$C_{iii}$ (molal$^{-2}$) [±95% CI]** | **$R^2_{adj,\mathrm{RTO}}$** | **Order-Limiting Criterion** |
|---|---|---|---|---|---|---|
| NaCl [142] | 5.111 | 1.678 [±0.016] | 0.044 [±0.002] | 0 | 1.000 | $R^2_{adj,\mathrm{RTO}}$ |
| KCl [142] | 2.004 | 1.772 [±0.003] | 0 | 0 | 1.000 | $R^2_{adj,\mathrm{RTO}}$ |
| DMSO [8,24,51,109] | 14.975 | 1 | 0.108 [±0.005] | 0 | 0.996 | $R^2_{adj,\mathrm{RTO}}$ |
| Glycerol [8,24,89,142] | 16.288 | 1 | 0.023 [±0.001] | 0 | 0.998 | $R^2_{adj,\mathrm{RTO}}$ |
| PG [8,89,142,145] | 19.713 | 1 | 0.039 [±0.001] | 0 | 0.998 | $R^2_{adj,\mathrm{RTO}}$ |
| EG [89,142] | 24.166 | 1 | 0.020 [±0.001] | 0 | 0.998 | $R^2_{adj,\mathrm{RTO}}$ |
| Ethanol [142] | 46.125 | 1 | 0.012 [±0.003] | -0.0004 [±0.0001] | 0.995 | $R^2_{adj,\mathrm{RTO}}$ |
| Methanol [142,145] | 66.323 | 1 | 0.0036 [±0.0002] | 0 | 0.999 | $R^2_{adj,\mathrm{RTO}}$ |
| Mannitol [142] | 0.969 | 1 | 0 | 0 | 1.000 | $R^2_{adj,\mathrm{RTO}}$ |
| Sucrose [43,142] | 5.329 | 1 | 0.116 [±0.004] | 0 | 0.998 | $R^2_{adj,\mathrm{RTO}}$ |
| Dextrose [142] | 2.379 | 1 | 0.044 [±0.001] | 0 | 1.000 | $R^2_{adj,\mathrm{RTO}}$ |
| Trehalose [92] | 1.108 | 1 | 0 | 0 | 0.997 | Both |
| Hemoglobin [17] | $1.23\times10^{-2}$ | 1 | 49.3 [±18.6] | $3.07\times10^{4}$ [$\pm0.18\times10^{4}$] | 1.000 | Both |
| BSA [140] | $9.72\times10^{-3}$ | 1 | 370.5 [±361.9] | $1.60\times10^{5}$ [$\pm0.42\times10^{5}$] | 0.997 | Both |
| OVL [149] | $1.95\times10^{-2}$ | 1 | 378.5 [±14.9] | 0 | 0.994 | $R^2_{adj,\mathrm{RTO}}$ |

Table 2.4. Elliott *et al.* mole fraction-based osmotic virial coefficients with corresponding 95% confidence intervals (CI), for use in Equation 2.17. The order-limiting criterion for each solute denotes which of the fitting criteria—adjusted $R^2$ ($R^2_{adj,\mathrm{RTO}}$), confidence interval (CI), or both—rejected further increases in the order of fit for that solute.

| **Solute [Source]** | **Maximum Mole Fraction** | $k_i^*$ **[±95% CI]** | $B_{ii}^*$ **[±95% CI]** | $C_{iii}^*$ **[±95% CI]** | $R^2_{adj,\mathrm{RTO}}$ | **Order-Limiting Criterion** |
|---|---|---|---|---|---|---|
| NaCl [142] | 0.084 | 1.644 [±0.021] | 3.80 [±0.17] | 0 | 1.000 | $R^2_{adj,\mathrm{RTO}}$ |
| KCl [142] | 0.035 | 1.818 [±0.004] | 0 | 0 | 1.000 | $R^2_{adj,\mathrm{RTO}}$ |
| DMSO [8,24,51,109] | 0.212 | 1 | 2.35 [±1.69] | 43.6 [±9.6] | 0.998 | Both |
| Glycerol [8,24,89,142] | 0.227 | 1 | 3.17 [±0.07] | 0 | 0.999 | $R^2_{adj,\mathrm{RTO}}$ |
| PG [8,89,142,145] | 0.262 | 1 | 4.98 [±0.14] | 0 | 0.998 | $R^2_{adj,\mathrm{RTO}}$ |
| EG [89,142] | 0.303 | 1 | 3.41 [±0.03] | 0 | 1.000 | Both |
| Ethanol [142] | 0.454 | 1 | 3.90 [±0.16] | −7.36 [±0.41] | 0.999 | $R^2_{adj,\mathrm{RTO}}$ |
| Methanol [142,145] | 0.544 | 1 | 2.63 [±0.07] | 0 | 0.997 | $R^2_{adj,\mathrm{RTO}}$ |
| Mannitol [142] | 0.017 | 1 | 0 | 0 | 0.999 | $R^2_{adj,\mathrm{RTO}}$ |
| Sucrose [43,142] | 0.088 | 1 | 8.68 [±0.25] | 0 | 0.999 | Both |
| Dextrose [142] | 0.041 | 1 | 3.65 [±0.06] | 0 | 1.000 | $R^2_{adj,\mathrm{RTO}}$ |
| Trehalose [92] | 0.020 | 1 | 0 | 0 | 0.997 | Both |
| Hemoglobin [17] | $2.21\times10^{-4}$ | 1 | $2.73\times10^{3}$ [$\pm1.03\times10^{3}$] | $9.46\times10^{7}$ [$\pm0.56\times10^{7}$] | 1.000 | Both |
| BSA [140] | $1.75\times10^{-4}$ | 1 | $2.05\times10^{4}$ [$\pm2.01\times10^{4}$] | $4.94\times10^{8}$ [$\pm1.31\times10^{8}$] | 0.997 | Both |
| OVL [149] | $3.51\times10^{-4}$ | 1 | $2.10\times10^{4}$ [$\pm0.08\times10^{4}$] | 0 | 0.994 | $R^2_{adj,\mathrm{RTO}}$ |

Table 2.5. Kleinhans and Mazur freezing point summation model coefficients with corresponding 95% confidence intervals (CI), for use with Equation 2.21. Bolded values indicate coefficients where the 95% confidence interval includes zero.

| **Solute [Source]** | **Maximum Molality (mol/kg)** | $C_{1i}$ **(°C/molal) [±95% CI]** | $C_{2i}$ **(°C/molal$^2$) [±95% CI]** | $C_{3i}$ **(°C/molal$^3$) [±95% CI]** | $R^2_{adj,\mathrm{RTO}}$ |
|---|---|---|---|---|---|
| NaCl [142] | 5.111 | –3.357 [±0.006] | –0.0043 [±0.0043] | $-2.56\times10^{-2}$ [$\pm0.07\times10^{-2}$] | 1.000 |
| KCl [142] | 2.004 | –3.398 [±0.018] | 0.1789 [±0.0283] | $-4.37\times10^{-2}$ [$\pm1.04\times10^{-2}$] | 1.000 |
| DMSO [8,24,51,109] | 14.975 | –1.599 [±0.503] | –0.1824 [±0.1057] | **$1.46\times10^{-3}$ [$\pm5.32\times10^{-3}$]** | 0.998 |
| Glycerol [8,24,89,142] | 16.288 | –1.998 [±0.075] | –0.0286 [±0.0162] | $1.26\times10^{-3}$ [$\pm0.78\times10^{-3}$] | 1.000 |
| PG [8,89,142,145] | 19.713 | –2.109 [±0.142] | –0.0375 [±0.0236] | **$5.67\times10^{-4}$ [$\pm8.96\times10^{-4}$]** | 0.999 |
| EG [89,142] | 24.166 | –1.814 [±0.034] | –0.0548 [±0.0045] | $1.76\times10^{-3}$ [$\pm0.14\times10^{-3}$] | 1.000 |
| Ethanol [142] | 46.125 | –2.389 [±0.100] | 0.0324 [±0.0074] | **$-7.23\times10^{-5}$ [$\pm12.47\times10^{-5}$]** | 0.998 |
| Methanol [142,145] | 66.323 | –2.044 [±0.024] | 0.0104 [±0.0012] | $-1.89\times10^{-5}$ [$\pm1.43\times10^{-5}$] | 1.000 |
| Mannitol [142] | 0.969 | –1.871 [±0.021] | **–0.0055 [±0.0680]** | **$-2.20\times10^{-2}$ [$\pm5.24\times10^{-2}$]** | 1.000 |
| Sucrose [43,142] | 5.329 | –1.824 [±0.145] | –0.2825 [±0.1080] | $1.84\times10^{-2}$ [$\pm1.65\times10^{-2}$] | 0.999 |
| Dextrose [142] | 2.379 | –1.851 [±0.014] | –0.0718 [±0.0202] | **$1.34\times10^{-5}$ [$\pm662.02\times10^{-5}$]** | 1.000 |
| Trehalose [92] | 1.108 | –1.709 [±0.532] | **0.3539 [±1.3955]** | **$-4.88\times10^{-1}$ [$\pm8.72\times10^{-1}$]** | 0.999 |
| Hemoglobin [17] | $1.23\times10^{-2}$ | –2.191 [±0.641] | **–14.1 [±154.7]** | $-6.13\times10^{4}$ [$\pm0.90\times10^{4}$] | 1.000 |
| BSA [140] | $9.72\times10^{-3}$ | **–5.091 [±10.692]** | **$2.29\times10^{2}$ [$\pm31.33\times10^{2}$]** | $-3.59\times10^{5}$ [$\pm2.22\times10^{5}$] | 0.997 |
| OVL [149] | $1.95\times10^{-2}$ | **2.239 [±3.442]** | $-1.13\times10^{3}$ [$\pm0.52\times10^{3}$] | **$1.05\times10^{4}$ [$\pm1.88\times10^{4}$]** | 0.997 |

Table 2.6. Isopleth-averaged regression-through-the-origin $R^2$ ($R_{RTO}^2$) values calculated for each of the multi-solute solution systems considered for predictions made using the molality- and mole fraction-based ideal dilute models, the ideal dissociation model, the Elliott *et al.* molality- and mole fraction-based multi-solute osmotic virial equations (MSOVE), and the Kleinhans and Mazur freezing point summation model.

| **Solution System** | **Maximum Osmolality (osmol/kg)** | **Molality Ideal Model $R_{RTO}^2$** | **Mole Fraction Ideal Model $R_{RTO}^2$** | **Ideal Dissociation Model $R_{RTO}^2$** | **Elliott *et al.* Molality MSOVE $R_{RTO}^2$** | **Elliott *et al.* Mole Fraction MSOVE $R_{RTO}^2$** | **Kleinhans and Mazur Freezing Point Summation Model $R_{RTO}^2$** |
|---|---|---|---|---|---|---|---|
| BSA + OVL | 0.07 | 0.325 | 0.325 | 0.325 | 0.992 | 0.992 | 0.867 |
| DMSO + Glycerol | 9.06 | 0.918 | 0.881 | 0.900 | 0.996 | 0.974 | 0.972 |
| DMSO + NaCl | 45.00 | 0.823 | 0.758 | 0.826 | 0.996 | 0.980 | 0.973 |
| EG + NaCl | 24.43 | 0.907 | 0.813 | 0.869 | 0.986 | 0.993 | 0.989 |
| Glycerol + NaCl | 31.09 | 0.948 | 0.884 | 0.950 | 0.974 | 0.989 | 0.991 |
| Methanol + NaCl | 8.43 | 0.990 | 0.967 | 0.984 | 0.995 | 0.994 | 0.997 |
| NaCl + PG | 10.06 | 0.939 | 0.906 | 0.936 | 0.989 | 0.997 | 0.994 |
| NaCl + Sucrose | 23.07 | 0.931 | 0.876 | 0.941 | 0.927 | 0.958 | 0.990 |
| EG + NaCl + Sucrose | 28.53 | 0.924 | 0.827 | 0.882 | 0.997 | 0.999 | 0.997 |
| Glycerol + NaCl + PG | 25.71 | 0.915 | 0.815 | 0.879 | 0.994 | 0.996 | 0.996 |
| **Overall Average:** | | **0.862** | **0.805** | **0.849** | **0.985** | **0.987** | **0.977** |

Table 2.7. Isopleth-averaged percent mean relative magnitude error (%*MRME*) values calculated for each of the multi-solute solution systems considered for predictions made using the molality- and mole fraction-based ideal dilute models, the ideal dissociation model, the Elliott *et al.* molality- and mole fraction-based multi-solute osmotic virial equations (MSOVE), and the Kleinhans and Mazur freezing point summation model.

| **Solution System** | **Maximum Osmolality (osmol/kg)** | **Molality Ideal Model *%MRME*** | **Mole Fraction Ideal Model *%MRME*** | **Ideal Dissociation Model *%MRME*** | **Elliott *et al.* Molality MSOVE *%MRME*** | **Elliott *et al.* Mole Fraction MSOVE *%MRME*** | **Kleinhans and Mazur Freezing Point Summation Model *%MRME*** |
|---|---|---|---|---|---|---|---|
| BSA + OVL | 0.07 | 65.84 | 65.84 | 65.84 | 11.29 | 11.27 | 34.91 |
| DMSO + Glycerol | 9.06 | 18.56 | 21.96 | 20.29 | 4.91 | 11.43 | 13.13 |
| DMSO + NaCl | 45.00 | 33.71 | 39.27 | 31.73 | 9.24 | 15.29 | 16.63 |
| EG + NaCl | 24.43 | 30.96 | 38.40 | 33.55 | 19.72 | 16.08 | 18.82 |
| Glycerol + NaCl | 31.09 | 17.78 | 25.06 | 14.22 | 8.13 | 7.18 | 6.61 |
| Methanol + NaCl | 8.43 | 11.70 | 18.21 | 13.56 | 8.80 | 8.28 | 6.21 |
| NaCl + PG | 10.06 | 20.36 | 23.78 | 19.78 | 12.24 | 8.50 | 7.48 |
| NaCl + Sucrose | 23.07 | 22.03 | 27.83 | 21.37 | 20.67 | 18.68 | 11.48 |
| EG + NaCl + Sucrose | 28.53 | 20.73 | 28.83 | 24.15 | 8.03 | 5.45 | 7.95 |
| Glycerol + NaCl + PG | 25.71 | 20.55 | 30.79 | 23.31 | 4.83 | 5.77 | 4.17 |
| **Overall Average:** | | **26.22** | **32.00** | **26.78** | **10.79** | **10.79** | **12.74** |

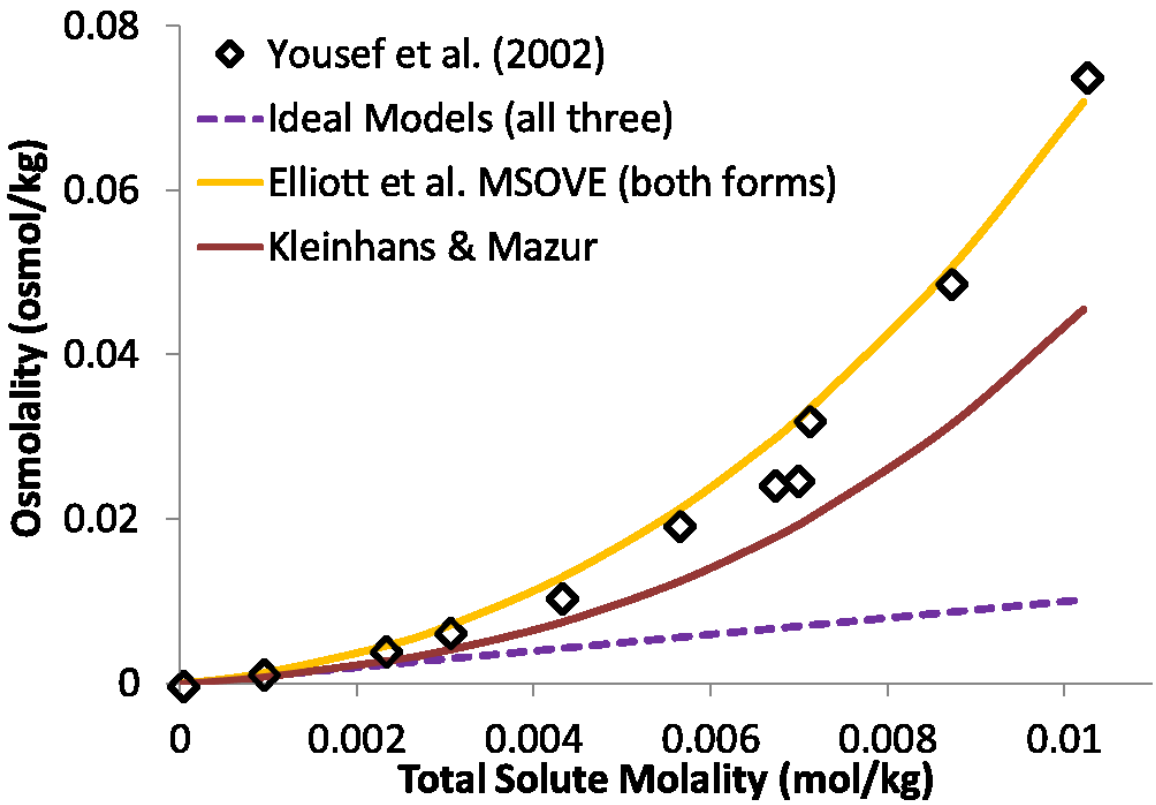


Figure 2.1. Experimental isopleth and model predictions for the solution system BSA + OVL, at a solute mass ratio of BSA:OVL = 3:2. Data are from Yousef *et al.* [150]. The predictions of the molality- and mole fraction-based multi-solute osmotic virial equations overlay directly, as do the predictions of the ideal dissociation model and the molality- and mole fraction-based ideal dilute models.

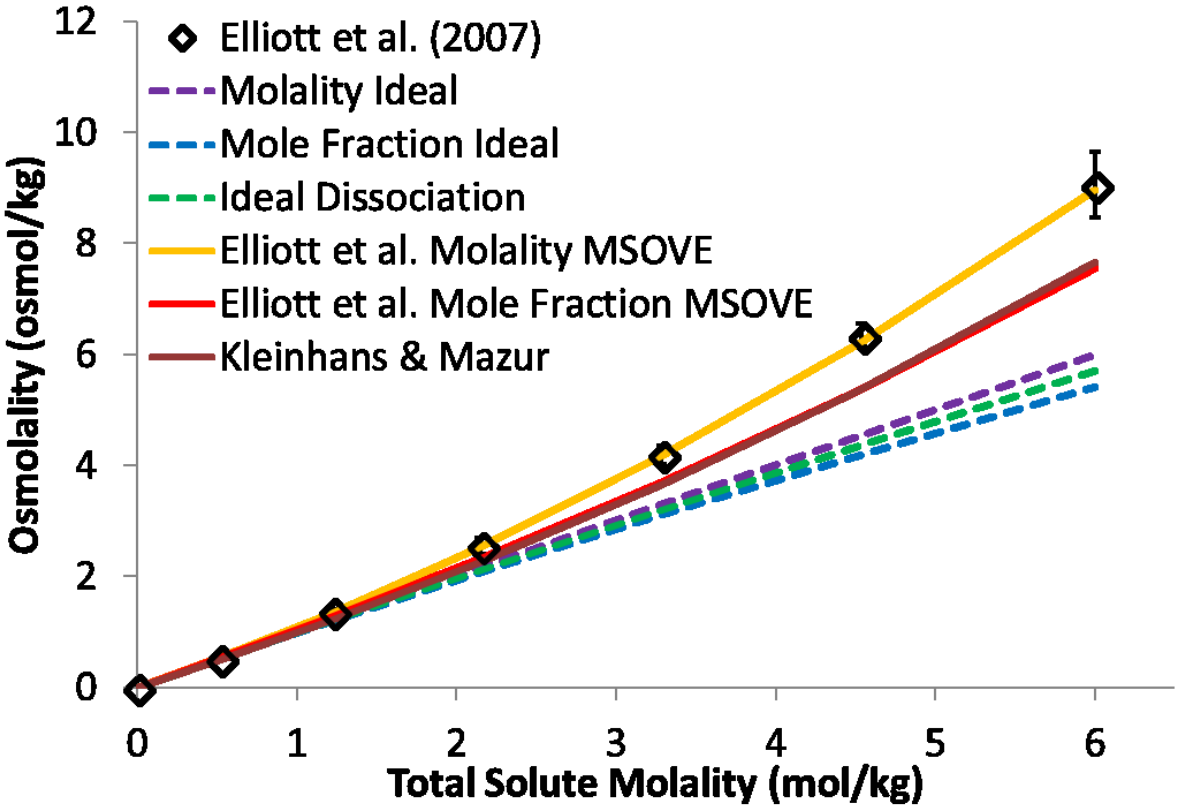


Figure 2.2. Experimental isopleth and model predictions for the solution system DMSO + glycerol, at a solute mass ratio of glycerol:DMSO = 1:2. Data are from Elliott *et al.* [24]. The error bars on the data points represent the standard deviations of the experimental measurements.

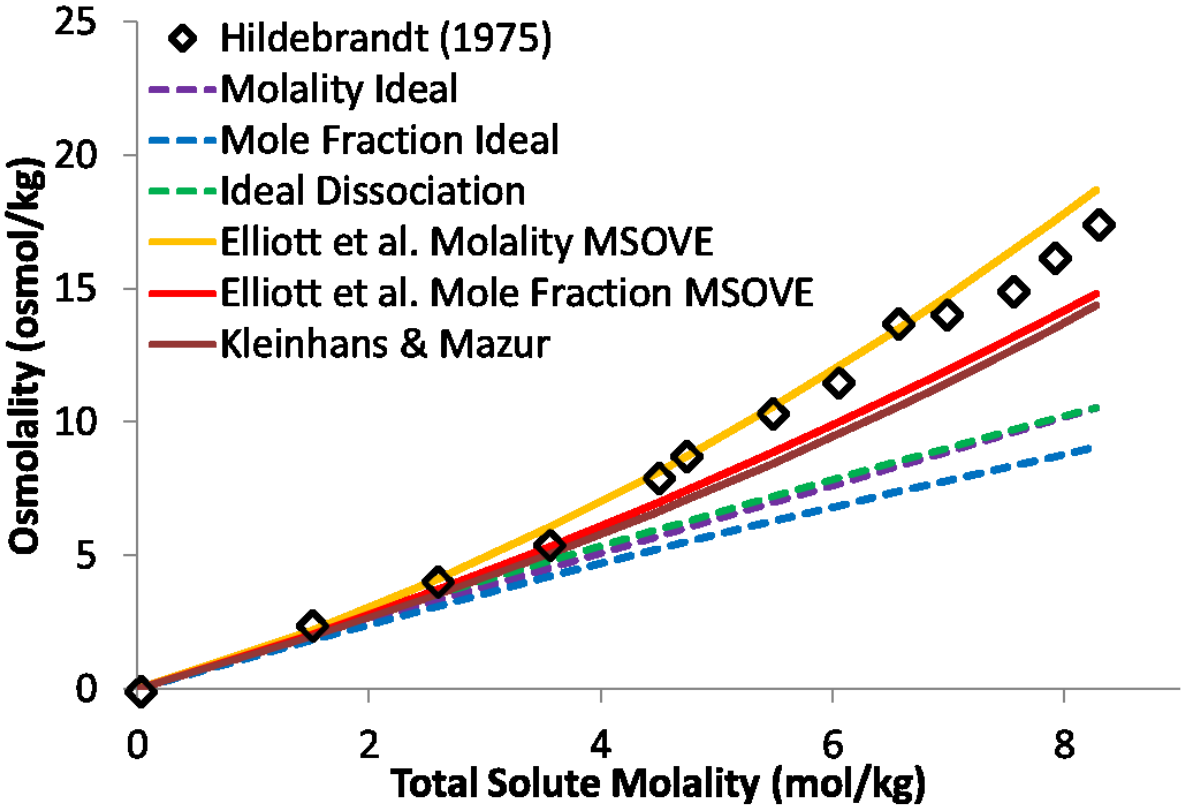


Figure 2.3. Experimental isopleth and model predictions for the solution system DMSO + NaCl, at a solute mass ratio of DMSO:NaCl = 2:1. Data are from Hildebrandt's thesis [51].

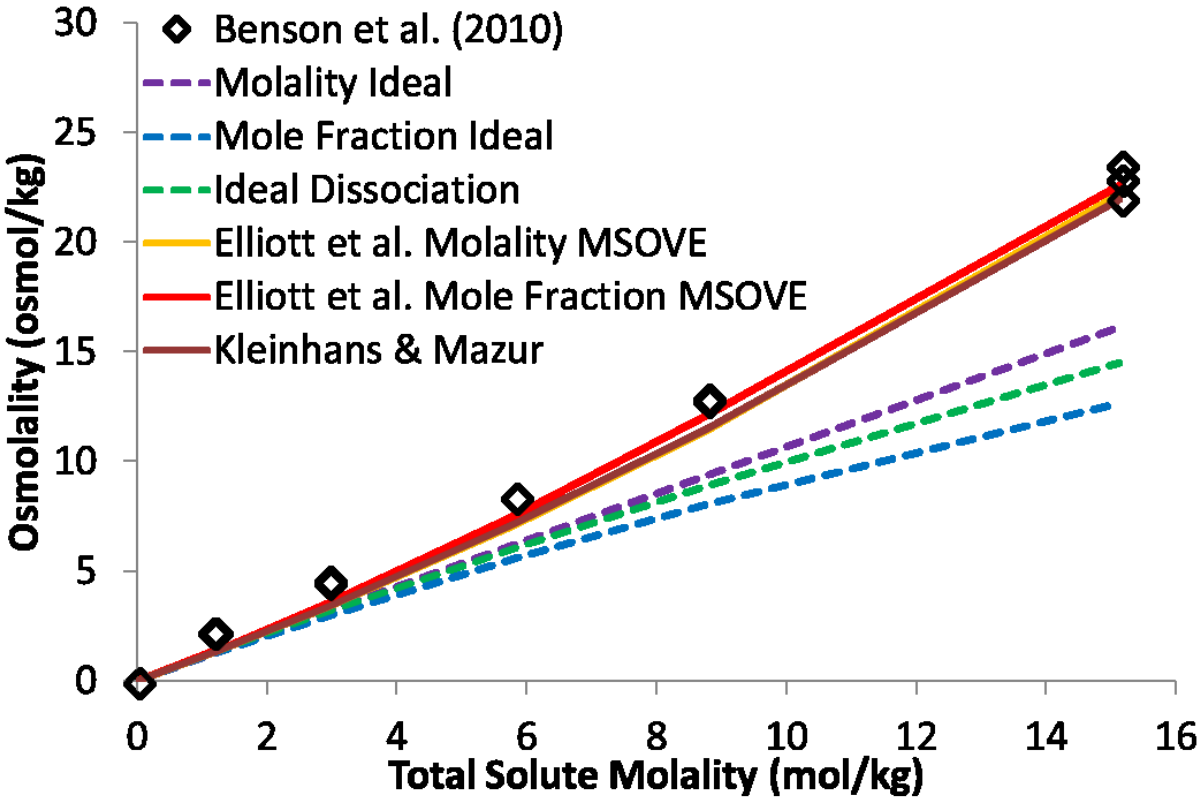


Figure 2.4. Experimental isopleth and model predictions for the solution system EG + NaCl, at a solute mass ratio of EG:NaCl = 10:1. Data are from Benson *et al.* [5].

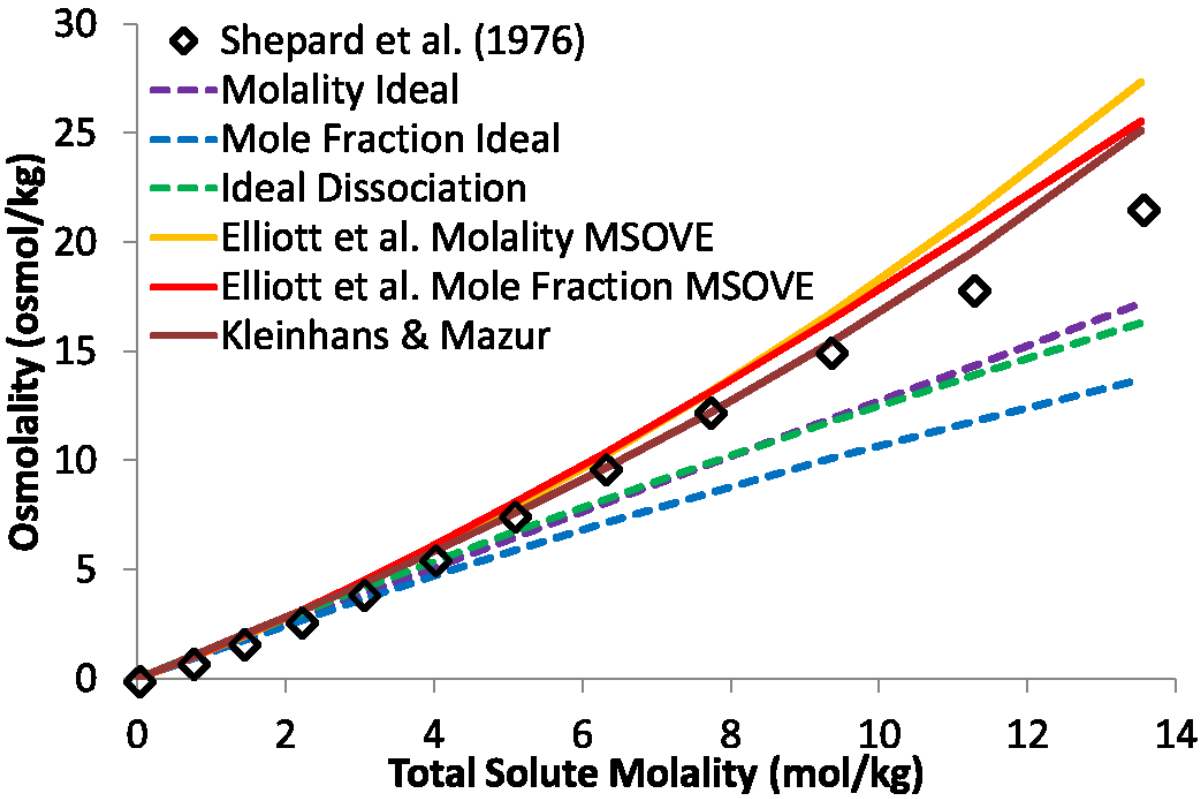


Figure 2.5. Experimental isopleth and model predictions for the solution system glycerol + NaCl, at a solute mass ratio of glycerol:NaCl = 7:3. Data are from Shepard *et al.* [128].

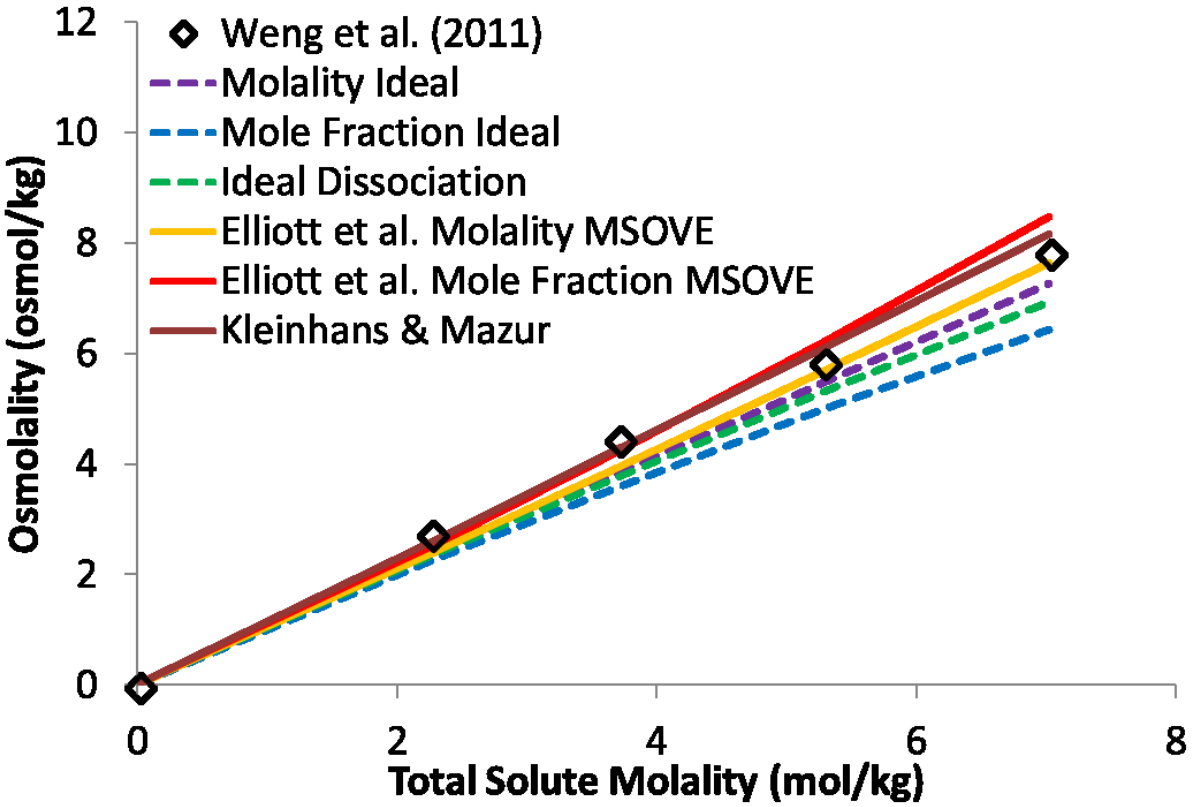


Figure 2.6. Experimental isopleth and model predictions for the solution system methanol + NaCl, at a solute mass ratio of methanol:NaCl = 10:1. Data are from Weng *et al.* [145].

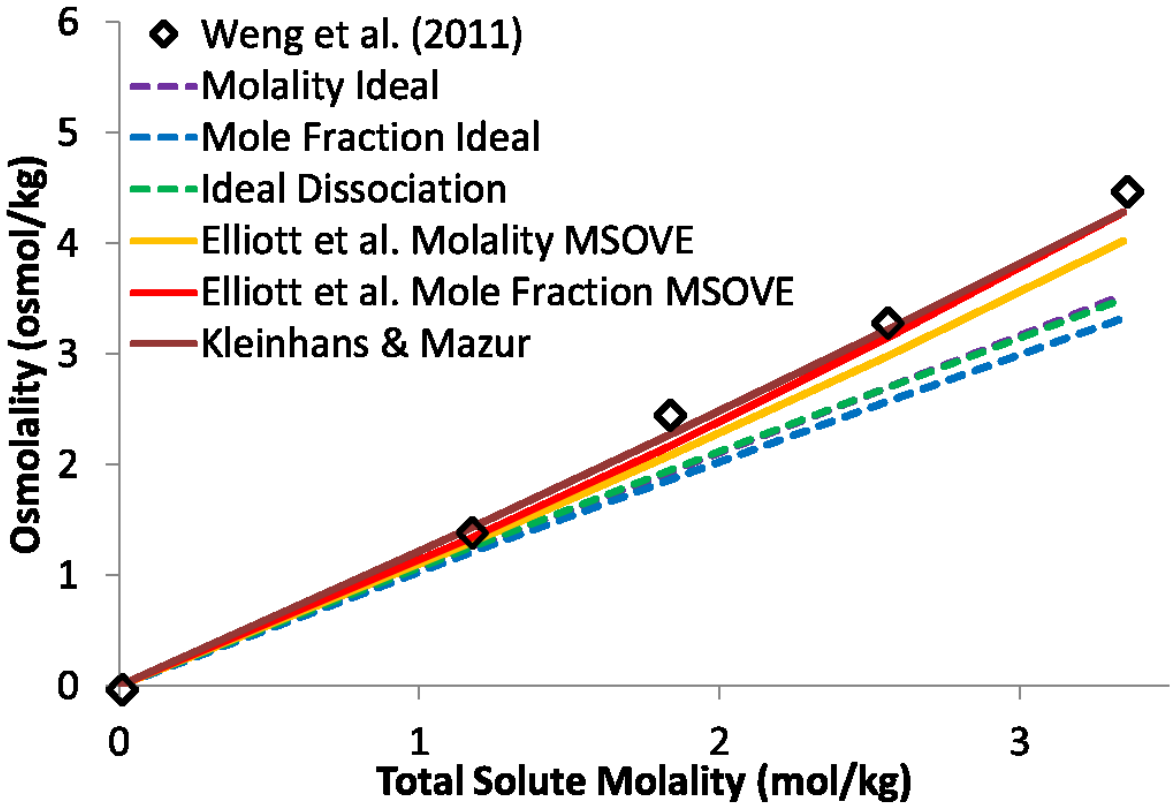


Figure 2.7. Experimental isopleth and model predictions for the solution system NaCl + PG, at a solute mass ratio of PG:NaCl = 15:1. Data are from Weng *et al.* [145].

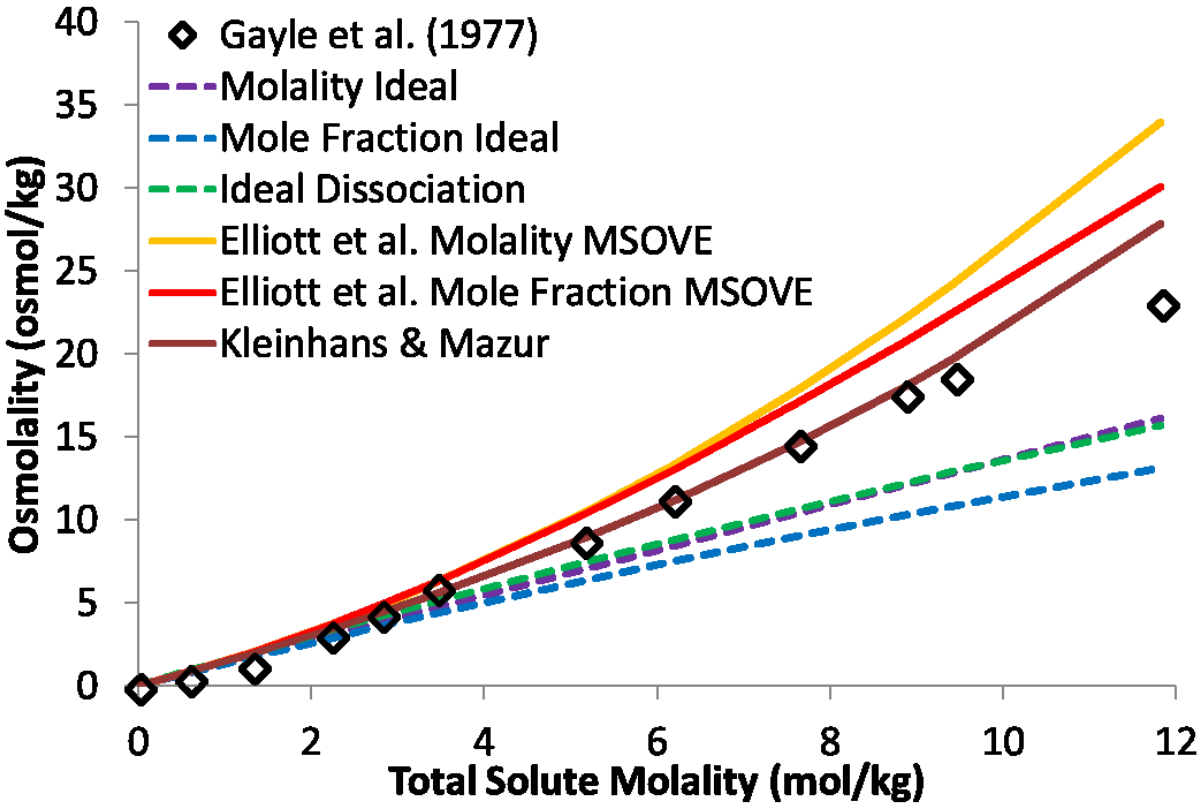


Figure 2.8. Experimental isopleth and model predictions for the solution system NaCl + sucrose, at a solute mass ratio of sucrose:NaCl = 5:1. Data are from Gayle *et al.* [43].

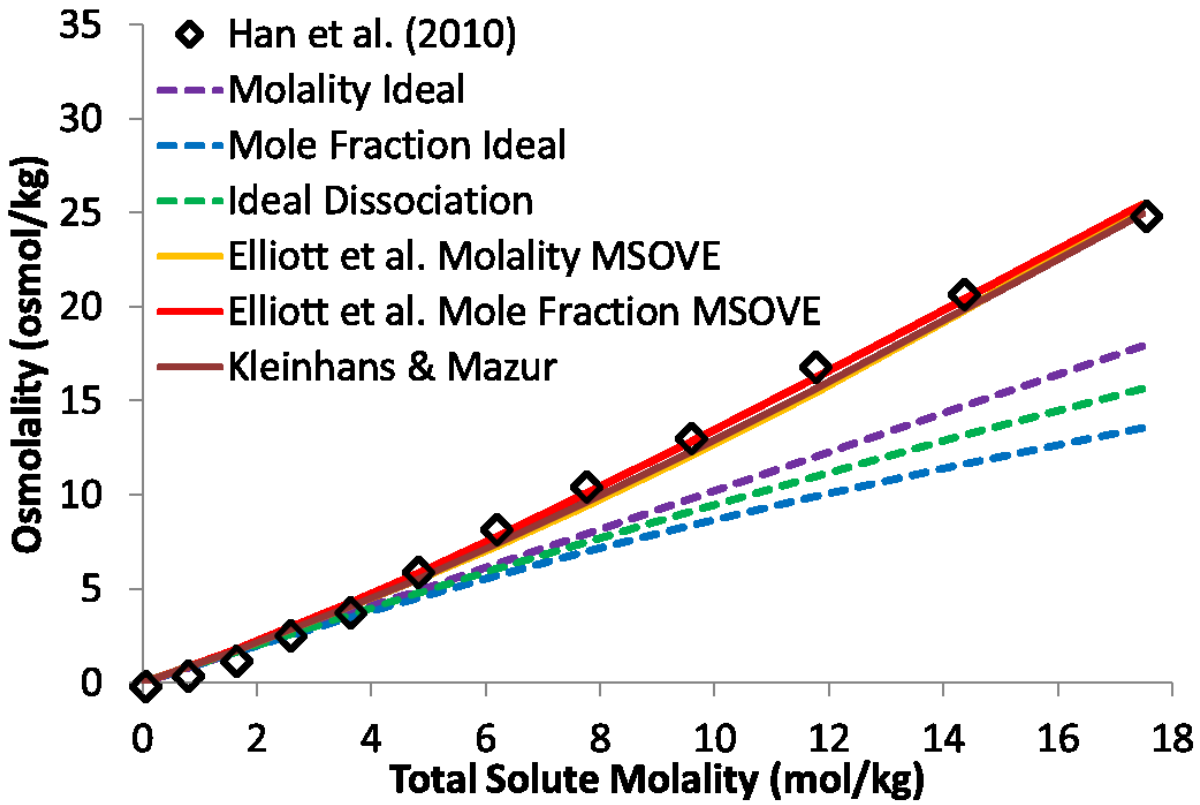


Figure 2.9. Experimental isopleth and model predictions for the solution system EG + NaCl + sucrose, at a solute mass ratio of EG:sucrose:NaCl = 30:5:1. Data are from Han *et al.* [47].

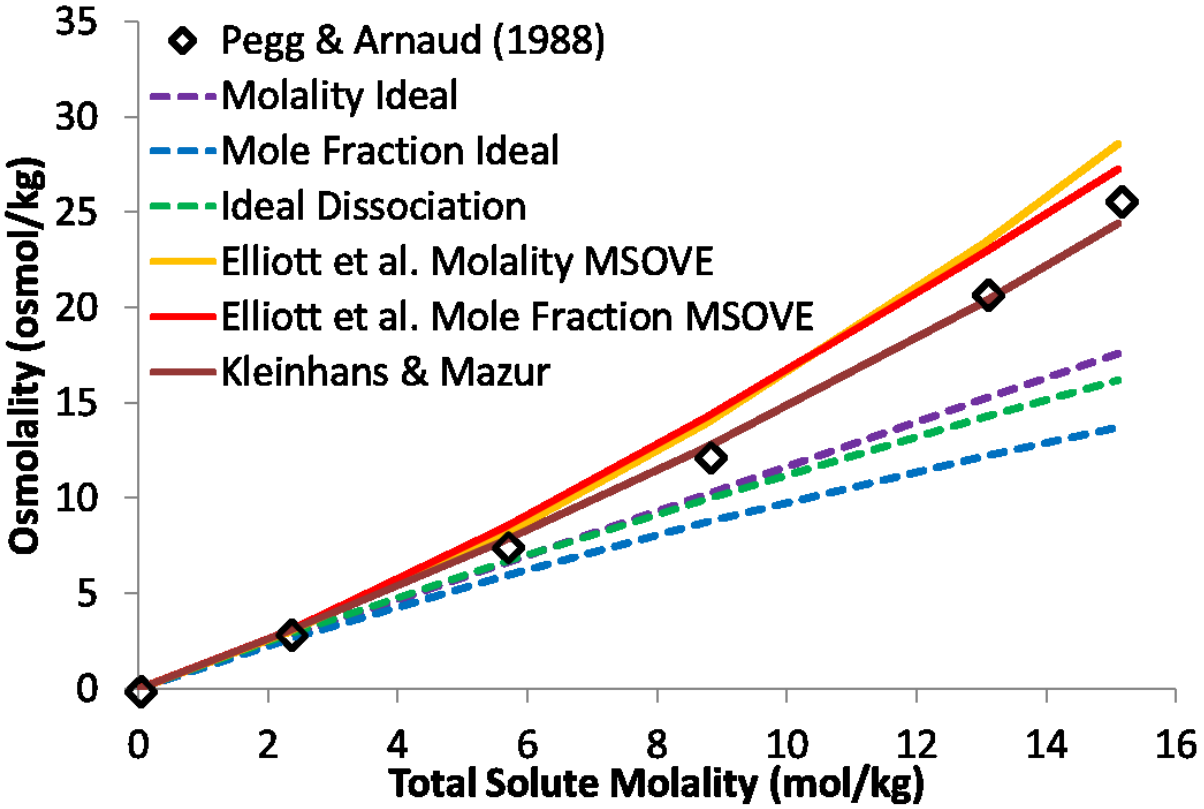


Figure 2.10. Experimental isopleth and model predictions for the solution system glycerol + NaCl + PG, at a solute mass ratio of glycerol:PG:NaCl ≈ 5:4:2. Data are from Pegg and Arnaud [100].

# Chapter 3. A non-ideal solute chemical potential equation and the validity of the grouped solute approach for intracellular solution thermodynamics[2]

**Chapter Summary:** The prediction of non-ideal chemical potentials in aqueous solutions is important in fields such as cryobiology, where models of water and solute transport—*i.e.,* osmotic transport—are used to help develop cryopreservation protocols, and where solutions contain many varied solutes and are generally highly concentrated and thus thermodynamically non-ideal. In this work, we further the development of a non-ideal multi-solute solution theory that has found application across a broad range of aqueous systems. This theory is based on the osmotic virial equation and does not depend on multi-solute data. Specifically, we derive herein a novel solute chemical potential equation that is thermodynamically consistent with the existing model, and we establish the validity of a grouped solute model for the intracellular space. With this updated solution theory, it is now possible to model cellular osmotic behaviour in non-ideal solutions containing multiple permeating solutes, such as those commonly encountered by cells during cryopreservation. In addition, because we show here that for the osmotic virial equation the grouped solute approach is mathematically equivalent to treating each solute separately, multi-solute solutions in other applications with fixed solute mass ratios can now be treated rigorously with such a model, even when all the solutes cannot be enumerated.

[2] This chapter, along with Appendices C and D, has been published as M.W. Zielinski, L.E. McGann, J.A. Nychka, J.A.W. Elliott, A Non-Ideal Solute Chemical Potential Equation and the Validity of the Grouped Solute Approach for Intracellular Solution Thermodynamics, J. Phys. Chem. B. 121 (2017) 10443–10456. This work is available at http://pubs.acs.org/articlesonrequest/AOR-38xihDTThrSv82dTdyFp.

### 3.1. Introduction

The modelling of aqueous solution thermodynamics—both water and solute chemical potential—has applications in a number of different fields, including biomolecule separation [67], microdrop concentrating processes [29–31], the study of micelle formation [76,77], and the primary focus of this work: cryopreservation [1,2,12,13,23,27,53,54,60,62,65,66,81,94,115,116, 127,129,137,139,153]. Recently, a form of the multi-solute osmotic virial equation has been demonstrated to have wide-ranging success in predicting water chemical potential in aqueous solutions [1,7,24,27,104–106,118,154,155]. In this work, we address two key theoretical aspects of this practically-important model in the general context of its application to cellular cryopreservation: *i)* we derive a novel and required equation for solute chemical potential that is thermodynamically consistent with the molality-based form of the osmotic virial equation, and *ii)* we provide a proof that the "grouped solute" modelling approach, practically necessary to model the cellular cytoplasm, is mathematically rigorous.

Cryopreservation refers to the storage of cells and tissues at low sub-zero temperatures. It offers a means of banking these biological materials for later use in transplantation and research. However, not all cell types and very few tissues can be successfully cryopreserved, due to damage—*i.e.,* cryoinjury—that occurs on cooling and/or warming [63,98,147]. The development of successful cryopreservation protocols hinges on understanding and minimizing this damage. During cryopreservation, differences in chemical potential caused by changing external conditions (*e.g.,* ice formation in the bulk solution) drive the passive transport of water and any permeating solutes through tissues and into and out of cells [1,27,53,54,65,66,139]. Collectively known as the osmotic response, these transport processes ultimately govern important mechanisms of cryoinjury. For example, in cells, the rate at which cooling occurs once ice starts to form in the

suspending solution has a profound effect on survival which is directly linked to the osmotic response [83]: due to the low solubility in ice of most solutes [124], low cooling rates expose cells to damagingly high solute concentrations for extended periods of time [83,91], whereas high cooling rates—while limiting exposure to concentrated solutions—allow insufficient time for the osmotic response to equilibrate the intra- and extracellular solutions, leading to conditions that promote intracellular ice formation, which is lethal under most conditions [82,83,91]. The addition of cryoprotective agents such as dimethyl sulphoxide to the extracellular solution can at least somewhat lessen this cryoinjury [85,90], but the effectiveness of these chemicals is limited by their toxicity [12,13,28,33,34]. Furthermore, their addition and removal can cause an osmotic response that leads to excessive—and potentially deadly—cell volume excursions [12,13,39,52,64]. In light of the above, mathematical models of osmotic response—which allow the prediction of cell behaviour during cryopreservation—are very useful tools in the development of cryopreservation protocols. However, modelling the osmotic response requires a means of simultaneously calculating solvent (*i.e.,* water) and solute chemical potentials in the complex solutions characteristic of cryobiology—that is, it requires an appropriate and complete thermodynamic solution theory. Herein, we build on existing work [11,24,27,105,106,154] based on the osmotic virial equation [87]—a foundational thermodynamic solution theory with important mathematical properties [7]—to further the development of such a solution theory. The resulting updated model accounts for all required chemical potentials and solution conditions relevant to cryopreservation.

From a thermodynamic perspective, cryobiological solutions can generally be considered non-ideal, on account of their tendency to be—or, as temperatures drop, to become—highly concentrated. Further, they tend to contain many different solutes with varied characteristics (*e.g.,* salts, alcohols, proteins). While an ideal dilute solution assumption can be used to simplify the

thermodynamic modelling of these solutions [39,53,54,60,61,64–66,81,137], it has been shown that ignoring the non-ideality of cryobiological solutions can negatively impact predictions of chemical potential [24,105,106,154]. The alternative is to use a non-ideal solution theory. These models account for solution deviation from thermodynamically ideal behaviour predominantly using empirically-obtained (*i.e.,* curve-fit) coefficients. A number of non-ideal solution theories have been proposed for use in cryobiology and have been demonstrated to accurately model the water chemical potential of multi-solute solutions of cryobiological interest [5,11,24,32,69,95,96, 99,104,105,145,153]. However, most of these models are solution-specific, requiring fitting to multi-solute data [5,32,96,97,100,146]—*i.e.,* every time a new combination of solutes is to be considered, it must first be curve-fit to the corresponding experimental multi-solute phase diagram in order to obtain the required coefficients. Given the extensive variety and number of solutes that are relevant in cryobiology, the myriad ways in which these solutes can be—and are—combined in cryobiological solutions, and the difficulties of measuring multi-solute phase diagrams [69], such solution-specific models are not well-suited for cryobiological solutions in general. Conversely, there are at least two non-ideal multi-solute solution theories that have been proposed for use with cryobiological solutions that do not depend on multi-solute data: the Kleinhans and Mazur freezing point summation model [69] and the Elliott *et al.* form of the multi-solute osmotic virial equation [11,24,27,105,106,154]. Both theories employ solute-specific thermodynamic coefficients to account for non-ideal behaviour, and for both theories these coefficients are obtained by curve-fitting to single solute (*i.e.,* binary) solution osmometric data. We have recently compared the performance of these two non-ideal solution theories in modelling the water chemical potential of several multi-solute solutions relevant to cryobiology, and found that both provide accurate predictions compared to ideal dilute models [154]. However, while the Kleinhans

and Mazur model allows the prediction of water chemical potential, it does not provide a corresponding means of calculating solute chemical potential, a requirement for modelling solute transport [69]. In contrast, the Elliott *et al.* form of the multi-solute osmotic virial equation—although its development has thus far been primarily focused on the chemical potential of water [11,24,105,106,154]—does include equations for both water and solute chemical potential [27]. Moreover, because this solution theory was originally obtained from fundamental thermodynamic theory [24,27], it is possible to derive further equations for solute chemical potential that are thermodynamically consistent with the existing model. The Elliott *et al.* model has been demonstrated to accurately predict experimentally-measured water chemical potentials in a wide variety of cryobiologically-relevant multi-solute aqueous solutions, including bovine serum albumin + ovalbumin [24,105,154], dimethyl sulphoxide + glycerol [24,105,154], dimethyl sulphoxide + NaCl [103,106,154], ethylene glycol + NaCl [154], glycerol + NaCl [103,106,154], methanol + NaCl [154], propylene glycol + NaCl [154], sucrose + NaCl [154], ethylene glycol + sucrose + NaCl [154], and glycerol + propylene glycol + NaCl [154]. Examples of the model's predictions in some of these solutions are contained in Figure 3.1. Note that the model can effectively account for both electrolyte and non-electrolyte solutes. The model's predictions of water chemical potential have also been successfully applied in the modelling of micelle formation in mixed surfactant solutions [76,77]. In light of the need in cryobiology to model the transport of both water and solutes, and in light of its demonstrated accuracy in modelling water chemical potential, the focus of this work will be the Elliott *et al.* model.

In order to model cellular osmotic behaviour, calculations of water and permeating solute chemical potential must be made both inside and outside the cell. In most circumstances, to calculate the chemical potential of a given species in a given solution, non-ideal solution theories

such as the Elliott *et al.* form of the multi-solute osmotic virial equation require knowledge of the concentration of every solute in solution (*e.g.,* see Equations 3.5, 3.6, and 3.8 below). This requirement severely complicates the calculation of intracellular chemical potentials, as—unlike in the extracellular solution—the concentrations of all osmotically-contributing solutes in the cytoplasm are generally not known. It has recently been proposed that this problem can be avoided altogether—at least, when using the Elliott *et al.* model—by modelling the inside of the cell using a "grouped intracellular solute" approach, where, for the purposes of calculating chemical potential, all non-permeating intracellular solutes are treated collectively as a single "grouped" solute (see Figure 3.2) [104]. A similar approach was used by Levin *et al*. with a non-ideal van Laar type solution theory to model the cytoplasm of red blood cells [75]. However, although the grouped intracellular solute approach has been applied in practice with the Elliott *et al.* model [104,118], its theoretical validity has never been addressed.

In this work, we have two distinct but related objectives with the overall goal of adding to the development of the Elliott *et al.* form of the multi-solute osmotic virial equation. The first objective stems from an important gap in the existing model related to the way in which solute concentrations are expressed. Although the Elliott *et al.* model currently includes equations for both water and solute chemical potential in terms of concentration in mole fraction (*i.e.,* moles of solute per total moles of all species) [24,27], in terms of molality (*i.e.,* moles of solute per kg of solvent), the model provides only a water chemical potential equation [24]. The choice of concentration units here is significant: the molality- and mole fraction-based forms of the model are obtained from different starting assumptions [24,27], use different solute-specific thermodynamic coefficients, and have been demonstrated to give different predictions of water chemical potential for the same solution [154,155]. Our earlier work [154] contains a more detailed

comparison of these two forms of the Elliott *et al.* model. A corresponding molality-based solute chemical potential equation has been derived separately [4], but this equation contains only terms up to second order, whereas the existing molality-based water chemical potential equation contains third order terms, an important requirement for certain solutes (*e.g.,* proteins and other macromolecules) [11,105,154]. As such, we derive here a novel molality-based equation for the non-ideal solute chemical potential that is thermodynamically consistent with the existing water chemical potential equation up to third order terms.

The second objective of this work concerns the grouped intracellular solute approach. Specifically, we use a thermodynamic proof to demonstrate that when calculating intracellular chemical potentials with the molality-based Elliott *et al.* form of the multi-solute osmotic virial equation, the grouped intracellular solute approach is theoretically valid—that is, we show this approach is mathematically equivalent to treating each non-permeating intracellular solute separately when calculating chemical potentials.

### 3.2. Current status of the Elliott *et al.* multi-solute osmotic virial equation

The Elliott *et al.* form of the multi-solute osmotic virial equation is based on the (single-solute) osmotic virial equation developed by McMillan and Mayer [87]. This equation of state models water chemical potential as a polynomial expansion in terms of solute concentration. For example, expressed in terms of concentration in molality, the osmotic virial equation is [24,87]

$$\pi = m_i + B_{ii}{m_i}^2 + C_{iii}{m_i}^3 + \cdots, \tag{3.1}$$

where $\pi$ is omolality (in osmoles/kg of water), $m_i$ is the molality of solute $i$, and $B_{ii}$ and $C_{iii}$ are the second and third molality-based osmotic virial coefficients of solute $i$, respectively (in [moles

of solute/kg of water]$^{-1}$ and [moles of solute/kg of water]$^{-2}$, respectively). Similarly, in terms of concentration in mole fraction, the osmotic virial equation is [87,105]

$$\pi = \frac{1}{M_1}[x_i + B_{ii}^{+}{x_i}^2 + C_{iii}^{+}{x_i}^3 + \cdots,] \tag{3.2}$$

where $x_i$ is the mole fraction of solute *i*, $M_1$ is the molar mass of water (in kg/mole), and $B_{ii}^{+}$ and $C_{iii}^{+}$ are the second and third mole fraction-based osmotic virial coefficients of solute *i*, respectively (unitless). Osmolality is the composition dependence of water chemical potential; the two properties are related by [24]

$$\pi = -\frac{\mu_1 - \mu_1^o}{RTM_1}, \tag{3.3}$$

where $\mu_1$ is the chemical potential of water (in J/mole), $\mu_1^o$ is the chemical potential of pure water (in J/mole), $R$ is the universal gas constant (in J/[mole K]), and $T$ is absolute temperature (in kelvin). Note that the subscript "1" is generally reserved for the solvent—in this case, water.

The osmotic virial coefficients ($B_{ii}$, $C_{iii}$, … or $B_{ii}^{+}$, $C_{iii}^{+}$, …) are important elements of the osmotic virial equation—and of solution theories based on it, such as the Elliott *et al.* model. These solute-specific thermodynamic parameters account for interactions between solute molecules: $B_{ii}$ (or $B_{ii}^{+}$) represents interactions between two molecules of solute *i*, $C_{iii}$ (or $C_{iii}^{+}$) represents interactions between three molecules of solute *i*, and so on. As a key assumption under the ideal dilute model is that there are no interactions between solute molecules in solution, these coefficients essentially represent the non-ideality of the solute: if they are all zero, then solute *i* is thermodynamically ideal. The osmotic virial coefficients for a given solute—and for a chosen unit of concentration—can be obtained by curve-fitting the appropriate osmotic virial equation to osmometric (*i.e.,* osmolality versus concentration) data for a binary (*i.e.,* single-solute) aqueous solution containing that solute (for example, see [154]).

For solutions containing multiple solutes, the single-solute osmotic virial equation can be extended through the use of osmotic virial cross-coefficients [24]. Using the molality-based osmotic virial equation (Equation 3.1) as an example, for a solution containing some number ($r$ – 1) of solutes, we can write

$$\pi = \sum_{i=2}^{r} m_i + \sum_{i=2}^{r}\sum_{j=2}^{r} B_{ij} m_i m_j + \sum_{i=2}^{r}\sum_{j=2}^{r}\sum_{k=2}^{r} C_{ijk} m_i m_j m_k + \cdots, \tag{3.4}$$

where $B_{ij}$, $C_{ijk}$, … are cross-coefficients—$B_{ij}$ represents interactions between a molecule of solute $i$ and a molecule of solute $j$; $C_{ijk}$ represents interactions between a molecule of solute $i$, a molecule of solute $j$, and a molecule of solute $k$; and so forth. However, unlike the single-solute coefficients in Equations 3.1 and 3.2, curve-fitting for these osmotic virial cross-coefficients requires multi-solute osmometric data, which, as discussed above, is undesirable. Alternatively, the cross-coefficients can be replaced using thermodynamic combining rules—that is, theoretical relationships between single-solute coefficients and cross-coefficients that allow the former to be used to predict the values of the latter. The Elliott *et al.* form of the osmotic virial equation essentially extends McMillan and Mayer's original model by proposing a specific set of combining rules for the second and third order coefficients.

Initially, the Elliott *et al.* model was derived in terms of concentration in mole fraction [24,27], based on the regular solution theory definition of Gibbs free energy [102]. For a pair of solutes "*i*" and "*j*", this mole fraction-based model consists of an osmolality equation

$$\pi = \frac{1}{M_1}\left[x_i + x_j + B_{ii}^{+} {x_i}^2 + B_{jj}^{+} {x_j}^2 + \left(B_{ii}^{+} + B_{jj}^{+}\right) x_i x_j\right], \tag{3.5}$$

and a solute chemical potential equation (*e.g.,* for solute *i*)

$$\mu_i = \psi_i^+ + RT\left[\ln(x_i) + \left(\frac{1}{2} - B_{ii}^+\right)(1 - x_i - x_j)(1 - x_i) - \left(\frac{1}{2} - B_{jj}^+\right)(1 - x_i - x_j)x_j\right], \tag{3.6}$$

where $\mu_i$ is the chemical potential of solute *i* (in J/mole) and $\psi_i^+$ is a concentration-independent function of temperature and pressure related to the standard state of solute *i* (in J/mole). In this case, the second order combining rule proposed by Elliott *et al.* is

$$B_{ij}^+ = \frac{B_{ii}^+ + B_{jj}^+}{2}. \tag{3.7}$$

It may be noted that the combining rule in Equation 3.7 appears to be what Guggenheim once called the "naïve assumption" [46,102], which has been demonstrated to not agree with experimental measurements of gaseous mixtures [46,102]. However, for liquid—and especially aqueous—solutions, which are the focus in this work, Equation 3.7 has been demonstrated to agree closely with experimental measurements [24,105,106,154,155] (see also Figure 3.1). Furthermore, for models of liquid solutions such as the osmotic virial equation, Equation 3.7 does not suffer from the same theoretical problem—*i.e.,* producing a mixing rule with a linear dependence on composition—as it does for models of gas mixtures, because—unlike the gas models—these liquid solution models do not provide coefficients to account for solvent interactions (for further details, see Appendix C).

With Equations 3.5 and 3.6, one can calculate the non-ideal chemical potentials of both water and permeating solutes in multi-solute solutions, as is required for osmotic modelling. However, a key *a priori* assumption made by the regular solution theory used in obtaining Equations 3.5 and 3.6—that is, that solute concentrations should be expressed in terms of mole fraction [102]—is not the only approach to concentration units. In Landau and Lifshitz solution theory [73], solute concentrations are instead expressed in terms of molality. Although they appear

similar, molality (*i.e.,* moles of solute per kg of solvent) and mole fraction (*i.e.,* moles of solute per total moles of all species) are in practice quite different, particularly from the perspective of multi-solute solution thermodynamics. With molality, a solute's concentration depends solely on the amount of that solute and on the amount of the solvent present in solution. With mole fraction, the solute's concentration also depends on the amount of every other solute present in solution. In multi-solute solution thermodynamics, where taking partial derivatives and integrals is common, this distinction becomes very important. Based on the Landau and Lifshitz solution theory, Equation 3.5 was rewritten in terms of concentration in molality, generalized to any number of solutes, and extended to third order [24], giving the following equation for the osmolality of a solution containing ($r$ – 1) solutes

$$\pi = \sum_{i=2}^{r} m_i + \sum_{i=2}^{r}\sum_{j=2}^{r}\left[\frac{\left(B_{ii}+B_{jj}\right)}{2} m_i m_j\right] + \sum_{i=2}^{r}\sum_{j=2}^{r}\sum_{k=2}^{r}\left[\left(C_{iii}C_{jjj}C_{kkk}\right)^{1/3} m_i m_j m_k\right]. \quad (3.8)$$

In this case, the proposed (molality-based) combining rules are

$$B_{ij} = \frac{B_{ii}+B_{jj}}{2} \quad (3.9)$$

and

$$C_{ijk} = \left(C_{iii}C_{jjj}C_{kkk}\right)^{1/3}. \quad (3.10)$$

Equation 3.8 has been demonstrated to provide accurate predictions of osmolality in a variety of cryobiologically-relevant multi-solute solutions [154]. Some examples of its effectiveness in predicting solution osmolality are contained in Figure 3.1. These examples show that this non-ideal model, which depends only on coefficients obtained from binary solution data, can be used to make predictions in multi-solute aqueous solutions containing proteins (*e.g.,* bovine serum albumin + ovalbumin), cryoprotectants (*e.g.,* dimethyl sulphoxide + glycerol), and/or electrolytes (*e.g.,* dimethyl sulphoxide + NaCl). Note that for electrolyte solutes, a slightly different form of

the equation is required (see Equation 3.33 below). However, Equation 3.8 was obtained without explicit derivation, and no corresponding solute chemical potential equation was provided.

Before continuing, it would be useful to make note of an important principle in solution thermodynamics that is referred to repeatedly in this work: thermodynamic consistency. Any set of equations making up a solution theory (*i.e.,* those equations used to simultaneously calculate solvent and solute chemical potentials) must be thermodynamically consistent—that is, the equations must collectively obey the Gibbs–Duhem equation. At constant temperature and pressure, this equation is [102]

$$N_1 d\mu_1 + N_2 d\mu_2 + N_3 d\mu_3 + \cdots = \sum_{i=1} N_i d\mu_i = 0, \tag{3.11}$$

where $N_i$ is the number moles of species *i* and $\mu_i$ is the chemical potential of *i*. If the equations of a solution theory do not satisfy the Gibbs–Duhem equation, then that solution theory cannot be correct. It should be noted that if Equation 3.11 is applied to the mole-fraction based form of the Elliott *et al.* model as written above—that is, to Equations 3.5 and 3.6—these two equations do not immediately appear to be thermodynamically consistent. This situation arises because in the derivation of Equation 3.5, a natural logarithm term was expanded and the resultant polynomial was truncated after second order terms, whereas in the derivation of Equation 3.6, no such approximation was made [25]. However, the precursors to these equations (*i.e.,* before the expansion of the natural logarithm) can be demonstrated to satisfy Equation 3.11 and are thus thermodynamically consistent [25]. Further, a thermodynamically consistent set of equations for osmolality and solute chemical potential can be obtained for a *single*-solute solution by directly using the Gibbs–Duhem equation (*i.e.,* Equation 3.11). Essentially, starting with the single solute mole fraction-based osmolality equation—Equation 3.2—one applies the Gibbs–Duhem equation in a manner analogous to that carried out below in Equations 3.15 to 3.18 for a molality-based set

of equations. Such a derivation ultimately yields the following equation for solute chemical potential

$$\mu_i = \psi_i^+ + RT\left(\ln x_i + [2B_{ii}^+ - 1]x_i - B_{ii}^+ {x_i}^2 + C_{iii}^+ {x_i}^2\left[\frac{3}{2} - x_i\right] + \cdots\right) \tag{3.12}$$

While this approach works for the single-solute system, the multi-solute derivation is more complex and requires the truncation made in obtaining Equations 3.5 and 3.6 [25].

In order to have a complete molality-based multi-solute osmotic virial equation, an equation for solute chemical potential that is thermodynamically consistent with Equation 3.8 is required. The existing mole fraction-based solute chemical potential equation (*i.e.,* Equation 3.6) cannot simply be rewritten in terms of molality as the mole fraction-based osmolality equation can be, as this process will not yield a thermodynamically consistent result. Previously, Benson [4] showed that starting from the Landau and Lifshitz definition of Gibbs free energy [73] and using the second order combining rule proposed by the Elliott *et al.* model (*i.e.,* Equation 3.9), one can derive corresponding molality-based water and solute chemical potential equations. However, these equations contain only up to second order terms (*i.e.,* $B_{ij}$), whereas Equation 3.8 contains third order terms (*i.e.,* $C_{ijk}$), and has been shown to provide accurate predictions in solutions containing solutes where those third order terms are required (*i.e.,* proteins) [154]. Thus, to complete the existing Elliott *et al.* model, we describe below the derivation and Gibbs–Duhem verification of a molality-based solute chemical potential equation that it is thermodynamically consistent with Equation 3.8 up to third order.

### 3.3. Derivation of molality-based solute chemical potential equation

The definition of chemical potential is

$$\mu_i = \left(\frac{\partial G}{\partial N_i}\right)_{T,P,N_{j\neq i}}, \tag{3.13}$$

where $G$ is the Gibbs free energy (in joules), $P$ is pressure, and the subscripts outside the brackets indicate that temperature, pressure, and the number of moles of all components other than $i$ are held constant during the differentiation. Given a model for Gibbs free energy, one can use this definition to derive chemical potential equations for any species of interest. As noted above, Equation 3.8 was obtained based on Landau and Lifshitz solution theory. According to this solution theory, for ($r$ – 1) solutes, Gibbs free energy is defined as [73]

$$G = N_1\mu_1^o + \sum_{i=2}^{r} N_i\psi_i + RT\sum_{i=2}^{r} N_i \ln\left(\frac{N_i}{N_1}\right) + \frac{1}{2}\sum_{i=2}^{r}\sum_{j=2}^{r}\left[\beta_{ij}\left(\frac{N_iN_j}{N_1}\right)\right], \tag{3.14}$$

where $\psi_i$ is a concentration-independent function of temperature and pressure specific to solute $i$ and $\beta_{ij}$ is a concentration-independent function of temperature and pressure specific to solutes $i$ and $j$. However, recall that Equation 3.8 was not explicitly derived from the Landau and Lifshitz definition of Gibbs free energy (*i.e.,* Equation 3.14)—rather, the mole fraction-based Equation 3.5 was rewritten in terms of molality [24]. Furthermore, Equation 3.14 contains only up to second order terms, whereas Equation 3.8 contains third order terms. Thus, it is apparent that the Landau and Lifshitz definition of Gibbs free energy as defined in Equation 3.14 does not actually give rise to the third order Equation 3.8 (indeed, as mentioned above, previous work by Benson [4] has shown that chemical potential equations of only second order can be obtained from Equation 3.14). As such, in order to derive a solute chemical potential equation that is thermodynamically consistent with Equation 3.8 to third order, we must first determine the form of the Gibbs free energy that does in fact give rise to Equation 3.8. We can subsequently use this Gibbs free energy equation along with Equation 3.13 to derive the desired solute chemical potential equation, and

then use the Gibbs–Duhem equation to verify that this new solute chemical potential equation is indeed thermodynamically consistent with Equation 3.8.

### *3.3.1. Use of the Gibbs–Duhem equation to derive unknown chemical potentials*

To find the required form of Gibbs free energy, we can use the Gibbs–Duhem equation (*i.e.,* Equation 3.11) itself. In fact, because it defines thermodynamic consistency, the Gibbs–Duhem equation is commonly used to derive unknown chemical potential equations for some components from known chemical potential equations for other components in the solution. Several groups have previously used the Gibbs–Duhem equation with various forms of the osmotic virial equation to develop complete thermodynamically consistent solution theories [18,21,42,50,141]. For example, Edmond and Ogston developed a second order molality-based model for ternary systems, starting with a solute equation and deriving a solvent equation through the Gibbs–Duhem relation [21]. This model was later extended to third order [50]. Solution models incorporating the molarity-based [18,42] and weight fraction-based [141] forms of the osmotic virial equation have also been developed using the Gibbs–Duhem equation.

### *3.3.2. Determination of required Gibbs free energy equation*

Here, we will use the Gibbs–Duhem equation to derive the Gibbs free energy that gives rise to Equation 3.8. To start, consider a binary aqueous solution containing a single solute "2"; for this solution, the Gibbs–Duhem equation at constant temperature and pressure is:

$$N_1 d\mu_1 + N_2 d\mu_2 = 0\,. \tag{3.15}$$

Converting to molality (using $m_2 = N_2/M_1 N_1$) and rearranging yields

$$\frac{d\mu_2}{dm_2} = -\frac{1}{M_1 m_2}\frac{d\mu_1}{dm_2}. \tag{3.16}$$

Truncating Equation 3.1 after third order terms, substituting into Equation 3.3, and rearranging gives

$$\mu_1 = \mu_1^o - RTM_1[m_2 + B_{22}{m_2}^2 + C_{222}{m_2}^3]\,. \tag{3.17}$$

Substituting Equation 3.17 into Equation 3.16, integrating and simplifying yields

$$\mu_2 = RT\left[\ln(M_1 m_2) + 2B_{22}m_2 + \frac{3}{2}C_{222}{m_2}^2\right] + \theta_2\,, \tag{3.18}$$

where $\theta_2$ is a concentration-independent integration constant specific to solute 2. Note that the molar mass of water ($M_1$) in Equation 3.18 was intentionally added to the equation in order to render the term within the natural logarithm (*i.e.,* $M_1 m_2$) unitless. This addition was accomplished by adding $RT\ln(M_1) - RT\ln(M_1) = 0$ to the right-hand side of the precursor of Equation 3.18—the positive $RT\ln(M_1)$ became a part of the natural logarithm that appears in Equation 3.18, while the negative $RT\ln(M_1)$ (a constant value at constant temperature) was absorbed into the integration constant $\theta_2$. By definition, the Gibbs free energy for this system is

$$G = N_1\mu_1 + N_2\mu_2\,. \tag{3.19}$$

Substituting Equations 3.17 and 3.18 into Equation 3.19 and converting to moles gives

$$G = N_1\mu_1^o + N_2\psi_2 + RTN_2\ln\left(\frac{N_2}{N_1}\right) + \frac{RT}{M_1}B_{22}\frac{{N_2}^2}{N_1} + \frac{1}{2}\frac{RT}{{M_1}^2}C_{222}\frac{{N_2}^3}{{N_1}^2}\,, \tag{3.20}$$

where $\psi_2 = \theta_2 - RT\ln M_1 - RT$ is a concentration-independent function of temperature and pressure specific to solute 2. Note that up to second order, Equation 3.20 is very similar to the Landau and Lifshitz definition of Gibbs free energy (Equation 3.14), and is, in fact, the same up to second order if we take $\frac{1}{2}\beta_{ij} = \frac{RT}{M_1}B_{ij}$. Based on this result, we propose that the following model of Gibbs free energy gives rise to Equation 3.8

$$G = N_1\mu_1^o + \sum_{i=2}^{r} N_i\psi_i + RT\sum_{i=2}^{r} N_i\, ln\left(\frac{N_i}{N_1}\right) + \frac{RT}{M_1}\sum_{i=2}^{r}\sum_{j=2}^{r}\left[B_{ij}\left(\frac{N_iN_j}{N_1}\right)\right] + \frac{1}{2}\frac{RT}{{M_1}^2}\sum_{i=2}^{r}\sum_{j=2}^{r}\sum_{k=2}^{r}\left[C_{ijk}\left(\frac{N_iN_jN_k}{{N_1}^2}\right)\right], \quad (3.21)$$

where the form of the added third-order term (*i.e.,* the one containing $C_{ijk}$) is based on the third-order term in Equation 3.20. We can verify the above hypothesis using the mathematical definition of chemical potential (*i.e.,* Equation 3.13). Substituting Equation 3.21 into Equation 3.13 for water (*i.e.,* $\mu_1$), evaluating the derivatives, simplifying, converting moles to molality, and using Equation 3.3 to relate chemical potential to osmolality gives

$$\pi = \sum_{i=2}^{r} m_i + \sum_{i=2}^{r}\sum_{j=2}^{r}\left[B_{ij}m_im_j\right] + \sum_{i=2}^{r}\sum_{j=2}^{r}\sum_{k=2}^{r}\left[C_{ijk}m_im_jm_k\right]. \quad (3.22)$$

Comparing Equation 3.22 to Equation 3.8, it can be seen that the two equations are identical if the Elliott *et al.* combining rules (*i.e.,* Equations 3.9 and 3.10) are applied. Therefore, Equation 3.21 is the model of Gibbs free energy that gives rise to Equation 3.8. We can thus use Equation 3.21 to derive a solute chemical potential equation that is thermodynamically consistent with Equation 3.8.

### *3.3.3. Derivation of non-ideal solute chemical potential equation*

Consider a single permeating solute "*s*" in a multi-solute solution. Substituting Equation 3.21 into Equation 3.13 for solute *s*, evaluating the derivative, simplifying, and rewriting in terms of molality gives

$$\mu_s = \theta_s + RT\left[\ln(M_1 m_s) + 2\sum_{i=2}^{r}[B_{is}m_i] + \frac{3}{2}\sum_{i=2}^{r}\sum_{j=2}^{r}[C_{ijs}m_i m_j]\right], \tag{3.23}$$

where $\theta_s$ is a concentration-independent function of temperature and pressure specific to solute *s*. Substituting the combining rules proposed by Elliott *et al.* (*i.e.,* Equations 3.9 and 3.10) into Equation 3.23 yields the following equation for solute chemical potential

$$\mu_s = \theta_s + RT\left[\ln(M_1 m_s) + \sum_{i=2}^{r}[(B_{ii} + B_{ss})m_i] + \frac{3}{2}\sum_{i=2}^{r}\sum_{j=2}^{r}\left[\left(C_{iii}C_{jjj}C_{sss}\right)^{1/3} m_i m_j\right]\right]. \tag{3.24}$$

Note that the above proof is independent of the combining rules used—that is, Equations 3.22 and 3.23 form a more general solution theory (which does not employ any combining rules) from which Equations 3.8 and 3.24 are obtained by substituting in the Elliott *et al.* combining rules. Other solution theories could be obtained by substituting different combining rules into Equations 3.22 and 3.23. Because of this relationship, if Equations 3.22 and 3.23 can be shown to be thermodynamically consistent, then Equations 3.8 and 3.24 must also be thermodynamically consistent—as must any other solution theory obtained by applying combining rules to Equations 3.22 and 3.23.

### *3.3.4. Verification of new non-ideal solute chemical potential equation*

To show that Equation 3.23 is thermodynamically consistent with Equation 3.22, we consider an aqueous solution containing some number ($r - 1$) of solutes, including the solute "2"—chosen arbitrarily as we must have a single solute with respect to which we can differentiate. For this solution, the Gibbs–Duhem equation at constant temperature and pressure is

$$N_1 d\mu_1 + N_2 d\mu_2 + \sum_{i=3}^{r} N_i d\mu_i = 0\,. \tag{3.25}$$

Converting to molality, writing out the exact differentials of all terms at constant $m_{x\neq 2}$, and simplifying gives

$$\frac{1}{M_1}\left(\frac{\partial \mu_1}{\partial m_2}\right)_{m_{x\neq 2}} + m_2\left(\frac{\partial \mu_2}{\partial m_2}\right)_{m_{x\neq 2}} + \sum_{i=3}^{r} m_i\left(\frac{\partial \mu_i}{\partial m_2}\right)_{m_{x\neq 2}} = 0\,. \tag{3.26}$$

Rewriting Equation 3.22 in terms of water chemical potential such that solute "2" is considered separately yields

$$\begin{aligned}\mu_1 = \mu_1^o - RTM_1\Bigg[m_2 + \sum_{i=3}^{r} m_i + B_{22}{m_2}^2 + 2\sum_{i=3}^{r}[B_{2i}m_2 m_i] \\ + \sum_{i=3}^{r}\sum_{j=3}^{r}\left[B_{ij}m_i m_j\right] + C_{222}{m_2}^3 + 3\sum_{i=3}^{r}[C_{22i}{m_2}^2 m_i] \\ + 3\sum_{i=3}^{r}\sum_{j=3}^{r}\left[C_{2ij}m_2 m_i m_j\right] + \sum_{i=3}^{r}\sum_{j=3}^{r}\sum_{k=3}^{r}\left[C_{ijk}m_i m_j m_k\right]\Bigg].\end{aligned} \tag{3.27}$$

Rewriting Equation 3.23 for solute "2" such that solute "2" is considered separately gives

$$\begin{aligned}\mu_2 = \theta_2 + RT\Bigg[\ln(M_1 m_2) + 2B_{22}m_2 + \frac{3}{2}C_{222}{m_2}^2 + 2\sum_{i=3}^{r}[B_{2i}m_i] \\ +3\sum_{i=3}^{r}[C_{22i}m_2 m_i] + \frac{3}{2}\sum_{i=3}^{r}\sum_{i=3}^{r}\left[C_{2ij}m_i m_j\right]\Bigg].\end{aligned} \tag{3.28}$$

Rewriting Equation 3.23 for each other solute "*i*" such that solute "2" is considered separately gives

$$\mu_i = \theta_i + RT\left[\ln(M_1 m_i) + 2B_{2i}m_2 + 2\sum_{j=3}^{r}\left[B_{ij}m_j\right] + \frac{3}{2}C_{22i}{m_2}^2 + 3\sum_{j=3}^{r}\left[C_{2ij}m_2 m_j\right] + \frac{3}{2}\sum_{j=3}^{r}\sum_{k=3}^{r}\left[C_{ijk}m_j m_k\right]\right]. \quad (3.29)$$

Taking the derivatives of Equations 3.27, 3.28, and 3.29 with respect to $m_2$ yields

$$\left(\frac{\partial \mu_1}{\partial m_2}\right)_{m_{x\neq 2}} = -RTM_1\left[1 + 2B_{22}m_2 + 2\sum_{i=3}^{r}[B_{2i}m_i] + 3C_{222}{m_2}^2 + 6\sum_{i=3}^{r}[C_{22i}m_2 m_i] + 3\sum_{i=3}^{r}\sum_{j=3}^{r}\left[C_{2ij}m_i m_j\right]\right], \quad (3.30)$$

$$\left(\frac{\partial \mu_2}{\partial m_2}\right)_{m_{x\neq 2}} = RT\left[\frac{1}{m_2} + 2B_{22} + 3C_{222}m_2 + 3\sum_{i=3}^{r}[C_{22i}m_i]\right], \quad (3.31)$$

and

$$\left(\frac{\partial \mu_i}{\partial m_2}\right)_{m_{x\neq 2}} = RT\left[2B_{2i} + 3C_{22i}m_2 + 3\sum_{j=3}^{r}\left[C_{2ij}m_j\right]\right], \quad (3.32)$$

respectively. When Equations 3.30, 3.31, and 3.32 are substituted into Equation 3.26, all terms on the left-hand side of Equation 3.26 cancel, making the equation true. Therefore, up to third order terms, Equation 3.23 is thermodynamically consistent with Equation 3.22, and, correspondingly, Equation 3.24 is thermodynamically consistent with Equation 3.8.

### *3.3.5. Addendum: for solutes which dissociate in solution (i.e., electrolytes)*

Here, we briefly extend the above derivation and verification of a solute chemical potential equation to a special case in the Elliott *et al.* model: electrolyte solutes (*i.e.,* salts). For electrolyte

solutes, an additional fitting parameter must be added to the osmotic virial equation: the dissociation constant [105,106]. This parameter is multiplied onto each molality term of its corresponding solute. It should be noted that when dealing with electrolyte solutes here, the molality to be considered and used in all calculations is the molality of the salt itself (*e.g.,* the number of moles of NaCl per kg of water).

For electrolyte solutes, the dissociation constant empirically accounts for all electrolyte effects. For non-electrolyte solutes, this term can be considered as effectively having a value of one. If we consider a solution where every solute is (potentially) an electrolyte, Equation 3.8 becomes [105,106]

$$\pi = \sum_{i=2}^{r} k_i m_i + \sum_{i=2}^{r}\sum_{j=2}^{r}\left[\frac{\left(B_{ii}+B_{jj}\right)}{2} k_i m_i k_j m_j\right] + \sum_{i=2}^{r}\sum_{j=2}^{r}\sum_{k=2}^{r}\left[\left(C_{iii}C_{jjj}C_{kkk}\right)^{1/3} k_i m_i k_j m_j k_k m_k\right] + \cdots, \tag{3.33}$$

where $k_i$ is the dissociation constant of solute *i*. This approach of using a dissociation constant to account for electrolyte solutes has been demonstrated by Prickett *et al.* to be at least as accurate in predicting experimental results as the more complex Pitzer–Debye–Huckel approach [106].

Starting with Equation 3.33 (instead of Equation 3.8) and following the same procedure as that used above for non-electrolyte solutes yields the following equation for solute chemical potential

$$\mu_s = k_s\theta_s + RTk_s\left[\ln(M_1 m_s) + \sum_{i=2}^{r}[(B_{ii} + B_{ss})k_i m_i] + \frac{3}{2}\sum_{i=2}^{r}\sum_{j=2}^{r}\left[\left(C_{iii}C_{jjj}C_{sss}\right)^{1/3}k_i m_i k_j m_j\right]\right]. \quad (3.34)$$

Note that if all of the solutes are non-electrolytes (*i.e.,* $k_i = 1$ for all *i*), Equation 3.34 simplifies to Equation 3.24. As with Equations 3.8 and 3.24, Equations 3.33 and 3.34 can also be shown to be thermodynamically consistent.

### 3.4. Thermodynamic proof of grouped intracellular solute validity

Now that we have a complete molality-based non-ideal solution theory (*i.e.,* Equations 3.8 and 3.24), we can determine whether or not the grouped intracellular solute approach is theoretically valid when using this solution theory. To begin, we explicitly define the grouped intracellular solute approach. Recall that this model states that for thermodynamic purposes, all non-permeating intracellular solutes can be considered as a single non-permeating intracellular "grouped" solute without affecting the outcomes of chemical potential calculations. Thus, in all thermodynamic considerations (*i.e.,* calculations and system definitions), the grouped intracellular solute represents all of the actual non-permeating solutes inside the cell. Furthermore, although it is important to remember that the grouped intracellular solute is a theoretical construction and not a "real" solute, in all thermodynamic considerations, the osmotic virial equation applies to the grouped intracellular solute as it would to any real solute—that is, the grouped intracellular solute has its own osmotic virial coefficients. Finally, the number of moles of the grouped intracellular

solute in solution is equal to the sum of the number of moles of each of the actual non-permeating solutes in the intracellular solution.

In addition to the grouped intracellular solute approach, we also need to define the alternative approach: that is, treating each non-permeating solute inside the cell separately, as if their concentrations were known. Throughout this work, we will refer to this approach as the "exact" approach. In order to establish that the grouped intracellular solute approach is valid, we need to show that it is mathematically equivalent to the exact approach.

From a thermodynamic modelling perspective, equivalence here means that two conditions must be simultaneously satisfied for *any given intracellular composition*: namely, the two approaches (exact and grouped) must have equal intracellular osmolalities, and—if any permeating solutes are involved—equal intracellular permeating solute chemical potentials. We will start by showing that the grouped intracellular solute approach is valid in the case of a cell that is in the presence of only non-permeating solutes (Figure 3.3a)—in this case, since there are no permeating solutes involved, we must satisfy only the first condition. Keeping this initial proof in mind, we will then show that the grouped intracellular solute approach is valid in the case of a cell that is in the presence of any number of non-permeating solutes and any number of permeating solutes (Figure 3.3b)—in this case, we must simultaneously satisfy both of the above conditions.

### *3.4.1. Considering a cell in the absence of permeating solutes*

Consider an aqueous intracellular solution containing $(n - 1)$ non-ideal non-permeating solutes, where $n$ is any number greater than 1, and no permeating solutes. For this system, the number of moles of each solute in the solution is fixed, since all solutes are non-permeating (and therefore cannot move into or out of the intracellular solution), while the number of moles of water

(*i.e.,* the solvent) in the solution is variable (since water can move freely across the cell membrane and thus into and out of the intracellular solution). Let the osmolality (*i.e.,* water chemical potential) be defined by Equation 3.8, such that

$$\pi^{exact} = \sum_{i=2}^{n} m_i + \sum_{i=2}^{n}\sum_{j=2}^{n}\left[\frac{\left(B_{ii} + B_{jj}\right)}{2} m_i m_j\right] + \sum_{i=2}^{n}\sum_{j=2}^{n}\sum_{k=2}^{n}\left[\left(C_{iii}C_{jjj}C_{kkk}\right)^{1/3} m_i m_j m_k\right] \tag{3.35}$$

and

$$\pi^{grouped} = m_g + B_{gg}{m_g}^2 + C_{ggg}{m_g}^3 , \tag{3.36}$$

where $m_g$ is the molality of the grouped intracellular solute $g$, and $B_{gg}$ and $C_{ggg}$ are the second and third osmotic virial coefficients of the grouped intracellular solute $g$. Given that the number of moles of each solute in solution is fixed in this case, the grouped intracellular solute approach will be equivalent to the exact approach if

$$\pi^{exact} = \pi^{grouped} \tag{3.37}$$

for any number of moles of water present in solution.

Since the number of moles of each solute is fixed, the ratios of their concentrations are constant—that is, the ratio of the concentration of any given solute to the concentration of any other solute is constant, for all solutes. Therefore, we can choose one solute—for example, solute "2"—and express the concentrations of all other solutes in terms of the concentration of that solute, *i.e.,*

$$m_i = R_i m_2 , \tag{3.38}$$

where $R_i$ is the ratio of the molality of solute $i$ to that of solute 2 (and is constant).

By definition, because solute $g$ is a grouped intracellular solute, its molality is the sum of the molalities of all the solutes which it represents. Therefore, we can write

$$m_g = \sum_{i=2}^{n} m_i = \left( \sum_{i=2}^{n} R_i \right) m_2 \,. \tag{3.39}$$

Substituting Equations 3.35, 3.36, 3.38, and 3.39 into Equation 3.37 and simplifying gives

$$\begin{aligned} &\sum_{i=2}^{n}\sum_{j=2}^{n}\left[\frac{\left(B_{ii}+B_{jj}\right)}{2}R_iR_j\right] + \sum_{i=2}^{n}\sum_{j=2}^{n}\sum_{k=2}^{n}\left[\left(C_{iii}C_{jjj}C_{kkk}\right)^{1/3}R_iR_jR_k\right]m_2 \\ &\qquad = B_{gg}\left(\sum_{i=2}^{n} R_i\right)^2 + C_{ggg}\left(\sum_{i=2}^{n} R_i\right)^3 m_2 \,. \end{aligned} \tag{3.40}$$

In order to establish the equivalence of the grouped intracellular solute and exact approaches, we must show that Equation 3.40 is true.

Before continuing on, there are a few important points of which to make note regarding the terms in Equation 3.40. First, according to our definition of the system, all of the osmotic virial coefficients ($B_{ii}$, $C_{iii}$) of all the real solutes in solution (*i.e.,* not the grouped intracellular solute) must be constant, as per the definition of the osmotic virial equation. The concentration ratios $\vec{R}_i$ of all the solutes are also constant because the number of moles of each solute in solution is fixed. The molality of solute 2, $m_2$, is variable because $m_2$ depends on the number of moles of water in solution, which is not fixed—in fact, it is the only variable in the system. Finally, the osmotic virial coefficients of the grouped intracellular solute $g$ (*i.e.,* $B_{gg}$ and $C_{ggg}$) are not defined and are unknowns, to be solved for. Note that if the osmotic virial equation is to apply to the grouped intracellular solute $g$ as it would to any real solute in solution, then $B_{gg}$ and $C_{ggg}$ should have unique constant values. Therefore, keeping all of the above points in mind, if we can show that Equation 3.40 is true for any value of $m_2$ such that $B_{gg}$ and $C_{ggg}$ have unique constant values, we

will have satisfied the condition contained in Equation 3.37 for any number of moles of water present in solution, as required.

In fact, if $B_{gg}$ and $C_{ggg}$ are defined as

$$B_{gg} = \sum_{i=2}^{n}\sum_{j=2}^{n}\left[\frac{(B_{ii}+B_{jj})}{2}R_iR_j\right]\Big/\left(\sum_{i=2}^{n}R_i\right)^2 = \text{constant} \tag{3.41}$$

and

$$C_{ggg} = \sum_{i=2}^{n}\sum_{j=2}^{n}\sum_{k=2}^{n}\left[\left(C_{iii}C_{jjj}C_{kkk}\right)^{1/3}R_iR_jR_k\right]\Big/\left(\sum_{i=2}^{n}R_i\right)^3 = \text{constant,} \tag{3.42}$$

then the Equation 3.40 is true for any value of $m_2$. Therefore, in the case of a cell in the absence of any permeating solutes, the grouped intracellular solute approach is equivalent to the exact approach when osmolality is defined by the Equation 3.8. We can now repeat the above proof with permeating solutes present.

### *3.4.2. Considering a cell in the presence of any number of permeating solutes*

Consider an aqueous intracellular solution containing both permeating and non-permeating solutes. Let there be ($n$ – 1) non-ideal non-permeating solutes (2, 3,..., $n$), where $n$ is any number greater than 1. Let there be $q$ non-ideal permeating solutes $\vec{p}$ $(p_1, p_2, \ldots, p_q)$, where $q$ is any number greater than or equal to 1. For this system, the number of moles of each non-permeating solute in solution is fixed, while the number of moles of each permeating solute and the number of moles of water in solution are variable. Let the osmolality be defined by Equation 3.8, such that

$$\pi^{exact} = \sum_{i=2}^{p_q} m_i + \sum_{i=2}^{p_q}\sum_{j=2}^{p_q}\left[\frac{\left(B_{ii} + B_{jj}\right)}{2} m_i m_j\right] + \sum_{i=2}^{p_q}\sum_{j=2}^{p_q}\sum_{k=2}^{p_q}\left[\left(C_{iii}C_{jjj}C_{kkk}\right)^{1/3} m_i m_j m_k\right] \tag{3.43}$$

and

$$\pi^{grouped} = m_g + \sum_{i=p1}^{p_q} m_i + B_{gg}{m_g}^2 + \sum_{i=p1}^{p_q}\left[\left(B_{ii} + B_{gg}\right)m_i m_g\right] + \sum_{i=p1}^{p_q}\sum_{j=p1}^{p_q}\left[\frac{\left(B_{ii} + B_{jj}\right)}{2} m_i m_j\right] + C_{ggg}{m_g}^3 + 3\sum_{i=p1}^{p_q}\left[\left(C_{iii}{C_{ggg}}^2\right)^{\frac{1}{3}} m_i {m_g}^2\right] + 3\sum_{i=p_1}^{p_q}\sum_{j=p_1}^{p_q}\left[\left(C_{iii}C_{jjj}C_{ggg}\right)^{\frac{1}{3}} m_i m_j m_g\right] + \sum_{i=p_1}^{p_q}\sum_{j=p_1}^{p_q}\sum_{k=p_1}^{p_q}\left[\left(C_{iii}C_{jjj}C_{kkk}\right)^{1/3} m_i m_j m_k\right]. \tag{3.44}$$

Let the chemical potentials of all permeating solutes $\vec{p}$ be defined by Equation 3.24, such that for any given permeating solute $p_x$, where $x$ = 1, 2,..., $q$, we can write

$${\mu_{p_x}}^{exact} = \theta_{p_x} + RT\left[\ln\left(M_1 m_{p_x}\right) + \sum_{i=2}^{p_q}\left[\left(B_{ii} + B_{p_x p_x}\right)m_i\right] + \frac{3}{2}\sum_{i=2}^{p_q}\sum_{j=2}^{p_q}\left[\left(C_{iii}C_{jjj}C_{p_x p_x p_x}\right)^{1/3} m_i m_j\right]\right] \tag{3.45}$$

and

$$\mu_{p_x}{}^{grouped} = \theta_{p_x} + RT\left[\ln\left(M_1 m_{p_x}\right) + \left(B_{gg} + B_{p_x p_x}\right)m_g + \sum_{i=p_1}^{p_q}\left[\left(B_{ii} + B_{p_x p_x}\right)m_i\right]\right.$$

$$+\frac{3}{2}\left(C_{ggg}{}^2 C_{p_x p_x p_x}\right)^{\frac{1}{3}} m_g{}^2 + 3\sum_{i=p_1}^{p_q}\left[\left(C_{iii} C_{ggg} C_{p_x p_x p_x}\right)^{\frac{1}{3}} m_i m_g\right] \quad (3.46)$$

$$\left.+\frac{3}{2}\sum_{i=p_1}^{p_q}\sum_{j=p_1}^{p_q}\left[\left(C_{iii} C_{jjj} C_{p_x p_x p_x}\right)^{1/3} m_i m_j\right]\right].$$

Given that the number of moles of each non-permeating solute in solution is fixed in this case, and given that if $\mu^{exact} = \mu^{grouped}$ for *any one given* permeating solute (*e.g.,* permeating solute "$p_x$"), it will be true for *all* permeating solutes $\vec{p}$ (as all permeating solutes follow the same equations, *i.e.,* Equations 3.45 and 3.46), the grouped intracellular solute approach will be equivalent to the exact approach if

$$\pi^{exact} = \pi^{grouped} \quad (3.37)$$

and

$$\mu_{p_x}{}^{exact} = \mu_{p_x}{}^{grouped} \quad (3.47)$$

for any number of moles of water and for any number of moles of each of the permeating solutes $\vec{p}$ present in solution.

To simplify later parts of this proof, we can use the linearity and commutativity of finite sums to rewrite Equations 3.43 and 3.45 such that the non-permeating solutes and permeating solutes are considered as separately as possible, giving

$$\pi^{exact} = \sum_{i=2}^{n} m_i + \sum_{i=p_1}^{p_q} m_i + \sum_{i=2}^{n}\sum_{j=2}^{n}\left[\frac{\left(B_{ii}+B_{jj}\right)}{2} m_i m_j\right] + 2\sum_{i=2}^{n}\sum_{j=p_1}^{p_q}\left[\frac{\left(B_{ii}+B_{jj}\right)}{2} m_i m_j\right] + \sum_{i=p_1}^{p_q}\sum_{j=p_1}^{p_q}\left[\frac{\left(B_{ii}+B_{jj}\right)}{2} m_i m_j\right] + \sum_{i=2}^{n}\sum_{j=2}^{n}\sum_{k=2}^{n}\left[\left(C_{iii}C_{jjj}C_{kkk}\right)^{1/3} m_i m_j m_k\right] + 3\sum_{i=2}^{n}\sum_{j=2}^{n}\sum_{k=p_1}^{p_q}\left[\left(C_{iii}C_{jjj}C_{kkk}\right)^{1/3} m_i m_j m_k\right] + 3\sum_{i=2}^{n}\sum_{j=p_1}^{p_q}\sum_{k=p_1}^{p_q}\left[\left(C_{iii}C_{jjj}C_{kkk}\right)^{1/3} m_i m_j m_k\right] + \sum_{i=p_1}^{p_q}\sum_{j=p_1}^{p_q}\sum_{k=p_1}^{p_q}\left[\left(C_{iii}C_{jjj}C_{kkk}\right)^{1/3} m_i m_j m_k\right] \tag{3.48}$$

and

$$\mu_{p_x}{}^{exact} = \theta_{p_x} + RT\left[\ln\left(M_1 m_{p_x}\right) + \sum_{i=2}^{n}\left[\left(B_{ii}+B_{p_x p_x}\right)m_i\right] + \sum_{i=p_1}^{p_q}\left[\left(B_{ii}+B_{p_x p_x}\right)m_i\right] + \frac{3}{2}\sum_{i=2}^{n}\sum_{j=2}^{n}\left[\left(C_{iii}C_{jjj}C_{p_x p_x p_x}\right)^{\frac{1}{3}} m_i m_j\right] + 3\sum_{i=2}^{n}\sum_{j=p_1}^{p_q}\left[\left(C_{iii}C_{jjj}C_{p_x p_x p_x}\right)^{1/3} m_i m_j\right] + \frac{3}{2}\sum_{i=p_1}^{p_q}\sum_{j=p_1}^{p_q}\left[\left(C_{iii}C_{jjj}C_{p_x p_x p_x}\right)^{1/3} m_i m_j\right]\right]. \tag{3.49}$$

As above, we can choose one non-permeating solute—again, for example, solute "2"—and express the concentrations of all other non-permeating solutes in terms of the concentration of that solute, *i.e.,*

$$m_i = R_i m_2 \,. \tag{3.38}$$

Note that Equation 3.38 does not apply to any of the permeating solutes. Using the definition of the grouped intracellular solute, we can again write

$$m_g = \sum_{i=2}^{n} m_i = \left( \sum_{i=2}^{n} R_i \right) m_2 \,. \tag{3.39}$$

Substituting Equations 3.38, 3.39, 3.44, 3.46, 3.48 and 3.49 into Equations 3.37 and 3.47, simplifying and rearranging gives

$$
\begin{aligned}
&{m_2}^2 \sum_{i=2}^{n}\sum_{j=2}^{n}\left[\frac{\left(B_{ii}+B_{jj}\right)}{2}R_iR_j\right] + m_2\sum_{i=2}^{n}\sum_{j=p_1}^{p_q}\left[\left(B_{ii}+B_{jj}\right)R_im_j\right] \\
&+ {m_2}^3\sum_{i=2}^{n}\sum_{j=2}^{n}\sum_{k=2}^{n}\left[\left(C_{iii}C_{jjj}C_{kkk}\right)^{1/3}R_iR_jR_k\right] \\
&+ 3{m_2}^2\sum_{i=2}^{n}\sum_{j=2}^{n}\sum_{k=p_1}^{p_q}\left[\left(C_{iii}C_{jjj}C_{kkk}\right)^{1/3}R_iR_jm_k\right] \\
&+ 3m_2\sum_{i=2}^{n}\sum_{j=p_1}^{p_q}\sum_{k=p_1}^{p_q}\left[\left(C_{iii}C_{jjj}C_{kkk}\right)^{1/3}R_im_jm_k\right] \qquad (3.50)\\
&\qquad = {m_2}^2B_{gg}\left(\sum_{i=2}^{n}R_i\right)^2 + m_2\left(\sum_{i=2}^{n}R_i\right)\left(\sum_{i=p_1}^{p_q}\left[\left(B_{ii}+B_{gg}\right)m_i\right]\right) \\
&\qquad\quad + {m_2}^3C_{ggg}\left(\sum_{i=2}^{n}R_i\right)^3 + 3{m_2}^2{C_{ggg}}^{2/3}\left(\sum_{i=2}^{n}R_i\right)^2\left(\sum_{i=p_1}^{p_q}\left[{C_{iii}}^{1/3}m_i\right]\right) \\
&\qquad\quad + 3m_2{C_{ggg}}^{1/3}\left(\sum_{i=2}^{n}R_i\right)\left(\sum_{i=p_1}^{p_q}\sum_{j=p_1}^{p_q}\left[\left(C_{iii}C_{jjj}\right)^{1/3}m_im_j\right]\right).
\end{aligned}
$$

and

$$m_2\sum_{i=2}^{n}\left[\left(B_{ii}+B_{p_xp_x}\right)R_i\right]+\frac{3}{2}{m_2}^2{C_{p_xp_xp_x}}^{\frac{1}{3}}\sum_{i=2}^{n}\sum_{j=2}^{n}\left[\left(C_{iii}C_{jjj}\right)^{1/3}R_iR_j\right]$$

$$+3m_2{C_{p_xp_xp_x}}^{\frac{1}{3}}\sum_{i=2}^{n}\sum_{j=p_1}^{p_q}\left[\left(C_{iii}C_{jjj}\right)^{1/3}R_im_j\right] \tag{3.51}$$

$$=m_2\left(B_{gg}+B_{p_xp_x}\right)\left(\sum_{i=2}^{n}R_i\right)+\frac{3}{2}{m_2}^2{C_{p_xp_xp_x}}^{1/3}{C_{ggg}}^{2/3}\left(\sum_{i=2}^{n}R_i\right)^2$$

$$+3m_2{C_{p_xp_xp_x}}^{1/3}{C_{ggg}}^{1/3}\left(\sum_{i=2}^{n}R_i\right)\sum_{i=p_1}^{p_q}\left[{C_{iii}}^{1/3}m_i\right].$$

As for Equation 3.40 above, we can look at Equations 3.50 and 3.51 and make note of several observations. Again, all the of osmotic virial coefficients ($B_{ii}$, $C_{iii}$) of all the real solutes in solution and all the concentration ratios $\vec{R}_i$ must be constant, while the molalities of non-permeating solute 2 ($m_2$) and of all permeating solutes $\vec{p}$ ($\vec{m}_i$) are variable. The osmotic virial coefficients of the grouped intracellular solute $g$, $B_{gg}$ and $C_{ggg}$, are once again unknowns. Note that if we can show that Equations 3.50 and 3.51 are simultaneously true for any set of values of $m_2$ and $\vec{m}_i$ such that $B_{gg}$ and $C_{ggg}$ have unique constant values, we will have satisfied the conditions contained in Equations 3.37 and 3.47 for any number of moles of water and for any number of moles of each of the permeating solutes $\vec{p}$ present in solution, as required.

The necessary unique and constant values of $B_{gg}$ and $C_{ggg}$ can be found by considering independently corresponding terms on the left and right sides of Equations 3.50 and 3.51 as written above, *i.e.,*

$$m_2{}^2 \sum_{i=2}^{n}\sum_{j=2}^{n}\left[\frac{(B_{ii}+B_{jj})}{2}R_iR_j\right] = m_2{}^2 B_{gg}\left(\sum_{i=2}^{n}R_i\right)^2, \tag{3.52}$$

$$m_2 \sum_{i=2}^{n}\sum_{j=p_1}^{p_q}\left[(B_{ii}+B_{jj})R_im_j\right] = m_2\left(\sum_{i=2}^{n}R_i\right)\left(\sum_{i=p_1}^{p_q}\left[(B_{ii}+B_{gg})m_i\right]\right), \tag{3.53}$$

$$m_2{}^3 \sum_{i=2}^{n}\sum_{j=2}^{n}\sum_{k=2}^{n}\left[\left(C_{iii}C_{jjj}C_{kkk}\right)^{1/3}R_iR_jR_k\right] = m_2{}^3 C_{ggg}\left(\sum_{i=2}^{n}R_i\right)^3, \tag{3.54}$$

$$\begin{aligned} &3m_2{}^2 \sum_{i=2}^{n}\sum_{j=2}^{n}\sum_{k=p_1}^{p_q}\left[\left(C_{iii}C_{jjj}C_{kkk}\right)^{1/3}R_iR_jm_k\right] \\ &\qquad = 3m_2{}^2 C_{ggg}{}^{2/3}\left(\sum_{i=2}^{n}R_i\right)^2\left(\sum_{i=p_1}^{p_q}\left[C_{iii}{}^{1/3}m_i\right]\right), \end{aligned} \tag{3.55}$$

$$\begin{aligned} &3m_2 \sum_{i=2}^{n}\sum_{j=p_1}^{p_q}\sum_{k=p_1}^{p_q}\left[\left(C_{iii}C_{jjj}C_{kkk}\right)^{1/3}R_im_jm_k\right] \\ &\qquad = 3m_2 C_{ggg}{}^{1/3}\left(\sum_{i=2}^{n}R_i\right)\left(\sum_{i=p_1}^{p_q}\sum_{j=p_1}^{p_q}\left[\left(C_{iii}C_{jjj}\right)^{1/3}m_im_j\right]\right), \end{aligned} \tag{3.56}$$

$$m_2 \sum_{i=2}^{n}\left[(B_{ii}+B_{p_xp_x})R_i\right] = m_2(B_{gg}+B_{p_xp_x})\left(\sum_{i=2}^{n}R_i\right), \tag{3.57}$$

$$\frac{3}{2}m_2{}^2 C_{p_xp_xp_x}{}^{1/3}\sum_{i=2}^{n}\sum_{j=2}^{n}\left[\left(C_{iii}C_{jjj}\right)^{1/3}R_iR_j\right] = \frac{3}{2}m_2{}^2 C_{p_xp_xp_x}{}^{1/3}C_{ggg}{}^{2/3}\left(\sum_{i=2}^{n}R_i\right)^2, \tag{3.58}$$

and

$$3m_2 C_{p_x p_x p_x}{}^{1/3} \sum_{i=2}^{n} \sum_{j=p_1}^{p_q} \left[ \left( C_{iii} C_{jjj} \right)^{1/3} R_i m_j \right] = 3m_2 C_{p_x p_x p_x}{}^{1/3} C_{ggg}{}^{1/3} \left( \sum_{i=2}^{n} R_i \right) \sum_{i=p_1}^{p_q} \left[ C_{iii}{}^{1/3} m_i \right]. \tag{3.59}$$

If all of Equations 3.52 through 3.59 are simultaneously true under a given set of conditions, then Equations 3.50 and 3.51 will also be simultaneously true under those conditions. By inspection, Equation 3.52 can only be true for any set of values of $m_2$ and $\vec{m}_i$ if $B_{gg}$ is defined by Equation 3.41. Similarly, Equation 3.54 can only be true for any set of values of $m_2$ and $\vec{m}_i$ if $C_{ggg}$ is defined by Equation 3.42. Using the multiplication rule for finite sums (see Appendix D), it can be shown that Equations 3.53 and 3.55 through 3.59 are also true for any set of values of $m_2$ and $\vec{m}_i$ if $B_{gg}$ and $C_{ggg}$ are defined by Equations 3.41 and 3.42, respectively. Therefore, in the case of a cell in the presence of some number of permeating solutes $q$, the grouped intracellular solute approach is equivalent to the exact approach when osmolality is defined by Equation 3.8 and permeating solute chemical potential is defined by Equation 3.24. A similar proof using Equations 3.33 and 3.34 to define osmolality and solute chemical potential, respectively, shows that the grouped intracellular solute approach continues to be equivalent to the exact approach when there are electrolytes present among the non-permeating solutes consolidated into the grouped solute.

### 3.5 Conclusions

Here, we have derived a molality-based non-ideal solute chemical potential equation which is thermodynamically consistent with the molality-based Elliott *et al.* form of the multi-solute osmotic virial equation to third order. We have also shown that when calculating water and solute chemical potentials within a cell using these molality-based equations, considering all non-

permeating intracellular solutes as a single non-permeating "grouped" solute (*i.e.,* using the grouped intracellular solute approach) is equivalent to treating each non-permeating intracellular solute separately—that is, the grouped intracellular solute approach does not affect model predictions of chemical potential. As such, we now have a complete thermodynamically consistent molality-based non-ideal solution theory to third order for any number of solutes, as well as a theoretically-verified method for modelling the intracellular solution without knowledge of its exact composition. Therefore, we can now model the osmotic behaviour of cells under non-ideal conditions (such as those found in cryobiology) and in the presence of multiple permeating solutes. Furthermore, the proof of mathematical equivalence between the grouped intracellular solute approach—when used with the multi-solute osmotic virial equation—and the approach of independently considering each non-permeating intracellular solute has ramifications outside of osmotic modelling, as it means that multi-solute solutions in other applications where there are some solutes with fixed mass ratios can be rigorously treated with such a grouped solute model. An example of such an application is the determination of vapor pressure of solutions of multiple non-volatile solutes.

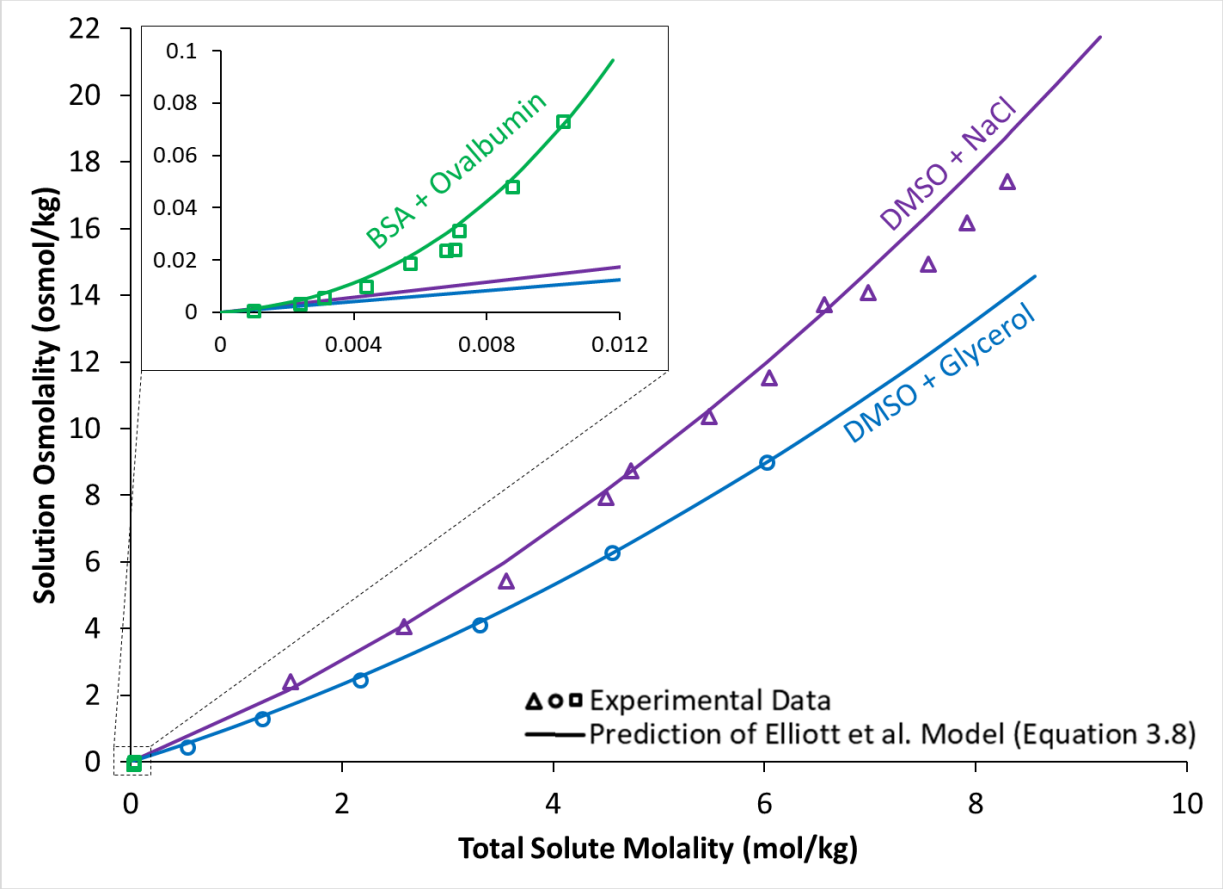


Figure 3.1. Comparison of experimental measurements and predictions by the Elliott *et al.* form of the multi-solute osmotic virial equation of multi-solute solution osmolality as a function of total solute molality. Adapted from Zielinski *et al*. [154]. The triangles, circles, and squares represent experimental measurements for each of the multi-solute solutions, while the correspondingly-coloured solid lines represent the predictions of Equation 3.8 in each solution. The triangles (purple) represent data from Hildebrandt's thesis [51] for a solution of dimethyl sulphoxide (DMSO) and NaCl, at a solute mass ratio of DMSO:NaCl = 2:1. The circles (blue) represent data from Elliott *et al*. [24]. for a solution of DMSO and glycerol, at a solute mass ratio of DMSO:glycerol = 2:1. The squares (green) represent data from Yousef *et al*. [150]. for a solution of bovine serum albumin (BSA) and ovalbumin, at a solute mass ratio of BSA:ovalbumin = 3:2. The inset at top left provides a closer look at the lower end of both the molality and osmolality

axes. This scale is more convenient than that of the main figure for visualizing the data and predictions for the BSA + ovalbumin system, which have values that are three orders of magnitude lower than those for the other three systems.

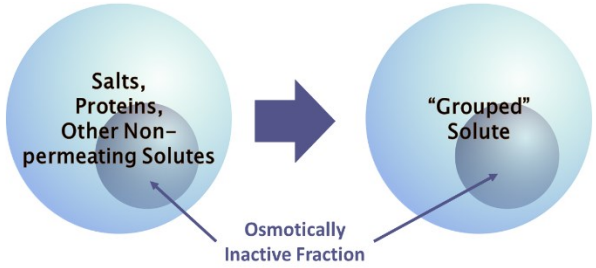


Figure 3.2. The grouped solute approach for modelling the cytoplasm. All non-permeating intracellular solutes are considered as a single, non-permeating "grouped" solute. The osmotically inactive fraction refers to those components of the cytoplasm which do not participate osmotically.

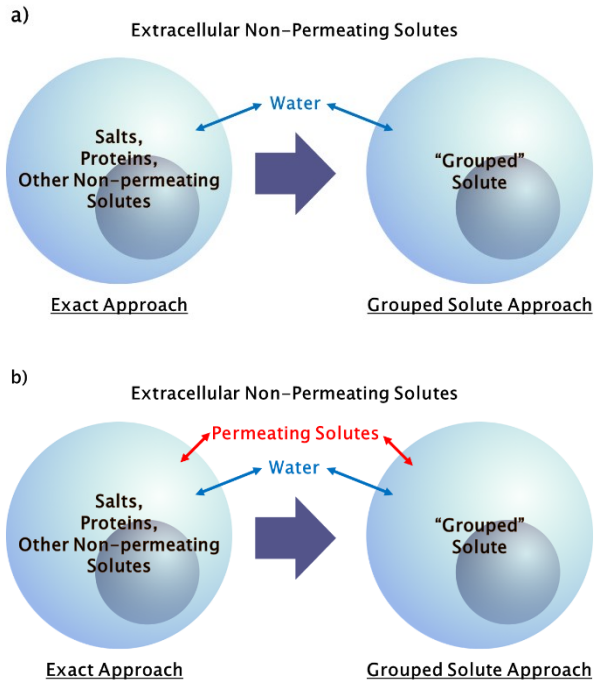


Figure 3.3. Schematic depicting the cell situation for the grouped intracellular solute proof. a) In the presence of non-permeating solutes only. b) In the presence of permeating and non-permeating solutes.

# Chapter 4. Measurement of grouped intracellular solute osmotic virial coefficients[3]

**Chapter Summary:** Models of cellular osmotic behaviour depend on thermodynamic solution theories to calculate chemical potentials in the solutions inside and outside of the cell. These solutions are generally thermodynamically non-ideal under cryobiological conditions. The molality-based Elliott *et al.* form of the multi-solute osmotic virial equation is a solution theory which has been demonstrated to provide accurate predictions in cryobiological solutions, accounting for the non-ideality of these solutions using solute-specific thermodynamic parameters called osmotic virial coefficients. However, this solution theory requires as inputs the exact concentration of every solute in the solution being modeled, which poses a problem for the cytoplasm, where such detailed information is rarely available. This problem can be overcome by using a grouped solute approach for modeling the cytoplasm, where all the non-permeating intracellular solutes are treated as a single non-permeating "grouped" intracellular solute. We have recently shown that such a grouped solute approach is theoretically valid when used with the Elliott *et al.* model, and Ross-Rodriguez *et al*. (*Biopreservation and Biobanking*, 2012) have recently developed a method for measuring the cell type-specific osmotic virial coefficients of the grouped intracellular solute. However, this method suffers from a lack of precision, which—as we demonstrate in this work—can severely impact the accuracy of osmotic model predictions under certain conditions. Thus, we herein develop a novel method for measuring grouped intracellular

[3] This chapter, with modifications, is being prepared for submission as M.W. Zielinski, L.E. McGann, J.A. Nychka, J.A.W. Elliott, Measurement of grouped intracellular solute osmotic virial coefficients.

solute osmotic virial coefficients which yields more precise values than the existing method, and apply this new method to measure these coefficients for human umbilical vein endothelial cells.

## 4.1. Introduction

The cytoplasm of a cell is a complex solution containing a myriad of different solutes (*e.g.*, salts, sugars, proteins), the specific combination depending on the cell type. The ability to accurately thermodynamically model this intracellular space is important to fields such as cryobiology, where a solution model of the cytoplasm is a critical component of mathematical models of cellular behaviour during cryopreservation [12,13,23,27,53,54,62,65,66,81,115, 116,129,139,153]. In this work, we introduce a novel technique for measuring a cell type-specific set of characteristic thermodynamic parameters that enable modeling of the cytoplasm, and demonstrate the application of this technique by measuring these parameters for human umbilical vein endothelial cells.

Cryopreservation is the process by which cells (or larger structures, *e.g.*, tissues) are cooled to low subzero temperatures (*e.g.*, –196 °C, the boiling point of nitrogen), stored until needed, and subsequently warmed back up to ambient conditions. Ideally, cryopreservation could—and in some cases [74,101,130,133], does—enable the long-term banking of cells and tissues for use in transplantation and research. However, at present, many types of cells (and the vast majority of tissues) cannot be successfully cryopreserved [63,98,147]—that is, they cannot be brought down to, and back from, storage temperatures with an acceptable level of survival.

With regards to the cryopreservation of cells, at least four potential mechanisms of damage that can have a negative impact on cell survival have been recognized. Two of these damage mechanisms, described by the two-factor hypothesis of Mazur *et al.* [83], are directly related to

the rate at which the cells are cooled. Intracellular ice formation, which is generally lethal for cells in suspension [82,91,99], becomes increasingly likely as the cooling rate is increased. Conversely, solution effects injury, which refers to damage resulting from cells being exposed to the high solute concentrations inherent to cryopreservation for extended periods of time [83,91], intensifies as the cooling rate is decreased. Briefly, these two mechanisms can be explained as follows. In general, ice initially nucleates and grows outside of cells as they are cooled down below freezing temperatures [81]. Due to the low solubility of most solutes in ice [124], as the temperature drops and increasing amounts of liquid water solidify to ice, nearly all of the solute ions and molecules that were in that liquid are rejected from the resulting solid and into the remaining liquid fraction. As a consequence, this remaining liquid becomes increasingly concentrated. At low cooling rates, this concentration of the liquid fraction during freezing can lead to solution effects injury. At high cooling rates, if osmotic equilibration across the cell membrane cannot occur quickly enough, then the intracellular solution will become increasingly supercooled as the temperature lowers. If the cooling rate is too high, such intracellular supercooling can result in the nucleation of intracellular ice.

Although it is possible to find a single "optimum" cooling rate at which the net effect from both intracellular ice formation and solution effects injury is minimized and—to an extent—cell survival maximized [83], survival can be further enhanced by using more complex, non-linear cooling protocols (*e.g.,* [36,37,86,117]) and by adding chemicals known as cryoprotectants [85,90]. It is the addition of cryoprotectants—and in particular those that can permeate the cell membrane—that gives rise to the other two mechanisms of damage: cryoprotectant toxicity—which increases with temperature, concentration, and exposure time [12,13,28,33,34], and osmotic damage arising from excessive cell volume excursions [12,13,39,52,64]. The latter can occur when

permeating cryoprotectants are added or removed too quickly (*e.g.,* if trying to minimize exposure time to a cryoprotectant with potent toxic effects). The development of successful cryopreservation protocols requires that the damage caused by all four of these mechanisms be minimized.

With the exception of solution effects injury, the above damage mechanisms are governed by the transport of water and permeating solutes (*e.g.,* cryoprotectants) across the cell membrane, a set of processes known as the cellular osmotic response. As such, mathematical models enabling the prediction of this osmotic response are useful in the development of cryopreservation protocols. A key component of these kinetic osmotic models is the ability to calculate the chemical potentials of water and of permeating solutes both inside and outside of the cell [12,13,23,27,53,54,62,65,66,81,115,116,129,139,153], as differences in chemical potential are the driving force for transport. A set of equations that allows the simultaneous, consistent calculation of both the water (*i.e.*, solvent) and solute chemical potentials in a given solution is called a thermodynamic solution theory. In cryobiology, ideal dilute solution theories are commonly used [12,13,39,53,54,60,61,64–66,81,129,137]. However, the ideal dilute approach does not account for the complex and highly thermodynamically non-ideal nature of cryobiological solutions, most of which contain multiple and varied solutes (*e.g.,* salts, sugars, proteins, alcohols) at high concentrations. Indeed, it has been shown that predictions of chemical potential in even relatively simple cryobiologically relevant multi-solute solutions are considerably more accurate when non-ideal—as opposed to ideal—solution theories are used [24,105,106,154].

One such non-ideal solution theory is the Elliott *et al.* form of the multi-solute osmotic virial equation [11,24,27,105,106,154,156]. This model is based on the osmotic virial equation of McMillan and Mayer [87], which expresses water chemical potential as a polynomial in terms of solute concentration. Solution non-ideality is accounted for by the coefficients of the polynomial.

These osmotic virial coefficients are solute-specific and can be obtained by curve-fitting to experimental osmometric measurements of water chemical potential in binary—*i.e.* single-solute—aqueous solutions containing the solute of interest [24,105,154]. The Elliott *et al.* model proposes thermodynamic combining rules for these coefficients that extend the application of the osmotic virial equation to multi-solute solutions without ignoring inter-solute interactions and without the need for fitting to multi-solute—*i.e.* solution-specific—data [24]. This flexibility is particularly useful in cryobiology, where—given the wide range of solutes that are relevant—the number of distinct solutions that can be encountered is effectively unlimited. The Elliott *et al.* model also introduces thermodynamically consistent equations for calculating solute chemical potential [27,156], thus providing a complete non-ideal solution theory that relies on only single-solute data.

As noted above, modeling the cellular osmotic response requires the prediction of chemical potentials both inside and outside the cell. However, in order to calculate chemical potentials in a solution of interest, the osmotic virial equation—and, by extension, the Elliott *et al.* model—requires that the concentration of every solute in that solution be known. This requirement is generally not a problem for the extracellular solution, as this solution—that is, the solution in which the cells are suspended—is usually controlled and thus defined. Conversely, the exact concentration of every solute in the intracellular solution—*i.e.* the cytoplasm—is typically not known, making the calculation of intracellular chemical potentials challenging. One way to overcome this problem without making any assumptions about the contents of the cell or resorting to an ideal dilute solution theory is to use a "grouped intracellular solute" approach, where, for the purposes of thermodynamic modeling, all of the non-permeating solutes inside the cell are treated as a single, non-permeating "grouped" solute. This approach has been successfully applied with a

number of different cell types [104,118], and we have recently shown that, when used with the Elliott *et al.* form of the multi-solute osmotic virial equation, it is theoretically valid—*i.e.* using the grouped intracellular solute approach with the Elliott *et al.* model does not affect the model's predictions of chemical potential (as compared to treating each non-permeating intracellular solute separately) [156].

However, just as for any other solute, in order for the grouped intracellular solute to be used within an osmotic virial model, its osmotic virial coefficients must be known. Furthermore, given that the grouped solute represents all of the non-permeating solutes inside the cell, and that the exact composition of the cytoplasm can vary widely between one type of cell and another, the grouped intracellular solute osmotic virial coefficients must be cell type-specific. Thus, in order to use the grouped intracellular solute approach in the Elliott *et al.* model to predict cellular osmotic responses, a method of measuring these coefficients for any cell type of interest is required. Previously, Ross-Rodriquez *et al.* developed such a method and applied it to measure the grouped intracellular solute osmotic virial coefficients for a variety of cell types [118]. However, their approach suffers from a lack of precision, which is problematic for models of the cellular osmotic response because, in the presence of one or more permeating solutes, these models can be highly sensitive to the values of the grouped intracellular solute osmotic virial coefficients (see Figures 4.6 to 4.9 below).

The objective herein is to develop a novel method of measuring grouped intracellular solute osmotic virial coefficients that has greater precision than the existing method, and to use this new method to measure these coefficients for a particular cell type: human umbilical vein endothelial cells (HUVEC).

The overall approach to this novel technique consists of two main steps. First, measurements of equilibrium cell volume are made in two different types of solutions: the first type containing only non-permeating solutes at specified osmolalities, and the second type containing defined concentrations of a single permeating cryoprotectant. Subsequently, a model of equilibrium cell volume is curve-fit to these measurements in order to obtain the cell type-specific grouped intracellular solute osmotic virial coefficients. In this work, the process was performed for HUVEC exposed to two different permeating cryoprotectants: dimethyl sulphoxide (DSMO) and ethylene glycol (EG).

## 4.2. Experimental methods

### *4.2.1. Overview*

As noted above, the measurement technique described herein requires two different types of experimental data. The first type of data consists of measurements of equilibrium cell volume as a function of solution osmolality in solutions of only non-permeating solutes. Such measurements have already been conducted for HUVEC by Ross-Rodriguez *et al.* in their work on grouped intracellular solute osmotic virial coefficients [118]. Accordingly, their data was used in this work, and no further measurements of this type were made. The second type of data consists of measurements of equilibrium cell volume as a function of cryoprotectant concentration in solutions containing a single permeating cryoprotectant. No such data appears to exist in the literature for HUVEC. As such, these type of measurements were the focus of the experimental work in this study.

*4.2.2. Cell culture*

Human umbilical vein endothelial cells (HUVEC) (LONZA, Walkersville, MD) were cultured aseptically at 37 °C in an atmosphere with 5% $CO_2$ and in a culturing medium consisting of Endothelial Cell Basal Medium-2 (EBM-2) plus a set of growth supplements (BulletKit) comprising hydrocortisone, human fibroblast growth factor B (hFGF-B), vascular endothelial growth factor (VEGF), R3 insulin-like growth factor (R3-IGF-1), ascorbic acid, heparin, fetal bovine serum (FBS), and human endothelial growth factor (hEGF). It should be noted that no antibiotic was included in this culturing medium. Cells were seeded at a density of 5000 cells/$cm^2$. Media was replaced at least every other day, and the cells were not cultured beyond 15 population doublings post-thaw (the maximum recommended by LONZA).

For continuous culture, cells were passaged using 0.025% trypsin/0.01% EDTA (LONZA) once they had reached approximately 80% of flask coverage. For experiments, cell were passaged with trypsin/EDTA once they had reached 100% flask coverage. In both cases, the resulting cell suspension was subsequently centrifuged (1000 RPM for 5 minutes at 20 °C) and resuspended in either fresh culture medium (for continuous culture) or HEPES buffered saline solution (for experiments). Cell suspensions for experiments had a minimum cell concentration of $6\times10^6$ cells/mL. Immediately after resuspension, experimental cell suspensions were placed into an ice–water bath, where they remained until used in the experiment.

*4.2.3. Exposure to cryoprotectant solutions*

Cells were exposed to solutions containing a single cryoprotectant: either dimethyl sulphoxide (DMSO) or ethylene glycol (EG). These cryoprotectant solutions consisted of a HEPES buffered saline solution (isotonic) to which the corresponding cryoprotectant was added in the

amount required to give the desired cryoprotectant concentration. The cryoprotectant concentrations used were 0.5, 1.0, 1.5, 2.0, 2.5, and 3.0 molal.

In order to establish the isotonic cell volume (required to calculate relative cell volumes), subsets of each cell sample were removed and analyzed separately in the absence of any cryoprotectant, both before (pre-treatment controls) and after (post-treatment controls) the experimental measurements. For each cell sample, six pre-treatment and six post-treatment controls were analysed. The isotonic volume was designated as the average value of all twelve controls.

The experimental portion of each cell sample (*i.e.*, the portion not used for pre/post-treatment controls) was subdivided into twelve experimental samples. Each of these samples was exposed to a single defined cryoprotectant concentration.

Cryoprotectant addition to the experimental samples was carried out one sample at a time. The remaining experimental samples remained cryoprotectant-free in the ice–water bath until each one was needed. Cryoprotectant addition was carried out at room temperature. The cryoprotectant was added to the cell samples in 0.5 molal increments (*i.e.,* sufficient cryoprotectant was added to increase the concentration by 0.5 molal), with each increment being added dropwise and with pipette mixing occurring between each incremental addition (this approach minimizes osmotic damage). Once all the cryoprotectant had been added for a given sample, the timer was started. From this point onward, the sample was left at room temperature (*i.e.,* not replaced back into the ice–water bath).

Each experimental sample was analyzed once after a cryoprotectant-specific exposure time. For any given cryoprotectant, the exposure time was defined to be the amount of time that is required for cryoprotectant equilibration at room temperature for all considered cryoprotectant

concentrations. Here, for both DMSO and EG, exposure time was determined to be 7 minutes post-cryoprotectant addition (see Appendix E).

Each unique cryoprotectant solution (*i.e.*, combination of cryoprotectant and concentration) was analysed a total of six times with the analyses distributed over three experiments, each experiment using an independent cell sample. The order in which the solutions were sampled was varied between experiments as outlined in Table 4.1.

### *4.2.4. Volume and membrane integrity assessment*

Although the ultimate goal of this experimental work was to obtain measurements of equilibrium cell volume in the solutions of interest, only membrane-intact cells could be considered, as the mathematical model of equilibrium cell volume that was used herein (see below) assumes that the cell is intact (*i.e.*, it assumes that the cell membrane is still semi-permeable). Therefore, in addition to measuring volume, the membrane integrity of the cells was also measured.

For each experimental and control sample, cell volume and membrane integrity were analysed using bright-field optical microscopy and trypan blue staining at room temperature. For each sample analysis, the cell suspension was mixed with equal parts 0.4% trypan blue solution and left to incubate for 3 minutes [134] at room temperature. For experimental samples, the trypan blue solution contained the same concentration of cryoprotectant as the cell suspension. After incubating, a small volume (10 μL) of the trypan blue-stained cell suspension was placed onto a haemocytometer.

For each sample, the outer edges of the haemocytometer grid were used as a guide to take twelve photos—in twelve different locations on the haemocytometer, as depicted in Figure 4.1—

of the cells using bright-field optical microscopy with a 40× objective lens. In addition, an initial photo was taken in the central portion of the haemocytometer grid for scale calibration purposes when calculating cell volume. In taking this scale calibration photo, the image focus was adjusted such that the top edges of the haemocytometer grid were in focus; this focus level was maintained for the remaining twelve images.

Cell volumes were analysed by measuring the cross-sectional area of the cells in the photos and converting this area to volume using the spherical cell assumption. Membrane integrity was analysed using the trypan blue exclusion assay. This assay is based on the principle that cells with intact cell membranes exclude trypan blue [134]. Thus, when exposed to trypan blue, intact cells will appear clear, while membrane-compromised cells will appear blue. A custom ImageJ software (National Institutes of Health, Bethesda, MD) macro script (described in greater detail below) was used with the photos both to obtain the cross-sectional cell areas required for volume measurement and to determine whether each cell was intact or membrane-compromised. For all analyses, at least 200 intact cells were measured across the twelve images.

### 4.3. Image analysis

The custom macro script used in ImageJ to determine cell cross-sectional area and membrane integrity is outlined in Figure 4.2, and the script itself is contained in Appendix F. The procedure in Figure 4.2 was carried out for each image individually, although the images were processed in batches of twelve, each batch corresponding to a single sample.

Prior to carrying out any other analysis, the lighting in each image was calibrated to account for any unevenness due to the microscope setup. Image lighting calibration was carried out by subtracting a microscope setup-specific calibration image from each cell image. The calibration

image was created as outlined in Figure 4.3. First, a haemocytometer filled with only HEPES buffered saline solution (*i.e.*, no cells) was placed under the microscope and at least two photos were taken in different locations in the off-grid region of the haemocytometer. Using ImageJ, these images were then averaged to account for (*i.e.*, remove) any bubbles, scratches, or other location-specific image artifacts, and a Gaussian blur filter with a radius of $\sigma = 5$ was applied to the resulting average. The image was then split into its red, green, and blue channels. For each colour channel, the mean pixel value of that channel's image was calculated and subtracted from the channel's image, with any pixels that would have been reduced below a value of zero reduced to zero instead. The colour channels were then merged back together to produce the final calibration image to be used to process all the experimental cell images. A separate calibration image was generated on the day of each experiment, prior to imaging any of the experimental samples. Apart from adjusting the image focus, neither the microscope nor its settings were changed in any way in the time between the generation of the calibration image and the completion of all experimental measurements.

Once calibrated, the image was processed and analyzed to locate all cells (*i.e.*, both membrane-intact and membrane-compromised). The bulk of the macro steps for this stage are contained in the "identifyCells" function of the macro script (see Appendix F). These steps are briefly summarized as follows. The first step of the identifyCells function is essentially a rough scan of the image to find all potential regions of interest (ROIs) that could contain a cell. The image is subjected to ImageJ's "Find Edges" algorithm, converted to 8-bit black-and-white, binarized/thresholded,[4] and then subjected to a series of binary operations that fill in holes in the

[4] Thresholding is an image analysis technique where a threshold pixel value is automatically determined based on the distribution of pixel values in the image, and then all pixels at or above this threshold value are set to white and all pixels below are set to black (or *vice-versa*) [44]. As a result, the image becomes binary, consisting of two types of areas: regions of interest, and background.

ROIs, identify and separate adjacent ROIs, and smooth out the ROI borders. At this point, the ROIs are marked and recorded. Next, the outermost layer of pixels of each ROI is repeatedly removed in order to find the approximate central region of each ROI (*i.e.*, of each potential cell). These ROI centres are then also marked and recorded, and the image is reverted to its calibrated state (*i.e.*, all processing is reversed). The next step of the function involves removing two specific types of artifacts from the image: haemocytometer gridlines and the bright rings or "halos" that often appear around cells (*e.g.*, see Figure 4.4(a)). In both cases, the considerably brighter pixels of the gridlines and halos are replaced by average background pixels. Finally, the last step of the function is a more aggressive search of the processed image (*i.e.*, with gridlines and halos removed) for cells and cell borders. At this point, only the ROIs identified in the first step are considered (*i.e.*, the rest of the image is not analyzed), and each ROI is scanned independently. Before scanning, the ROI centres also identified in the first step are drawn on to the image to help avoid cells being lost due to poorly-imaged or obscured edges. This measure is necessary because in this last step—unlike in the first step—only regions with a circularity ratio greater than a defined minimum value (0.6 for equilibrium measurements; 0.7 for kinetic measurements) are actually considered to be cells. Thus, if a cell's edge cannot be clearly distinguished all the way around its perimeter, the corresponding region on the image may appear hollowed out or crescent-shaped, thus removing the cell from consideration. Drawing in the ROI centre can prevent this from occurring. It should be noted that the particular set of steps used in the identifyCells function is not necessarily the optimal image analysis approach for cell location, and better approaches may exist; however, this approach was found to be effective for the application required herein (*i.e.*, determining cell volumes of HUVEC). Figure 4.4 contains a representative example image before and after cell identification by the macro. When all the cells in an image had been identified, the

cross-sectional area of each cell was measured and recorded and the image was reverted to its calibrated state.

The final stage of the image analysis procedure was to distinguish between membrane-intact and membrane-compromised cells, because—as noted above—only the volumes of intact cells can be used to fit for the grouped intracellular solute osmotic virial coefficients. The trypan blue assay used in this work to determine cell membrane integrity causes membrane-compromised cells to appear blue while not affecting the appearance of membrane-intact cells (*i.e.*, leaving them clear). As such, the macro identified the blue—and therefore membrane-compromised—cells and removed them from consideration. As a general overview, to identify blue cells, the calibrated cell image was first split into its red, green, and blue channels. Subsequently, the ratios of blue-to-green and blue-to-red pixel values within each cell were compared to the corresponding ratios for the whole image. If either ratio was greater within the cell than for the image as a whole—*i.e.*, if the cell was more blue as compared to green or as compared to red than the image as a whole—then the cell was considered to be membrane-compromised. For further details, see Appendix F.

### 4.4. Thermodynamic model of equilibrium cell state

Equilibrium cell volumes were calculated using a thermodynamic model of the cell state at equilibrium. This model consists of four conditions, described in detail below. The equilibrium cell volume is obtained from the model when all four of these conditions (*i.e.*, Equations 4.11, 4.12, 4.7, and 4.10 in Table 4.2 below) are simultaneously satisfied.

At equilibrium, there will be no chemical potential differences across the cell membrane (*i.e.*, no driving force for transport). As such, the first two conditions of the model are chemical potential balances for water

$$\mu_1{}^{in} = \mu_1{}^{ex} \tag{4.1}$$

and for any permeating solute in solution

$$\mu_p{}^{in} = \mu_p{}^{ex}\,, \tag{4.2}$$

where $\mu_1$ is the chemical potential of water (in J/mole), $\mu_p$ is the chemical potential of permeating solute *p* (in J/mole), and the superscripts "*in*" and "*ex*" refer to the intracellular and extracellular solutions, respectively. In this work, the chemical potentials in Equations 4.1 and 4.2 were calculated using the molality-based Elliott *et al.* form of the multi-solute osmotic virial equation, which models water and solute chemical potentials, respectively, as [24,105,156]

$$\mu_1 = \mu_1^o - RTM_1\pi\,, \tag{4.3}$$

with $\pi$, the solution osmolality (in osmoles/kg of water), defined as

$$\pi = \sum_{i=2}^{r} k_i m_i + \sum_{i=2}^{r}\sum_{j=2}^{r}\left[\frac{\left(B_{ii}+B_{jj}\right)}{2} k_i m_i k_j m_j\right] + \sum_{i=2}^{r}\sum_{j=2}^{r}\sum_{k=2}^{r}\left[\left(C_{iii}C_{jjj}C_{kkk}\right)^{1/3} k_i m_i k_j m_j k_k m_k\right], \tag{4.4}$$

and

$$\mu_p = k_p\theta_p + RTk_p\left[\ln\left(M_1 m_p\right) + \sum_{i=2}^{r}\left[\left(B_{ii}+B_{pp}\right)k_i m_i\right] + \frac{3}{2}\sum_{i=2}^{r}\sum_{j=2}^{r}\left[\left(C_{iii}C_{jjj}C_{ppp}\right)^{1/3} k_i m_i k_j m_j\right]\right], \tag{4.5}$$

where $m_i$ is the molality (a measure of concentration) of solute *i* (in moles of solute *i*/kg of water), $B_{ii}$ and $C_{iii}$ are the second and third osmotic virial coefficients of solute *i,* respectively (in [moles of solute *i*/kg of water]$^{-1}$ and [moles of solute *i*/kg of water]$^{-2}$, respectively), $k_i$ is the empirical dissociation constant of solute *i* (unitless), $R$ is the universal gas constant (in J/[mole K]), $T$ is

absolute temperature (in K), $M_1$ is the molar mass of water (in kg/mole), $\mu_1^o$ is the chemical potential of pure water (in J/mole), $\theta_p$ is a function of temperature and pressure only that is specific to solute $p$ (in J/mole), and $(r - 1)$ is the number of solutes in solution. The solution osmolality $\pi$ represents the composition dependence of water chemical potential. Water chemical potential also depends on solution temperature and pressure. However, since at equilibrium there are no temperature or pressure gradients across the cell membrane, the first condition of the model reduces to

$$\pi^{in} = \pi^{ex}\,, \tag{4.6}$$

which will be used instead of Equation 4.1.

As mentioned earlier, the osmotic virial coefficients of a solute (*i.e.*, $B_{ii}$, $C_{iii}$) account for its non-ideal thermodynamic behaviour. Specifically, osmotic virial coefficients represent the increasing orders of thermodynamic interactions that occur between solute molecules. The second osmotic virial coefficient $B_{ii}$ corresponds to interactions between two molecules of solute $i$, while the third osmotic virial coefficient $C_{iii}$ corresponds to interactions between three molecules of solute $i$. The greater the absolute values of these coefficients, the more thermodynamically non-ideal the behaviour of the solute; a solute with ideal thermodynamic behaviour would have coefficient values of zero.

The dissociation constant $k_i$ is a term that is required by the Elliott *et al.* model for any electrolyte solute [105,106]. It empirically accounts for all electrolyte-specific effects such as ionic dissociation and charge screening, and is obtained simultaneously with the solute's osmotic virial coefficients when curve-fitting to experimental osmometric data. For solutes that are not electrolytes, the value of the dissociation constant is one in all calculations.

Many solutes, including the two cryoprotectants used in this study, DMSO [78] and EG [3], exhibit near-ideal volumetric behaviour in aqueous solution. (As an aside, it should, however, be noted that both DMSO and EG exhibit non-ideal thermodynamic behaviour in terms of chemical potential [154]). That is, when mixed with water, the volumes of these solutes are essentially directly additive with the solvent (water) volume. The third condition in this model is needed for any such solutes which can permeate the cell membrane. That is, for each permeating solute $p$ which exhibits near-ideal volumetric behaviour in solution, it is required that

$$m_p^{in} M_p \rho_1 \left( \frac{V_{cell}}{V_{cell}^o} - b - \frac{\sum {V_p}^{in}}{V_{cell}^o} \right) = \frac{\text{intracellular mass of permeating solute } s}{\text{isotonic cell volume}} = \rho_p \frac{{V_p}^{in}}{V_{cell}^o}, \tag{4.7}$$

where $m_p^{in}$ is the intracellular molality of solute $p$ (in moles of solute $p$/kg of water), ${V_p}^{in}$ is the intracellular volume of solute $p$ (in μm$^3$), $M_p$ is the molar mass of solute $p$ (in kg/mole), $\rho_p$ is the density of solute $p$ (in kg/μm$^3$), $\sum {V_p}^{in}$ is the sum of the intracellular volumes of all of the permeating solutes present in solution (including $p$) (in μm$^3$), $\rho_1$ is the density of water (in kg/μm$^3$), $V_{cell}$ is the equilibrium cell volume (in μm$^3$), $V_{cell}^o$ is the equilibrium cell volume under isotonic conditions (in μm$^3$), and $b$ is the osmotically inactive fraction of the cell. This condition ensures that the intracellular volume and concentration of solute $p$, which are independent variables in this model, remain consistent with one another and with the cell volume $V_{cell}$ (also an independent variable).

From the perspective of thermodynamic modeling, the term isotonic refers to a solution having an osmolality equal to that found under normal physiological conditions. For human cells, this is typically approximately 0.3 osmoles/kg [9,19,20,24,38,82,84,104,108,118,139]. In this model, the isotonic cell state is used as a reference point, with values such as equilibrium cell

volume being calculated and reported relative to the isotonic—*i.e.*, we use the relative equilibrium cell volume, $V_{cell}/V_{cell}^{o}$.

The osmotically inactive fraction, $b$, is the fraction of the overall cell volume which does not participate osmotically—that is, it represents a volume of the cell which is not at all considered in calculations of chemical potential. This property is a cell-specific constant and is typically measured for a cell type of interest by curve-fitting to experimental measurements of equilibrium cell volume in increasingly concentrated anisotonic solutions containing only non-permeating solutes [19,38,52,104,117,118,129,139,152]. The equation used for these fits is the Boyle van't Hoff relation [104,138], typically applied in the following form [19,38,52,104,117,118, 129,139,152]:

$$\frac{V_{cell}}{V_{cell}^{o}} = (1-b)\frac{\pi^{o}}{\pi} + b\,, \tag{4.8}$$

where $\pi^{o}$ is the solution osmolality under isotonic conditions. Previously, Prickett *et al.* [104] showed that there is an inherent ideal dilute assumption in Equation 4.8, and recommended that a non-ideal form of the Boyle van't Hoff relation be used instead when determining osmotically inactive fraction—specifically, the following form [104]:

$$\frac{V_{cell}}{V_{cell}^{o}} = (1-b)\frac{m^{o}}{m^{in}} + b\,, \tag{4.9}$$

where $m^{in}$ is the combined molality of all non-permeating intracellular solutes, and $m^{o}$ is the combined molality of all non-permeating intracellular solutes under isotonic conditions. Equation 4.9 was obtained from a mass balance for the non-permeating solutes inside the cell: it states that, since these solutes cannot—by definition—cross the cell membrane, their mass must be constant and thus equal to the mass in some reference state—in this case, the isotonic state. The fourth

condition in this model of equilibrium cell state is effectively an extension of Equation 4.9 to additionally consider the presence of permeating solutes—*i.e.*,

$$\frac{V_{cell}}{V_{cell}^{o}} = (1 - b)\frac{m^{o}}{m^{in}} + \frac{\sum {V_p}^{in}}{V_{cell}^{o}} + b \, . \tag{4.10}$$

Thus, to summarize, the general model of equilibrium cell volume used in this work consists of the four conditions listed in Table 4.2, which are represented by Equations 4.11 (obtained by substituting Equation 4.4 into Equation 4.6), 4.12 (obtained by substituting Equation 4.5 into Equation 4.2), 4.7, and 4.10. This model is also schematically represented in Figure 4.5. However, depending on the circumstances being modeled, two of these conditions require multiple instances. The second condition—permeating solute chemical potential balance (Equation 4.12)—must be satisfied for each permeating solute being modeled, and the third condition—Equation 4.7—must be satisfied for each permeating solute which exhibits near-ideal volumetric behaviour in solution. In contrast, the first condition—water chemical potential balance (Equation 4.11)—and the fourth condition—non-permeating solute mass balance (Equation 4.10)—are each always only required once. Note that if there are no permeating solutes present in the solution, the model consists solely of the first and fourth conditions—*i.e.*, Equations 4.11 and 4.10. Essentially, the model is a system of equations, ranging in size from two equations (if there are no permeating solutes) upwards, depending on the number and nature of permeating solutes present. The organization of this general model of equilibrium cell volume, as described above, is summarized in Table 4.2.

The unknowns—*i.e.*, the independent variables—in the system of equations comprising the model are the relative cell volume ($V_{cell}/V_{cell}^{o}$), the combined molality of all non-permeating intracellular solutes ($m^{in}$), the intracellular molalities of any permeating solutes ($m_p^{in}$), and the relative intracellular volumes of any permeating solutes which exhibit near-ideal volumetric

behaviour in solution ($V_p{}^{in}/V_{cell}^{o}$). All other parameters are fixed and characteristic of the physical system being modeled.

The solution to the model for a given set of parameters is the set of values for the unknowns that simultaneously satisfies all of the equations in the system. As the equilibrium cell volume is one of these unknowns, once the model is solved, the equilibrium cell volume can be obtained directly from the model solution.

In this work, the ultimate aim is to measure cell type-characteristic grouped solute osmotic virial coefficients. As such, we model the cell cytoplasm using the grouped solute approach—that is, we consider the intracellular solution to contain a single non-permeating solute (the grouped solute). Further, consistent with the experimental measurements described above, we model the extracellular solution as containing a concentration of NaCl (a non-permeating solute) that would, on its own, yield an isotonic solution plus a specified concentration of a permeating cryoprotectant—*i.e.*, either DMSO or EG. Note that any permeating solute that is present in the extracellular solution (*i.e.*, the cryoprotectant, DMSO or EG) may also enter the intracellular solution. Under these circumstances, employing the model described above (specifically, Equation 4.4), the intra- and extracellular osmolalities (*i.e.*, water chemical potentials) are

$$\begin{aligned}\pi^{in} = {} & m_p^{in} + m_g^{in} + B_{pp}\left(m_p^{in}\right)^2 + B_{gg}\left(m_g^{in}\right)^2 + \left(B_{pp} + B_{gg}\right)m_p^{in}m_g^{in} + C_{ppp}\left(m_p^{in}\right)^3 \\ & + 3\left(C_{ppp}{}^2 C_{ggg}\right)^{1/3}\left(m_p^{in}\right)^2 m_g^{in} + 3\left(C_{ppp}C_{ggg}{}^2\right)^{1/3} m_p^{in}\left(m_g^{in}\right)^2 \\ & + C_{ggg}\left(m_g^{in}\right)^3\end{aligned} \tag{4.13}$$

and

$$\pi^{ex} = m_p^{ex} + k_N m_N^{ex} + B_{pp}\left(m_p^{ex}\right)^2 + B_{NN}(k_N m_N^{ex})^2 + \left(B_{pp} + B_{NN}\right)m_p^{ex} k_N m_N^{ex}$$
$$+ C_{ppp}\left(m_p^{ex}\right)^3 + 3\left({C_{ppp}}^2 C_{NNN}\right)^{1/3}\left(m_p^{ex}\right)^2 k_N m_N^{ex} \quad (4.14)$$
$$+ 3\left(C_{ppp}{C_{NNN}}^2\right)^{1/3} m_p^{ex}(k_N m_N^{ex})^2 + C_{NNN}(k_N m_N^{ex})^3$$

respectively, where $m_g^{in}$ is the intracellular molality of the grouped solute $g$, $B_{gg}$ and $C_{ggg}$ are the second and third osmotic virial coefficients of the grouped solute, respectively (in [moles of grouped solute $g$/kg of water]$^{-1}$ and [moles of grouped solute $g$/kg of water]$^{-2}$, respectively), $m_N^{ex}$ is the extracellular molality of NaCl, $B_{NN}$ and $C_{NNN}$ are the second and third osmotic virial coefficients of NaCl, respectively (in [moles of NaCl/kg of water]$^{-1}$ and [moles of NaCl/kg of water]$^{-2}$, respectively), $k_N$ is the dissociation constant of NaCl, and solute $p$ in this case is the permeating cryoprotectant (DMSO or EG). Similarly, the intra- and extracellular chemical potentials of the permeating cryoprotectant $p$ are (per Equation 4.5)

$$\mu_p^{in} = \theta_p + RT\left[\ln\left(M_1 m_p^{in}\right) + \left(B_{pp} + B_{gg}\right)m_g^{in} + \frac{3}{2}\left(C_{ppp}{C_{ggg}}^2\right)^{1/3}\left(m_g^{in}\right)^2\right], \quad (4.15)$$

and

$$\mu_p^{ex} = \theta_p + RT\left[\ln\left(M_1 m_p^{ex}\right) + \left(B_{pp} + B_{NN}\right)m_N^{ex} + \frac{3}{2}\left(C_{ppp}{C_{NNN}}^2\right)^{1/3}(m_N^{ex})^2\right], \quad (4.16)$$

respectively. As there is only one permeating cryoprotectant present (at a time), Equation 4.7 becomes

$$m_p^{in} M_p \rho_1 \left(\frac{V_{cell}}{V_{cell}^o} - b - \frac{{V_p}^{in}}{V_{cell}^o}\right) = \rho_p \frac{{V_p}^{in}}{V_{cell}^o}, \quad (4.17)$$

Finally, Equation 4.10 can be rewritten as

$$\frac{V_{cell}}{V_{cell}^o} = (1 - b)\frac{m_g^o}{m_g^{in}} + \frac{{V_p}^{in}}{V_{cell}^o} + b\,, \quad (4.18)$$

where $m_g^o$ is the intracellular molality of the grouped solute under isotonic conditions. Thus, to summarize once again, for the purposes of this work, the specific model of equilibrium cell volume used consists of Equations 4.13 and 4.14 in Equation 4.6 (giving Equation 4.19 as listed in Table 4.3), Equations 4.15 and 4.16 in Equation 4.2 (giving Equation 4.20 as listed in Table 4.3), and Equations 4.17 and 4.18. The organization of this specific model is summarized in Table 4.3.

### 4.5. Sensitivity of model predictions to $b$, $B_{gg}$, and $C_{ggg}$

As noted above, the technique for measuring grouped solute osmotic virial coefficients previously developed by Ross-Rodriquez *et al.* [118] does not provide precise enough values of the coefficients for use with models of osmotic response in the presence of permeating cryoprotectants. This problem can be illustrated—and explained—using the above-described model of equilibrium cell volume (*i.e.*, the equations in Table 4.3).

To begin, it should be noted that the Ross-Rodriquez *et al.* technique is fundamentally similar to the one described in this work, except in that their technique involves fitting exclusively to solutions containing only non-permeating solutes, whereas the technique here involves fitting to both solutions of non-permeating solutes as well as solutions containing a permeating solute (*i.e.*, the cryoprotectant). As such, the Ross-Rodriquez *et al.* technique essentially uses only conditions 1 and 4 in Table 4.3 (*i.e.*, Equations 4.19 and 4.18, respectively), while the technique described herein uses all four conditions in Table 4.3.

The problem with using only non-permeating solute data to fit for the grouped solute osmotic virial coefficients (along with the osmotically inactive fraction) can be demonstrated by considering the effect of varying each of these fitting parameters on the model's equilibrium cell volume predictions, all other parameters held constant—*i.e.*, by examining the sensitivity of the

model to $b$ and $B_{gg}$. First, consider a cell placed into a series of solutions containing only non-permeating solutes at progressively increasing osmolality. Figure 4.6 contains model predictions of relative equilibrium cell volume under such circumstances in two different scenarios. The predictions in Figure 4.6(a) represent the scenario where $B_{gg}$ and $C_{ggg}$ are held constant at zero (*i.e.*, such that the cytoplasm is thermodynamically ideal) and $b$ is varied across a range of values from 0.2 to 0.8. The predictions in Figure 4.6(b) represent the scenario where $b$ is held constant at a value of 0.4, $C_{ggg}$ is held constant at zero, and $B_{gg}$ is varied across a range of values from 0 to 10 [moles of grouped solute/kg water]$^{-1}$. It is apparent from comparing these two sets of predictions that changes in $b$ have a far greater effect on model predictions than changes in $B_{gg}$—that is, in the presence of only non-permeating solutes, the model is more sensitive to $b$ than to $B_{gg}$. In fact, under these circumstances, the model has very little sensitivity to $B_{gg}$: even in the most concentrated solution considered (3 osmol/kg), the difference between the relative cell volume predictions for $B_{gg} = 0$ and $B_{gg} = 10$ [moles of grouped solute/kg water]$^{-1}$ is less than 0.1. As such, fitting for $B_{gg}$ under these conditions—as is done in the Ross-Rodriquez *et al.* technique—is unlikely to yield precise results, as demonstrated in practice [118]. This is problematic because, as shown immediately below, the model of equilibrium cell volume is very sensitive to the value of $B_{gg}$ when a permeating solute is introduced.

Consider now a cell placed into a series of solutions consisting of a non-permeating isotonic solution to which a permeating cryoprotectant—DMSO—has been added at progressively increasing concentrations. Figure 4.7 contains model predictions of relative equilibrium cell volume under such circumstances in the same two scenarios as in Figure 4.6 above: the predictions in Figure 4.7(a) represent the scenario where $B_{gg}$ and $C_{ggg}$ are held constant at zero and $b$ is varied across a range of values from 0.2 to 0.8, and the predictions in Figure 4.7(b) represent the scenario

where $b$ is held constant at a value of 0.4, $C_{ggg}$ is held constant at zero, and $B_{gg}$ is varied across a range of values from 0 to 10 [moles of grouped solute/kg water]$^{-1}$. Here, it is apparent from comparing the two sets of predictions that the model is more sensitive to $B_{gg}$ than to $b$. In fact, small changes in $B_{gg}$—especially for values below 2 [moles of grouped solute/kg water]$^{-1}$—can result in large changes not only in volume predictions, but also in the general trend of predictions as the DMSO concentration increases. Therefore, imprecision in the measurement of $B_{gg}$ can have a considerable impact on the accuracy of volume predictions when permeating cryoprotectants are present. That being said, the sensitivity of the model to $B_{gg}$ under such conditions can also be an advantage, as it means that fitting the model to experimental measurements of cell volume in the presence of permeating cryoprotectants—as is done in this work—should yield more precise values of $B_{gg}$ than using only measurements in the presence of non-permeating solutes.

One can also examine the effect of varying $C_{ggg}$ on model predictions. Figure 4.8 contains model predictions of equilibrium cell volume under the same conditions as for Figure 4.7(b) above, with $b$ still held constant at a value of 0.4, but where $B_{gg}$ and $C_{ggg}$ are both varied across a range of values (0 to 10 [moles of grouped solute/kg water]$^{-1}$ and 0 to 60 [moles of grouped solute/kg water]$^{-2}$, respectively). The general trends exhibited in Figures 4.7b and 4.8 are that increasing the value of $B_{gg}$ tends to decrease the predicted volume, while increasing the value of $C_{ggg}$ tends to attenuate the effect of $B_{gg}$.

### 4.6. Numerical and statistical methods

Fitting the above model of equilibrium cell volume—which yields the volume predictions $V_{cell}$—to experimental measurements of equilibrium cell volume—hereafter symbolized by $V_{cell}^{exp}$—essentially means finding the values of the osmotically inactive fraction $b$ and the grouped

solute osmotic virial coefficients $B_{gg}$ and (if necessary) $C_{ggg}$ that minimize the model's errors in predicting the experimental cell volume—*i.e.*, the values that minimize the difference between $V_{cell}$ and $V_{cell}^{exp}$. For a given cell type, the values of these three parameters—$b$, $B_{gg}$, and $C_{ggg}$—effectively characterize the solution thermodynamic behaviour of the cell cytoplasm. The overall fitting procedure is outlined in Figure 4.9.

*4.6.1. Quantification of error*

The first part of the procedure consists of determining the model prediction error of equilibrium cell volume associated with each set of values of $b$, $B_{gg}$, and $C_{ggg}$ in the range considered, calculated over all of the experimental measurements in a given data set (steps B–G in Figure 4.9). In this work, prediction error was quantified using root mean squared error (RMSE), defined as

$$RMSE = \sqrt{\frac{1}{n}\sum_{i=1}^{n}\left(y_{(i)} - \hat{y}_{(i)}\right)^2}, \tag{4.21}$$

where $n$ is the number of experimental data points, $y_{(i)}$ is the experimentally-measured value of the relative equilibrium cell volume at the *i*th data point $\left(V_{cell}^{exp}/V_{cell}^{o}\right)_i$, and $\hat{y}_{(i)}$ is the model prediction of the relative equilibrium cell volume at the *i*th data point $(V_{cell}/V_{cell}^{o})_i$.

RMSE values were obtained for predictions of equilibrium cell volume as compared to three sets of experimental measurements: one of HUVEC in the presence of only non-permeating solutes (data from Ross-Rodriguez *et al.* [118]), one of HUVEC in the presence of DSMO (data obtained in this work), and one of HUVEC in the presence of EG (data obtained in this work). The

range of values considered and the value resolutions used for $b$, $B_{gg}$, and $C_{ggg}$ are contained in Table 4.4. These ranges and resolutions were used for all three experimental data sets.

*4.6.2. Solution technique for model of equilibrium cell volume: vector-form Newton's method*

For each set of values of $b$, $B_{gg}$, and $C_{ggg}$, model predictions of relative equilibrium cell volume were calculated by applying Newton's method (in its vector form) [49,113] to solve the system of equations formed by Equations 4.19, 4.20, 4.17, and 4.18 (*i.e.*, the model of equilibrium cell volume) for each experimental data point. As a general numerical approach, the vector form of Newton's method allows one to solve a system of equations of the form $\vec{f}(\vec{x};\vec{c}) = 0$, where $\vec{x}$ are the system unknowns and $\vec{c}$ are the system parameters. Briefly, the method involves the iterative application of the following equation

$$\vec{x}^{(k+1)} = \vec{x}^{(k)} - \left[\underline{J}^{(k)}\right]^{-1} \vec{f}^{(k)} \tag{4.22}$$

where $k$ is the iteration number, such that $\vec{x}^{(k)}$ is the $k$th guess for $\vec{x}$, and $\underline{J}$ is the Jacobian matrix, defined as

$$\underline{J} = \begin{bmatrix} \frac{df_1}{dx_1} & \cdots & \frac{df_1}{dx_n} \\ \vdots & \ddots & \vdots \\ \frac{df_n}{dx_1} & \cdots & \frac{df_n}{dx_n} \end{bmatrix}, \tag{4.23}$$

where $x_1$, $x_2$,… $x_n$ are the unknown values and $n$ is the total number of unknowns (and correspondingly, the total number of equations in the system). Equation 4.22 is applied until one or more convergence criteria are satisfied. Two possible convergence criteria—both of which were used in this work—are

$$\text{norm}\left(\vec{x}^{(k+1)} - \vec{x}^{(k)}\right) \leq \epsilon \tag{4.24}$$

and

$$\text{norm}\left(\vec{f}^{(k)}\right) \leq \epsilon \tag{4.25}$$

where $\epsilon$ is a maximum allowable error and $\text{norm}(\vec{x})$ refers to the magnitude, or norm, of a vector $\vec{x}$, defined as

$$\text{norm}(\vec{x}) = \sqrt{\sum_{i}^{n} {x_i}^2}\,. \tag{4.26}$$

The first of these criteria (Equation 4.24) is effectively satisfied when two consecutive guesses for the unknowns $\vec{x}$ are the same (within allowable error), while the second criterion (Equation 4.25) is satisfied when there is a guess for the unknowns that makes all the equations $\vec{f}$ in the system true (again, within allowable error). In the context of this work, Equations 4.19, 4.20, 4.17, and 4.18 can be respectively rewritten into the format $\vec{f}(\vec{x};\vec{c}) = [f_1\,,\quad f_2\,,\quad f_3\,,\quad f_4] = 0$ as follows:

$$\begin{aligned} f_1 = \Big[ & m_p^{in} + m_g^{in} + B_{pp}\left(m_p^{in}\right)^2 + B_{gg}\left(m_g^{in}\right)^2 + \left(B_{pp} + B_{gg}\right)m_p^{in}m_g^{in} + C_{ppp}\left(m_p^{in}\right)^3 \\ & + 3\left({C_{ppp}}^2 C_{ggg}\right)^{\frac{1}{3}}\left(m_p^{in}\right)^2 m_g^{in} + 3\left(C_{ppp}{C_{ggg}}^2\right)^{\frac{1}{3}} m_p^{in}\left(m_g^{in}\right)^2 \\ & + C_{ggg}\left(m_g^{in}\right)^3 \Big] \\ & - \Big[ m_p^{ex} + k_N m_N^{ex} + B_{pp}\left(m_p^{ex}\right)^2 + B_{NN}(k_N m_N^{ex})^2 \\ & + \left(B_{pp} + B_{NN}\right)m_p^{ex}k_N m_N^{ex} + C_{ppp}\left(m_p^{ex}\right)^3 \\ & + 3\left({C_{ppp}}^2 C_{NNN}\right)^{1/3}\left(m_p^{ex}\right)^2 k_N m_N^{ex} \\ & + 3\left(C_{ppp}{C_{NNN}}^2\right)^{1/3} m_p^{ex}(k_N m_N^{ex})^2 + C_{NNN}(k_N m_N^{ex})^3 \Big] = 0\,, \end{aligned} \tag{4.27}$$

$$f_2 = \left[\ln\left(M_1 m_p\right) + \left(B_{pp} + B_{gg}\right) m_g^{in} + \frac{3}{2}\left(C_{ppp} {C_{ggg}}^2\right)^{\frac{1}{3}} \left(m_g^{in}\right)^2\right] - \left[\ln\left(M_1 m_p\right) + \left(B_{pp} + B_{NN}\right) k_N m_N^{ex} + \frac{3}{2}\left(C_{ppp} {C_{NNN}}^2\right)^{1/3} \left(k_N m_N^{ex}\right)^2\right] = 0\,, \tag{4.28}$$

$$f_3 = m_p^{in} M_p \rho_1 \left(\frac{V_{cell}}{V_{cell}^o} - b - \frac{{V_p}^{in}}{V_{cell}^o}\right) - \rho_p \frac{{V_p}^{in}}{V_{cell}^o} = 0\,, \tag{4.29}$$

and

$$f_4 = \frac{V_{cell}}{V_{cell}^o} - (1 - b)\frac{m_g^o}{m_g^{in}} - \frac{{V_p}^{in}}{V_{cell}^o} - b = 0\,. \tag{4.30}$$

The unknowns in these equations are $\vec{x} = \left[V_{cell}/V_{cell}^o\,,\ \ m_g^{in}\,,\ \ m_p^{in}\,,\ \ {V_p}^{in}/V_{cell}^o\right]$. These unknowns, along with all model parameters, corresponding units, and—where applicable—known constant values, are listed in Table 4.5.

One of the model parameters—the intracellular molality of the grouped solute under isotonic conditions, $m_g^o$—requires some additional explanation. Although this parameter is a constant for the purposes of the model of equilibrium cell volume, its value depends on the values of $B_{gg}$ and $C_{ggg}$. As such, this value must be calculated prior to predicting any equilibrium cell volumes for each set of $b$, $B_{gg}$, and $C_{ggg}$ (step D).

The value of $m_g^o$ can be obtained by finding the concentration of the grouped solute that, in the absence of any other intracellular solutes, would set the intracellular osmolality to its physiologically isotonic value. This concentration will depend on the values of $B_{gg}$ and $C_{ggg}$ because these parameters characterize the thermodynamic behaviour of the grouped solute, and thus the relationship between concentration and osmolality. Mathematically, the required concentration is that which satisfies

$$f\left(m_g^o\right) = m_g^o + B_{gg}\left(m_g^o\right)^2 + C_{ggg}\left(m_g^o\right)^3 - \pi^o = 0\,, \tag{4.31}$$

where $\pi^o$ is the isotonic osmolality (0.3 osmoles/kg). As such, the required value can be obtained by solving Equation 4.31 for $m_g^o$, which can be accomplished using the Newton method as outlined in Equation 4.22 (except for a single equation instead of for a system of equations—in this case, the Jacobian simplifies to the derivative $df/dm_g^o$).

Note also that there are other parameters in Table 4.5 without known values given: $m_p^{ex}$, $b$, $B_{gg}$, and $C_{ggg}$. Of these, $m_p^{ex}$ is defined by the experiment being modeled (and thus will have one of the experimental values: 0.5, 1.0, 1.5, 2.0, 2.5, or 3.0 molal), while $b$, $B_{gg}$, and $C_{ggg}$ are fitting parameters, the values of which will fall within the ranges set out in Table 4.4.

Another complication to solving for equilibrium cell volume arises from the Newton method's requirement for an initial guess for the unknowns $\vec{x}$—*i.e.*, an iteration where $k = 0$ in Equation 4.22. Unfortunately, the system defined herein by Equations 4.27 to 4.30 is highly sensitive to the values of the initial guess, and will not converge to an answer unless that guess is sufficiently close to the actual solution. This issue is further exacerbated by the fact that the solution values of the unknowns can vary widely depending on the system parameters. Since the solution values are, by definition, not known in advance, this set of circumstances can lead to a situation where the system cannot be solved without an impractical number of attempts with different initial guesses: without an appropriate initial guess, one cannot find the solution, but without the solution, it is extremely difficult and time-consuming to choose an appropriate initial guess. This impracticality is all the greater given the large number of times that the system must be solved (*i.e.*, for each data point for each set of values of $b$, $B_{gg}$, and $C_{ggg}$). To counteract this problem, we have developed an adaptive initial guess algorithm, which numerically finds the

appropriate initial guess for the unknowns for each set of system parameters (step E in Figure 4.9). This algorithm is outlined in Figure 4.10.

### *4.6.3. Adaptive initial guess algorithm*

The adaptive initial guess algorithm can best be described using system states. Here, what is meant by a "state" is a complete and consistent set of values of all of the unknowns/variables and parameters in a system of equations. In other words, using the terminology from above (*e.g.,* see Equation 4.22), a state is a complete set of values for $\vec{x}$ and $\vec{c}$ that satisfy all equations $\vec{f}$ such that $\vec{f}(\vec{x};\vec{c}) = 0$. Within this context, a "solved" state is one for which both the parameters and the variables are known, while an "unsolved" state is one for which only the parameters are known, with the variables remaining to be solved for.

In the most general terms, given an unsolved target state for which a solution is desired, the adaptive initial guess algorithm starts with a known, completely solved state as an initial guess and then attempts to solve for the target state using Newton's method as described above. If this initial guess does not converge to the target state, then the algorithm uses a series of intermediate states to systematically approach the target state. For the purposes of this algorithm, an intermediate state "Y" between two other states "X" and "Z" is defined to be a state for which certain parameters have values that are intermediate between those of states X and Z. The parameters which are to have intermediate values in state Y are any which do not have the same value in state X as they do in state Z. Any method or scheme can be used to calculate the intermediate values; the simplest method—and the one used in this work—is to calculate the state Y intermediate value of each parameter to be halfway between the parameter's value in state X and that in state Z.

Assuming that the known state, when used as an initial guess, does not converge to the target state, the adaptive initial guess algorithm continues by finding an intermediate state "A" between the known state and the target state to which the known state, when used as an initial guess, does converge. This intermediate state A is then set to be the initial guess, and the algorithm attempts to solve for the target state. If unsuccessful, the algorithm finds another intermediate state "B" between intermediate state A and the target state to which intermediate state A, when used as an initial guess, does converge. Intermediate state B is then set to be the initial guess for the target state. If intermediate state B does not converge to the target state, then the iterative process continues until an intermediate state is found that, when used as an initial guess, does converge to the target state.

The adaptive initial guess algorithm was applied to the problem in this work—that is, solving the model contained in Equations 4.27–4.30—as follows. The known state here is the cell under isotonic conditions: the cell at its isotonic volume, the grouped solute at its isotonic molality (*i.e.*, that which gives the isotonic osmolality), and no cryoprotectant inside or outside the cell (*i.e.*, $m_p^{in} = m_p^{ex} = 0$). In this state, the values of the variables are $\vec{x} = \left[V_{cell}/V_{cell}^o\,,\quad m_g^{in}\,,\quad m_p^{in}\,,\quad {V_p}^{in}/V_{cell}^o\right] = [1\,,\quad m_g^o\,,\quad 0\,,\quad 0]$. The target state is the cell at equilibrium in the presence of the cryoprotectant (at its defined extracellular concentration $m_s^{ex}$). This state is unsolved. The parameter to be varied in the intermediate states is the only parameter that changes between the isotonic and target states: the extracellular molality of the cryoprotectant, $m_p^{ex}$.

As an example of how the algorithm would be employed here, take a hypothetical calculation of the equilibrium volume of HUVEC in the 4 molal DMSO solution used in this work. In this case, the known state would be HUVEC under isotonic conditions as maintained by HEPES

buffered saline (*i.e.*, NaCl) solution, and the target state would be HUVEC in HEPES plus 4 molal DMSO. The first step to solve this system would be to use the isotonic state as an initial guess to attempt to solve for the target state. If this were unsuccessful, then the isotonic state would be used as an initial guess to attempt to solve for an intermediate state of HUVEC in HEPES plus 2 molal DMSO. If this attempt were also unsuccessful, the foregoing step would be repeated but with an intermediate state of HUVEC in HEPES plus 1 molal DMSO. This process would continue, with the intermediate states moving closer and closer to the isotonic state (*i.e.*, to 0 molal DMSO), until the isotonic state could successfully be used as an initial guess. Assuming for the purposes of this example that the isotonic state could be successfully used as an initial guess in solving for the intermediate state of HUVEC in HEPES plus 1 molal DMSO, this intermediate state would become the new default initial guess, and would be used to attempt to solve for the target state. If this attempt were unsuccessful, then this new initial guess would be used to attempt to solve a series of intermediate states starting at HUVEC in HEPES plus 2.5 molal DMSO and moving progressively closer to 1 molal DMSO (*i.e.*, 1.75 molal DMSO, 1.375 molal DMSO, 1.1875 molal DMSO, …). A successful attempt here would lead to the corresponding intermediate state being designated the new default initial guess, and the entire process would repeat itself—starting with an attempt to solve for the target state—until an intermediate state could be found that, when used as an initial guess, would lead to a solution for the target state.

#### *4.6.4. Finding optimal values of b, $B_{gg}$, and $C_{ggg}$*

Once the RMSE has been calculated for each set of values of $b$, $B_{gg}$, and $C_{ggg}$ for all experimental data sets, the optimal set—or sets—of these values can be determined (step H in Figure 4.9). Optimal in this respect means those values of $b$, $B_{gg}$, and $C_{ggg}$ that minimize model

prediction errors in as wide a variety of solutions as possible. In this work, we have primarily distinguished between solutions that contain only non-permeating solutes and those that contain a permeating cryoprotectant. Accordingly, we have herein defined the optimal set of values of $b$, $B_{gg}$, and $C_{ggg}$ as being that which simultaneously minimizes the RMSE of model predictions in both of these types of solutions. Specifically, for a given permeating cryoprotectant (*i.e.*, one of either DMSO or EG in this work), the optimal values are those that minimize the *combined* RMSE ($RMSE_{COM}$) of the model predictions, defined as

$$RMSE_{COM} = RMSE_{NP} + RMSE_{PC}\,, \tag{4.32}$$

where $RMSE_{NP}$ is the RMSE of model predictions in non-permeating solute solutions and $RMSE_{PC}$ is the RMSE of model predictions in solutions containing the cryoprotectant of interest. It should be emphasized that under this definition, if measurements of equilibrium cell volume are made with more than one permeating cryoprotectant (as was done in this work), a set of optimal values will be obtained for each cryoprotectant, although—theoretically—these values should be the same.

As a basic approach to account for the uncertainty of the fit for the optimal values, error tolerance ranges were calculated for each fit. These error tolerance ranges consist of the absolute ranges of each of $b$, $B_{gg}$, and $C_{ggg}$ which correspond to predictions with RMSE values within a specified tolerance of the minimum combined RMSE obtained for the overall fit. That is, the error tolerance ranges are defined as $\left[b_{(\min)}, b_{(\max)}\right]$, $\left[B_{gg(\min)}, B_{gg(\max)}\right]$, and $\left[C_{ggg(\min)}, C_{ggg(\max)}\right]$, where $b_{(\min)}$ (or $B_{gg(\min)}$ or $C_{ggg(\min)}$) and $b_{(\max)}$ (or $B_{gg(\max)}$ or $C_{ggg(\max)}$) are—respectively—the minimum and maximum values of $b$ (or $B_{gg}$ or $C_{ggg}$) found within all those sets of $b$, $B_{gg}$, and $C_{ggg}$ for which the $RMSE_{COM}$ is less than or equal to (1 + the specified tolerance) times the overall minimum $RMSE_{COM}$ obtained for the fit.

## 4.7. Results and discussion

Figure 4.11 contains experimental measurements of equilibrium HUVEC volume in solutions of only non-permeating solutes (data provided by Lisa Ross-Rodriguez [unpublished], with majority of data published in Ross-Rodriguez *et al*. [118]), in solutions containing DMSO (data obtained in this work), and in solutions containing EG (data obtained in this work). This data is also tabulated in Tables 4.6 and 4.7. It should be noted that in both cryoprotectant solutions (Figure 4.11(b)), equilibrium cell volume initially decreases with increasing cryoprotectant concentration before reaching a lower limit. This behaviour is not consistent with ideal dilute model predictions (see Figure 4.7 above and Figure 4.12 below).

The model of equilibrium cell volume described above (see Table 4.3) was fit to the data in Figure 4.11 to find an optimal set of $b$ and $B_{gg}$ (with $C_{ggg} = 0$)—*i.e.*, a second-order fit—and of $b$, $B_{gg}$, and $C_{ggg}$—*i.e.*, a third-order fit—corresponding to each of DMSO and EG. The values of the coefficients obtained, along with the corresponding 15% error tolerance ranges for the second-order fits and 2.5% error tolerance ranges for the third-order fits, are contained in Table 4.8. A 15% error tolerance range was used for the second-order fits because this error tolerance range roughly corresponds to the 95% confidence interval obtained by Ross-Rodriguez *et al.* in their measurement of $B_{gg}$ for HUVEC (also a second-order fit) [118]. Specifically—as is shown in greater detail in Table 4.8—if the model of equilibrium cell volume described in this work is fit to only the experimental measurements of HUVEC in solutions of only non-permeating solutes (*i.e.*, the data in Figure 4.11(a)) as was done by Ross-Rodriguez *et al*. in their approach [118], then the optimum value of $B_{gg}$ and the corresponding 15% error tolerance range obtained approximately match the value of $B_{gg}$ and the corresponding 95% confidence interval obtained by

Ross-Rodriguez *et al*. [118]. The discrepancy between the value of $B_{gg}$ obtained in this work as compared to the one obtained by Ross-Rodriquez *et al.* (*i.e.*, 2.8 versus 2.4 [moles of grouped solute/kg water]$^{-1}$) can likely be attributed to the different measures of goodness of fit used—RMSE here and adjusted $R^2$ in Ross-Rodriquez *et al.*'s approach [118]—and to the fact that the fitting resolution for $b$ in this work was limited to a value of 0.01 (see Table 4.4).

The 15% error tolerance ranges of the second-order fits for $B_{gg}$ contained in Table 4.8 are an order of magnitude lower than the 15% error tolerance range obtained from fitting to only the non-permeating solute data (see above) and—accordingly—than the corresponding 95% confidence intervals obtained by Ross-Rodriguez *et al*. in their measurements [118]. These results indicate that the novel technique developed in this work for measuring grouped intracellular solute osmotic virial coefficients has considerably greater precision than the previous method used by Ross-Rodriguez *et al*. That said, it should also be noted that—with one exception—the second-order values measured in this work using the novel technique do agree with the (second-order) values obtained by Ross-Rodriguez *et al*. within the measure of error used in that work (*i.e.*, the 95% confidence intervals). The one exception is the value of $b$ obtained from fitting to the EG data: 0.54. This value falls just outside of Ross-Rodriguez *et al*.'s 95% confidence interval for $b$ of [0.514, 0.534] [118].

The third-order results in Table 4.8 demonstrate that even with a 2.5% error tolerance range, the third-order fits to the DMSO and EG data overlap for all coefficients—that is, each of the best-fit coefficient values for each data set falls within the 2.5% error tolerance range of the corresponding fit in the other data set. This outcome—*i.e.*, similar/overlapping values obtained from two different data sets—is consistent with the thermodynamic theory underpinning the models used in this work.

Figure 4.12 shows the second- and third-order model fits to the experimental data—as represented by the coefficients in Table 4.8—for both the DMSO and EG solutions, and also contains *predictions of—i.e.*, not fits to—the data made using the values of $b$ and $B_{gg}$ obtained by Ross-Rodriquez *et al.*, as well as corresponding predictions made using an ideal dilute model. For the ideal model predictions, the model of equilibrium cell volume was fit to the measurements made in solutions of only non-permeating solutes (*i.e.*, Figure 4.11(a)) with $B_{gg}$ and $C_{ggg}$ set to zero in order to acquire a value of $b$ only. The value of $b$ so obtained—0.60—was then used in the model (with $B_{gg} = C_{ggg} = 0$) to make equilibrium cell volume predictions in the DMSO and EG solutions.

From the results in Figure 4.12, it is clear that a non-ideal model of equilibrium cell volume—*i.e.*, a model that incorporates the Elliott *et al*. form of the multi-solute osmotic virial equation—is required to capture the volumetric behaviour of HUVEC exposed to the DMSO and EG solutions considered in this work. The ideal dilute approach does not—and, from an examination of Figure 4.7, regardless of the value of $b$ used, cannot—allow for a decrease in equilibrium cell volume with increasing permeating cryoprotectant concentration. As such, for cells such as HUVEC which have a thermodynamically non-ideal cytoplasm, the use of only an ideal dilute model can introduce considerable error in the prediction of cell volumes where permeating cryoprotectants are present. Under such circumstances, a non-ideal model, such as the one described in this work, should be applied.

Figure 4.12 also clearly displays the deleterious effect of a lack of precision in the measurement of $B_{gg}$. The shaded areas on the graphs correspond to predictions that fall within the 95% confidence intervals for $B_{gg}$ measured by Ross-Rodriguez *et al*. [118]. The relatively large size of these areas—and the fact that they encompass the possibility of both an increase and

a decrease in volume with increasing cryoprotectant concentration—demonstrate that the measurement technique used by Ross-Rodriguez *et al*. does not yield values of $B_{gg}$ precise enough for use in modeling of cell behaviour in the presence of permeating cryoprotectants. Conversely, the purple shaded areas on the graphs in Figure 4.12 correspond to predictions that wall within the 15% error tolerance ranges for $B_{gg}$ measured in this work for a second-order fit. These areas are much smaller than the green areas, reflecting the increased precision of the new method.

Finally, as would be expected, the results in Figure 4.12 demonstrate that—for both the DMSO and EG data—the third-order fits obtained in this work are better (*i.e.*, more accurate) than the corresponding second-order fits (this outcome is also quantitatively reflected in lower $RMSE_{COM}$ values for the third-order fits as compared to the corresponding second-order fits). As such, we would recommend using the coefficients from the third-order fits when modeling HUVEC osmotic behaviour. While the third-order fits to the two data sets do not yield identical coefficients (see Table 4.8), as noted above, the values are within each other's 2.5% error tolerance ranges. Accordingly, we would further recommend using the averages of the values obtained for each coefficient from the two third-order fits—*i.e.*, $b = 0.43$, $B_{gg} = 3.0$ [moles of grouped solute/kg water]$^{-1}$, and $C_{ggg} = 20.8$ [moles of grouped solute/kg water]$^{-2}$.

*4.7.1. Effect of cytoplasm non-ideality on predictions of kinetic osmotic response*

The thermodynamic non-ideality of the cytoplasm can also have an impact on kinetic models of cell behaviour when exposed to permeating solutes. Consider, for example, the kinetic osmotic response of a cell when a permeating cryoprotectant such as DMSO is first added, and then removed. The cell behaviour in this situation can be predicted using the following form of the

two-parameter model [27,53,54,84], which accounts for the osmotic transport of both water and of permeating solutes using

$$\frac{dN_1}{dt} = \frac{L_1 A_{cell} {\rho_1}^2 RT}{M_1}\left(\pi^{in} - \pi^{ex}\right) \tag{4.33}$$

and

$$\frac{dN_p}{dt} = P_p A_{cell}\left(a_p^{ex} - a_p^{in}\right), \tag{4.34}$$

respectively, where $N_1$ is the intracellular number of moles of water, $N_p$ is the intracellular number of moles of the permeating cryoprotectant, $t$ is time (in minutes), $A_{cell}$ is the cell surface area (in μm$^2$), $L_1$ is the hydraulic conductivity of the cell (in μm/min/atm), $P_p$ is the permeability of the cell to the permeating cryoprotectant (in μm/min), and $a_p$ is the activity of the permeating cryoprotectant. $L_1$ and $P_p$ are cell-specific permeability parameters that are generally obtained by curve-fitting to experimental measurements of cellular kinetic osmotic response [27,117].

Activity is a thermodynamic property similar to chemical potential; for any given species *i* the two are related by [102]

$$RT \ln a_i = \mu_i - \mu_i^o, \tag{4.35}$$

where $\mu_i^o$ is the chemical potential of species *i* at an arbitrarily-chosen standard state. To combine the Elliott *et al.* form of the multi-solute osmotic virial equation—and, specifically, the solute chemical potential calculation in Equation 4.5—with Equation 4.35 in order to calculate the activity of a given cryoprotectant *p*, one can choose a standard state of a binary aqueous solution of the cryoprotectant at the same temperature and pressure as the cell being modeled, and at a concentration $m_p^o$ such that

$$\ln\left(M_1 m_p^o\right) + 2B_{pp} k_p m_p^o + \frac{3}{2} C_{ppp}\left(k_p m_p^o\right)^2 = 0. \tag{4.36}$$

Then, recalling that $\theta_p$ is a function of temperature and pressure only, substituting Equations 4.5 and 4.36 into Equation 4.35, and simplifying and rearranging yields

$$a_p = \exp\left[k_p\left[\ln\left(M_1 m_p\right) + \sum_{i=2}^{r}\left[\left(B_{ii} + B_{pp}\right)k_i m_i\right] + \frac{3}{2}\sum_{i=2}^{r}\sum_{j=2}^{r}\left[\left(C_{iii}C_{jjj}C_{ppp}\right)^{1/3}k_i m_i k_j m_j\right]\right]\right]. \tag{4.37}$$

As has been noted elsewhere [151], the standard state for a solute in the Elliott *et al.* model—represented by Equation 4.36 here—is a function of that solute's osmotic virial coefficients (*i.e.*, $B_{pp}$ and $C_{ppp}$).

The surface area of the cell $A_{cell}$ can be related to the cell volume using the spherical cell assumption, and the cell volume at any time is given by the sum of the volumes of intracellular water, intracellular permeating cryoprotectant, and the osmotically inactive fraction, that is,

$$V_{cell}(t) = \frac{M_1 N_1(t)}{\rho_1} + \frac{M_p N_p(t)}{\rho_p} + bV_{cell}^{o}\,. \tag{4.38}$$

To demonstrate the effect of cytoplasm non-ideality, the above model of kinetic osmotic response (*i.e.*, Equations 4.33 and 4.34) was applied to the specific situation where a cell with the same permeability parameters as a TF-1 cell is exposed to a 2 molal solution of DMSO for 10 minutes, and then immediately returned to an isotonic solution (*i.e.*, with no DMSO) for another 10 minutes. The resulting model predictions are contained in Figure 4.13. Solution osmolality and the chemical potential of DMSO were calculated using the Elliott *et al*. form of the multi-solute osmotic virial equation (*i.e.*, Equations 4.4 and 4.5), and the values of $B_{gg}$ and $C_{ggg}$ for the cell were varied from 0 to 8 [moles of grouped solute/kg water]$^{-1}$ and 0 to 80 [moles of grouped solute/kg water]$^{-2}$, respectively. All other relevant parameters for TF-1 were those measured by

Ross-Rodriguez *et al*. [117] at a temperature of 11 °C (284 K) and are summarized here in Table 4.9. Equations 4.33 and 4.34 were solved using the explicit adaptive Runge-Kutta-Fehlberg method for ordinary differential equations [114], with an initial step size of 0.00025 minutes.

Figure 4.13 clearly demonstrates that the value of $B_{gg}$ can have a considerable effect on model predictions of osmotic response, particularly upon cryoprotectant removal. Notably, all else held constant, the higher the value of $B_{gg}$, the lower the maximum volume reached on cryoprotectant removal. In fact, for the situation modeled here, $B_{gg}$ values above a minimum threshold (*e.g.*, $B_{gg} \geq 3$ [moles of grouped solute/kg water]$^{-1}$ for $C_{ggg} = 0$ [moles of grouped solute/kg water]$^{-2}$) actually resulted in the cell not swelling beyond its isotonic volume when the cryoprotectant was removed. The implications of this effect are particularly relevant to the use of modeling to avoid cell damage from excessive volume excursions (*i.e.*, exceeding osmotic tolerance limits) during cryopreservation [12,13,39,52,64]. Although the value of $C_{ggg}$ also affects model predictions, it has less of an impact than $B_{gg}$. Notably, as $C_{ggg}$ increases, the above-noted minimum threshold of $B_{gg}$ to avoid cell volume swelling above isotonic on cryoprotectant removal shifts to higher $B_{gg}$ values.

## 4.8. Conclusions

In this work, we have developed a novel method of measuring cell-specific grouped intracellular solute osmotic virial coefficients, along with the corresponding osmotically inactive fraction, using experimental measurements of equilibrium cell volume in solutions of non-permeating solutes and in solutions containing a permeating solute. These parameters can together completely characterize the composition-dependent non-ideal solution thermodynamic behaviour

of the cytoplasm. As such, they allow mathematical models of cellular osmotic behaviour to account for solution non-ideality, even inside the cell where the exact composition is not known.

Applying the method developed herein, we have obtained the grouped intracellular solute osmotic virial coefficients and osmotically inactive fraction for HUVEC using two different sets of experimental measurements of cell volume: in non-permeating solute solutions + DMSO solutions, and in non-permeating solute solutions + EG solutions. Our measurements clearly indicate that the cytoplasm of HUVEC is not ideal, and—accordingly—that the volumetric behaviour of HUVEC in the presence of permeating cryoprotectants cannot be effectively modeled using an ideal dilute approach. Our recommendation for applying these measurements to predict HUVEC osmotic behaviour is to use the non-ideal model described herein with the average values of the third order fits to the two data sets—*i.e.*, $b = 0.43$, $B_{gg} = 3.0$ [moles of grouped solute/kg water]$^{-1}$, and $C_{ggg} = 20.8$ [moles of grouped solute/kg water]$^{-2}$.

We have also shown that when modeling cellular osmotic behaviour in the presence of permeating solutes such as the cryoprotectants DMSO and EG, the values of the grouped intracellular solute osmotic virial coefficients can have a considerable impact on model predictions. For example, when modeling the kinetic cell response to cryoprotectant removal, an ideal dilute cytoplasm model (*i.e.*, grouped intracellular solute osmotic virial coefficients of zero) may predict swelling 50% above the isotonic volume, where a model corresponding to a reasonably non-ideal cytoplasm may predict no swelling at all. As such, it is important in such scenarios that the values of these grouped solute coefficients be both accurate and precise; otherwise, the predictions can veer far off course. Our results here indicate that the novel method we have developed for measuring these coefficients yields more precise values than the previously

existing method developed by Ross-Rodriguez *et al*. As such, our new measurement technique will allow for more effective modeling of osmotic behaviour.

However, it is important to note that modeling the full range of cellular osmotic behaviour while incorporating non-ideal solution thermodynamics will require more than just the measurements described in this work. In order to model the *kinetic* osmotic response for a cell type of interest, one must know not only the given cell type's grouped intracellular solute osmotic virial coefficients and osmotically inactive fraction, but also the hydraulic conductivity $L_1$ and—for each permeating cryoprotectant of interest—the solute permeability $P_p$. These cell-specific permeability coefficients can only be obtained from non-equilibrium (*i.e.*, kinetic) measurements of cell volume. Thus, for the purposes of mathematical modeling, the complete characterization of a given cell type's osmotic behaviour will require fitting to both equilibrium and kinetic cell volume data.

Table 4.1. Experimental sampling order.

| Sample Order | Cryoprotectant Concentration Added | | |
|---|---|---|---|
| | **Experiment 1** | **Experiment 2** | **Experiment 3** |
| 1 | 0.5 molal | 1.5 molal | 2.5 molal |
| 2 | 1.0 molal | 2.0 molal | 3.0 molal |
| 3 | 1.5 molal | 2.5 molal | 0.5 molal |
| 4 | 2.0 molal | 3.0 molal | 1.0 molal |
| 5 | 2.5 molal | 0.5 molal | 1.5 molal |
| 6 | 3.0 molal | 1.0 molal | 2.0 molal |
| 7 | 0.5 molal | 1.5 molal | 2.5 molal |
| 8 | 1.0 molal | 2.0 molal | 3.0 molal |
| 9 | 1.5 molal | 2.5 molal | 0.5 molal |
| 10 | 2.0 molal | 3.0 molal | 1.0 molal |
| 11 | 2.5 molal | 0.5 molal | 1.5 molal |
| 12 | 3.0 molal | 1.0 molal | 2.0 molal |

Table 4.2. Overview of general model of equilibrium cell volume.

| Condition Number | Equation | Equation Number |
|---|---|---|
| 1 (always required once) | $\sum_{i=2}^{r} k_i m_i^{in} + \sum_{i=2}^{r}\sum_{j=2}^{r}\left[\frac{(B_{ii}+B_{jj})}{2} k_i m_i^{in} k_j m_j^{in}\right] + \sum_{i=2}^{r}\sum_{j=2}^{r}\sum_{k=2}^{r}\left[(C_{iii}C_{jjj}C_{kkk})^{1/3} k_i m_i^{in} k_j m_j^{in} k_k m_k^{in}\right] = \sum_{i=2}^{r} k_i m_i^{ex} + \sum_{i=2}^{r}\sum_{j=2}^{r}\left[\frac{(B_{ii}+B_{jj})}{2} k_i m_i^{ex} k_j m_j^{ex}\right] + \sum_{i=2}^{r}\sum_{j=2}^{r}\sum_{k=2}^{r}\left[(C_{iii}C_{jjj}C_{kkk})^{1/3} k_i m_i^{ex} k_j m_j^{ex} k_k m_k^{ex}\right]$ | 4.11 |
| 2 (one instance required for each permeating solute) | $\ln(M_1 m_p^{in}) + \sum_{i=2}^{r}\left[(B_{ii}+B_{pp}) k_i m_i^{in}\right] + \frac{3}{2}\sum_{i=2}^{r}\sum_{j=2}^{r}\left[(C_{iii}C_{jjj}C_{ppp})^{1/3} k_i (B_{ii}+B_{pp}) k_i m_i^{in} k_j m_j^{in}\right] = \ln(M_1 m_p^{ex}) + \sum_{i=2}^{r}\left[(B_{ii}+B_{pp}) k_i m_i^{ex}\right] + \frac{3}{2}\sum_{i=2}^{r}\sum_{j=2}^{r}\left[(C_{iii}C_{jjj}C_{ppp})^{1/3} k_i (B_{ii}+B_{pp}) k_i m_i^{ex} k_j m_j^{ex}\right]$ | 4.12 |
| 3 (one instance required for each permeating solute which exhibits near-ideal volumetric behaviour) | $m_p^{in} M_p \rho_1 \left(\frac{V_{cell}}{V_{cell}^o} - b - \frac{\sum {V_p}^{in}}{V_{cell}^o}\right) = \rho_p \frac{{V_p}^{in}}{V_{cell}^o}$ | 4.7 |
| 4 (always required once) | $\frac{V_{cell}}{V_{cell}^o} = (1-b)\frac{m^o}{m^{in}} + \frac{\sum {V_p}^{in}}{V_{cell}^o} + b$ | 4.10 |

Table 4.3. Overview of specific model of equilibrium cell volume used in this work.

| Condition Number | Equation | Equation Number |
|---|---|---|
| 1 | $m_p^{in} + m_g^{in} + B_{pp}\left(m_p^{in}\right)^2 + B_{gg}\left(m_g^{in}\right)^2 + \left(B_{pp} + B_{gg}\right)m_p^{in}m_g^{in} + C_{ppp}\left(m_p^{in}\right)^3 + 3\left(C_{ppp}{}^2 C_{ggg}\right)^{1/3}\left(m_p^{in}\right)^2 m_g^{in} + 3\left(C_{ppp}C_{ggg}{}^2\right)^{1/3} m_p^{in}\left(m_g^{in}\right)^2 + C_{ggg}\left(m_g^{in}\right)^3 = m_p^{ex} + k_N m_N^{ex} + B_{pp}\left(m_p^{ex}\right)^2 + B_{NN}(k_N m_N^{ex})^2 + \left(B_{pp} + B_{NN}\right)m_p^{ex}k_N m_N^{ex} + C_{ppp}\left(m_p^{ex}\right)^3 + 3\left(C_{ppp}{}^2 C_{NNN}\right)^{1/3}\left(m_p^{ex}\right)^2 k_N m_N^{ex} + 3\left(C_{ppp}C_{NNN}{}^2\right)^{1/3} m_p^{ex}(k_N m_N^{ex})^2 + C_{NNN}(k_N m_N^{ex})^3$ | 4.19 |
| 2 | $\ln\left(M_1 m_p^{in}\right) + \left(B_{pp} + B_{gg}\right)m_g^{in} + \frac{3}{2}\left(C_{ppp}C_{ggg}{}^2\right)^{1/3}\left(m_g^{in}\right)^2 = \ln\left(M_1 m_p^{ex}\right) + \left(B_{pp} + B_{NN}\right)m_N^{ex} + \frac{3}{2}\left(C_{ppp}C_{NNN}{}^2\right)^{1/3}(m_N^{ex})^2$ | 4.20 |
| 3 | $m_p^{in} M_p \rho_1 \left(\frac{V_{cell}}{V_{cell}^o} - b - \frac{V_p{}^{in}}{V_{cell}^o}\right) = \rho_p \frac{V_p{}^{in}}{V_{cell}^o}$ | 4.17 |
| 4 | $\frac{V_{cell}}{V_{cell}^o} = (1-b)\frac{m_g^o}{m_g^{in}} + \frac{V_p{}^{in}}{V_{cell}^o} + b$ | 4.18 |

Table 4.4. Minimum, maximum, and resolution values over which to search for optimal values of $b$, $B_{gg}$, and $C_{ggg}$ which best fit the data.

| Fitting Parameter | Minimum | Maximum | Resolution |
|---|---|---|---|
| $b$ | 0.20 | 0.80 | 0.01 |
| $B_{gg}$ | 0.0 [moles of grouped solute/kg water]$^{-1}$ | 10.0 [moles of grouped solute/kg water]$^{-1}$ | 0.1 [moles of grouped solute/kg water]$^{-1}$ |
| $C_{ggg}$ | 0.0 [moles of grouped solute/kg water]$^{-2}$ | 100.0 [moles of grouped solute/kg water]$^{-2}$ | 0.1 [moles of grouped solute/kg water]$^{-2}$ |

Table 4.5. Parameters and unknowns for equilibrium cell volume model.

| **System Parameters $\vec{c}$** | | |
|---|---|---|
| **Symbol** | **Parameter** | **Value(s) and Units (if applicable)** |
| $b$ | Osmotically inactive fraction | * |
| $B_{gg}$ | Second osmotic virial coefficient of grouped intracellular solute | *[moles of grouped solute/kg water]$^{-1}$ |
| $C_{ggg}$ | Third osmotic virial coefficient of grouped intracellular solute | *[moles of grouped solute/kg water]$^{-2}$ |
| $B_{pp}$ | Second osmotic virial coefficient of cryoprotectant (DMSO or EG) | For DMSO: 0.108 [moles DMSO/kg water]$^{-1}$ [154]<br>For EG: 0.020 [moles of EG/kg water]$^{-1}$ [154] |
| $C_{ppp}$ | Third osmotic virial coefficient of cryoprotectant (DMSO or EG) | For DMSO: 0 [moles of DMSO/kg water]$^{-2}$ [154]<br>For EG: 0 [moles of EG/kg water]$^{-2}$ [154] |
| $k_N$ | Dissociation constant of NaCl | 1.678 [154] |
| $B_{NN}$ | Second osmotic virial coefficient of NaCl | 0.044 [moles of NaCl/kg water]$^{-1}$ [154] |
| $C_{NNN}$ | Third osmotic virial coefficient of NaCl | 0 [moles of NaCl/kg water]$^{-2}$ [154] |
| $\rho_1$ | Density of water (at 25 °C) | 0.9970 $\times$ 10$^{-15}$ kg/μm$^3$ [119] |
| $M_1$ | Molar mass of water | 0.018015 kg/mol [119] |
| $\rho_p$ | Density of cryoprotectant | For DMSO (at 25 °C): 1.1010 $\times$ 10$^{-15}$ kg/μm$^3$ [120]<br>For EG (at 20 °C): 1.1135 $\times$ 10$^{-15}$ kg/μm$^3$ [120] |
| $M_p$ | Molar mass of cryoprotectant | For DMSO: 0.078133 kg/mol [120]<br>For EG: 0.062068 kg/mol [120] |
| $m_g^o$ | Intracellular molality of grouped solute under isotonic conditions | †moles of grouped solute/kg water |
| $m_p^{ex}$ | Extracellular molality of cryoprotectant | 0 to 3.0 moles of cryoprotectant/kg water as set by experimental condition |
| $m_N^{ex}$ | Extracellular molality of NaCl | 0.17 moles of NaCl/kg water |
| **System Unknowns $\vec{x}$** | | |
| **Symbol** | **Unknown** | **Units (if applicable)** |
| $V_{cell}/V_{cell}^o$ | Relative equilibrium cell volume | |
| $m_g^{in}$ | Intracellular molality of grouped solute | moles of grouped solute/kg water |
| $m_p^{in}$ | Intracellular molality of cryoprotectant | moles of cryoprotectant/kg water |
| $V_p{}^{in}/V_{cell}^o$ | Relative intracellular volume of cryoprotectant | |

* Value set by overall numerical procedure (step B in Figure 4.9).

† Calculated in advance for each set of values of $B_{gg}$ and $C_{ggg}$ using Equation 4.31 (step D in Figure 4.9).

Table 4.6. Experimental measurements of relative equilibrium HUVEC volume ($V_{cell}/V_{cell}^{o}$), with corresponding standard deviation (SD), in solutions of only non-permeating solutes (data from Ross-Rodriguez *et al*. [118]).

| **Solution Osmolality (osmol/kg)** | $\boldsymbol{V_{cell}/V_{cell}^{o}}$ **[± SD]** |
|---|---|
| 0.29 | 1.00 |
| 0.57 | 0.80 [±0.05] |
| 0.86 | 0.75 [±0.05] |
| 1.14 | 0.72 [±0.06] |
| 1.43 | 0.69 [±0.06] |
| 1.73 | 0.67 [±0.06] |
| 2.03 | 0.66 [±0.06] |
| 2.33 | 0.64 [±0.07] |
| 2.67 | 0.63 [±0.06] |

Table 4.7. Experimental measurements of relative equilibrium HUVEC volume ($V_{cell}/V_{cell}^{o}$), with corresponding standard deviation (SD), in solutions containing DMSO or EG.

| **Cryoprotectant Concentration (mole/kg)** | $\boldsymbol{V_{cell}/V_{cell}^{o}}$ **[± SD] in DMSO** | $\boldsymbol{V_{cell}/V_{cell}^{o}}$ **[± SD] in EG** |
|---|---|---|
| 0.0 | 1.00 | 1.00 |
| 0.5 | 0.93 [±0.06] | 0.93 [±0.05] |
| 1.0 | 0.91 [±0.03] | 0.89 [±0.06] |
| 1.5 | 0.87 [±0.07] | 0.88 [±0.03] |
| 2.0 | 0.85 [±0.04] | 0.86 [±0.03] |
| 2.5 | 0.83 [±0.05] | 0.84 [±0.04] |
| 3.0 | 0.85 [±0.05] | 0.85 [±0.04] |

Table 4.8. HUVEC grouped intracellular solute osmotic virial coefficients and osmotically inactive fraction, along with corresponding confidence intervals (CIs) (Ross-Rodriguez *et al*. fit [118]) or error tolerance ranges (ETRs) (this work). NPS data refers to equilibrium cell volume measurements in solutions containing only non-permeating solutes. DMSO data refers to equilibrium cell volume measurements in solutions containing DMSO. EG data refers to equilibrium cell volume measurements in solutions containing EG.

| **Second-Order Fit, Ross-Rodriguez *et al.*** [118] | | | |
|---|---|---|---|
| **Description of Fit** | $b$ **±95% Confidence Interval** | $B_{gg}$ **±95% CI ([moles of grouped solute/kg water]$^{-1}$)** | $C_{ggg}$ **([moles of grouped solute/kg water]$^{-2}$)** |
| **To NPS Data Alone** | 0.524±0.010 | 2.4±1.9 | 0 |
| **Second-Order Fits, This Work** | | | |
| **Description of Fit** | $b$ **[15% ETR]** | $B_{gg}$ **[15% ETR] ([moles of grouped solute/kg water]$^{-1}$)** | $C_{ggg}$ **([moles of grouped solute/kg water]$^{-2}$)** |
| **To NPS Data Alone** | 0.52 [0.50, 0.55] | 2.8 [1.0, 6.2] | 0 |
| **To NPS + DMSO Data** | 0.53 [0.52, 0.55] | 1.7 [1.6, 1.8] | 0 |
| **To NPS + EG Data** | 0.54 [0.52, 0.55] | 1.5 [1.4, 1.7] | 0 |
| **Third-Order Fits, This Work** | | | |
| **Description of Fit** | $b$ **[2.5% ETR]** | $B_{gg}$ **[2.5% ETR] ([moles of grouped solute/kg water]$^{-1}$)** | $C_{ggg}$ **[2.5% ETR] ([moles of grouped solute/kg water]$^{-2}$)** |
| **To NPS + DMSO Data** | 0.42 [0.38, 0.45] | 3.3 [2.7, 4.6] | 23.9 [10.4, 79.2] |
| **To NPS + EG Data** | 0.43 [0.38, 0.46] | 2.7 [2.2, 4.0] | 17.6 [7.2, 75.4] |

Table 4.9. TF-1 parameters used for kinetic modeling of osmotic response in the presence of DMSO. All values were measured by Ross-Rodriguez *et al*. at 11 °C (284 K) [117].

| **Symbol** | **Parameter** | **Value and Units** |
|---|---|---|
| $T$ | Absolute temperature | 284 K |
| $V_{cell}^{o}$ | Isotonic volume | 916 μm$^3$ |
| $b$ | Osmotically inactive fraction | 0.368 |
| $L_1$ | Hydraulic conductivity | 0.17 μm/min/atm |
| $P_{DMSO}$ | DMSO permeability | 6.00 μm/min |

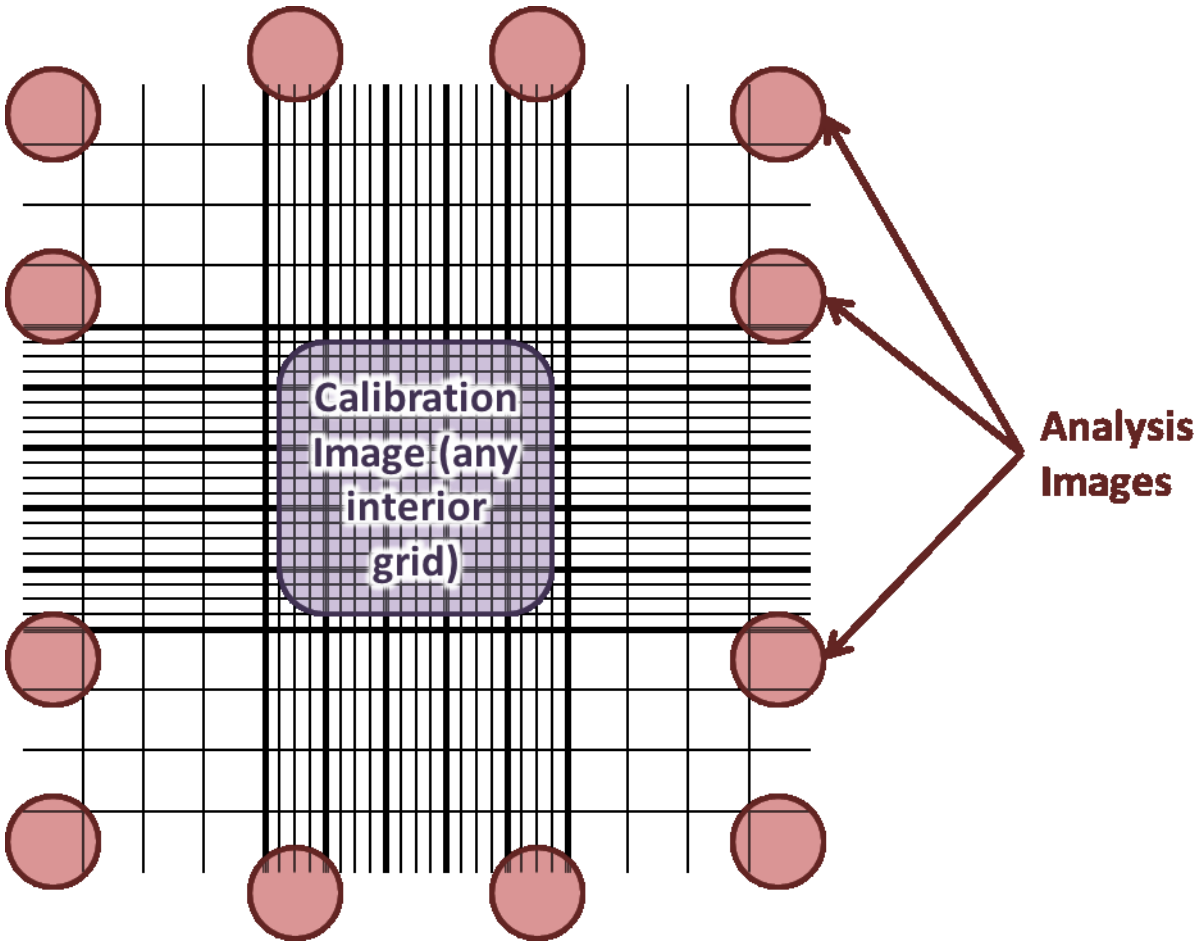


Figure 4.1. Photo locations on haemocytometer grid.

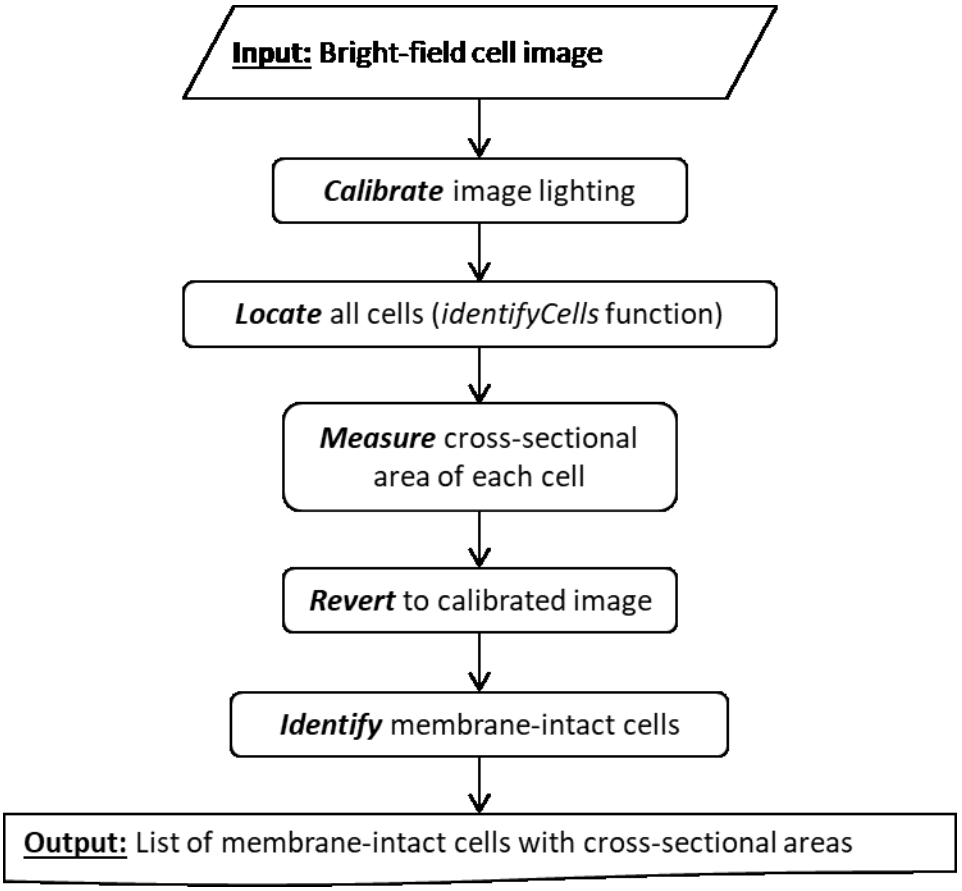


Figure 4.2. Image analysis procedure used to obtain cell cross-sectional area (and thus volume).

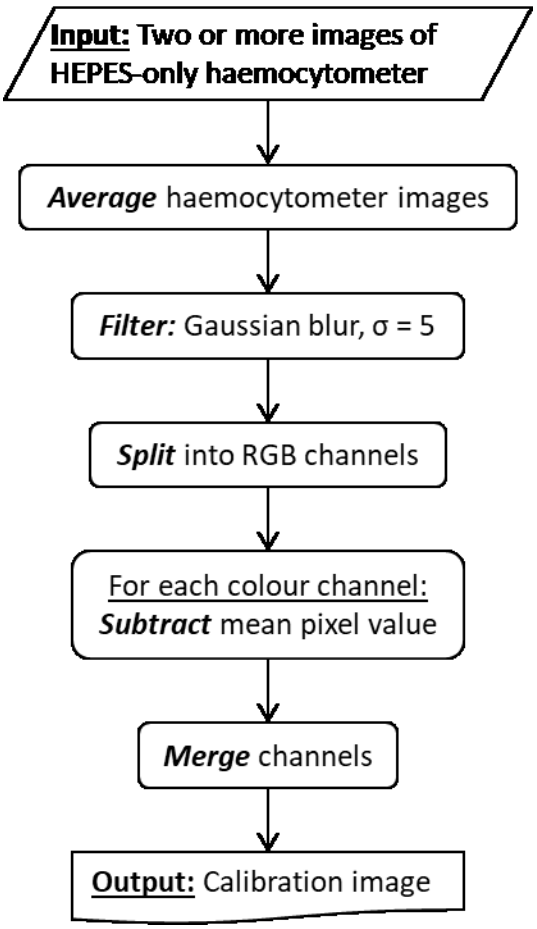


Figure 4.3. Procedure used to create calibration image for image analysis.

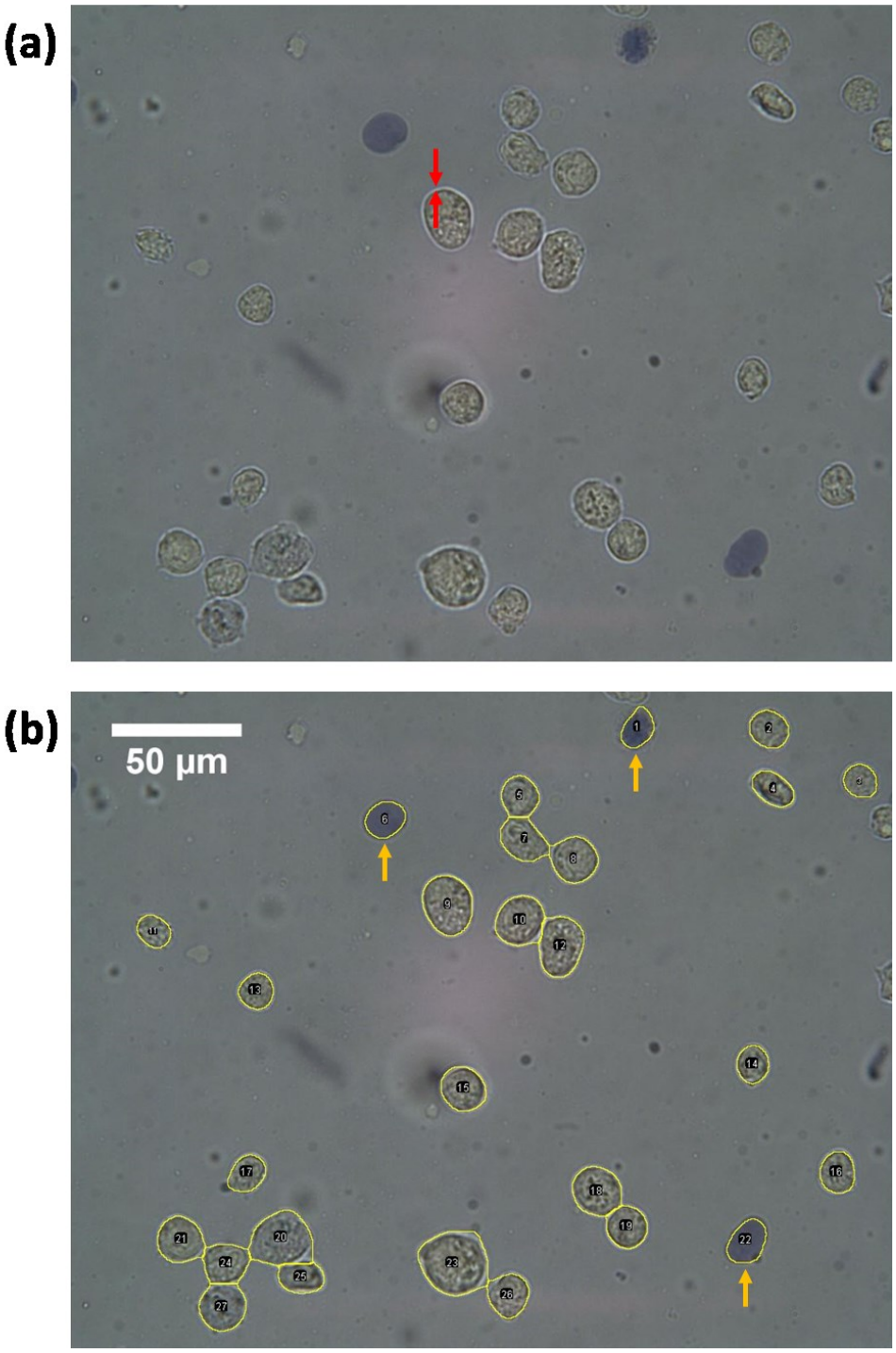


Figure 4.4. Representative example image depicting cell identification by the ImageJ macro used in this work. (a) Image input to macro. The red arrows denote an example of a cell "halo." (b) Macro output. The yellow borders correspond to identified cell edges. The cells marked with orange arrows were identified as membrane-compromised.

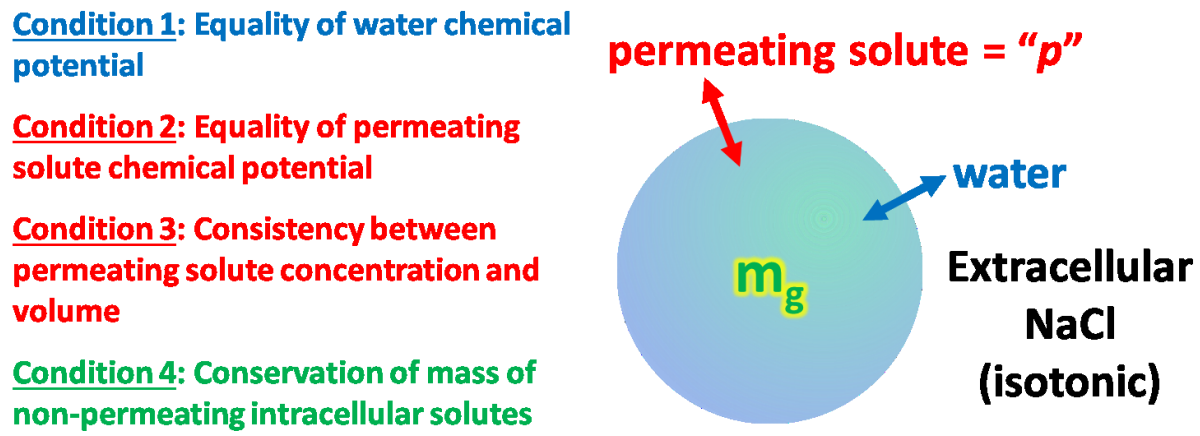


Figure 4.5. Schematic representation of the general model of equilibrium cell volume.

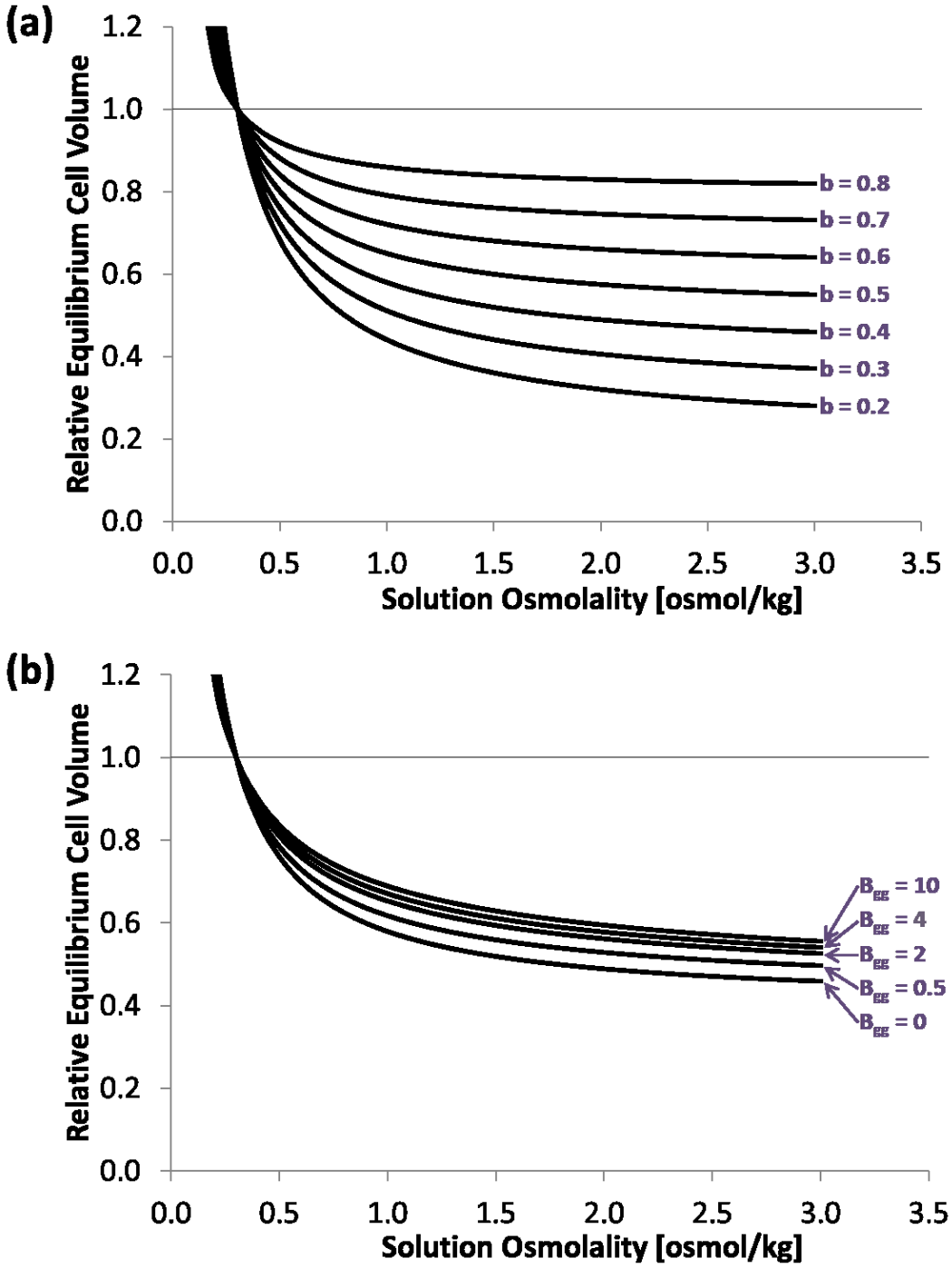


Figure 4.6. Model predictions of relative equilibrium cell volume for a cell placed into solutions of varying osmolality containing only non-permeating solutes. (a) For a range of values of $b$ with $B_{gg}$ and $C_{ggg}$ held constant at zero. (b) For a range of values of $B_{gg}$ (all in units of [moles of grouped solute/kg water]$^{-1}$) with $b$ and $C_{ggg}$ held constant at 0.4 and zero, respectively.

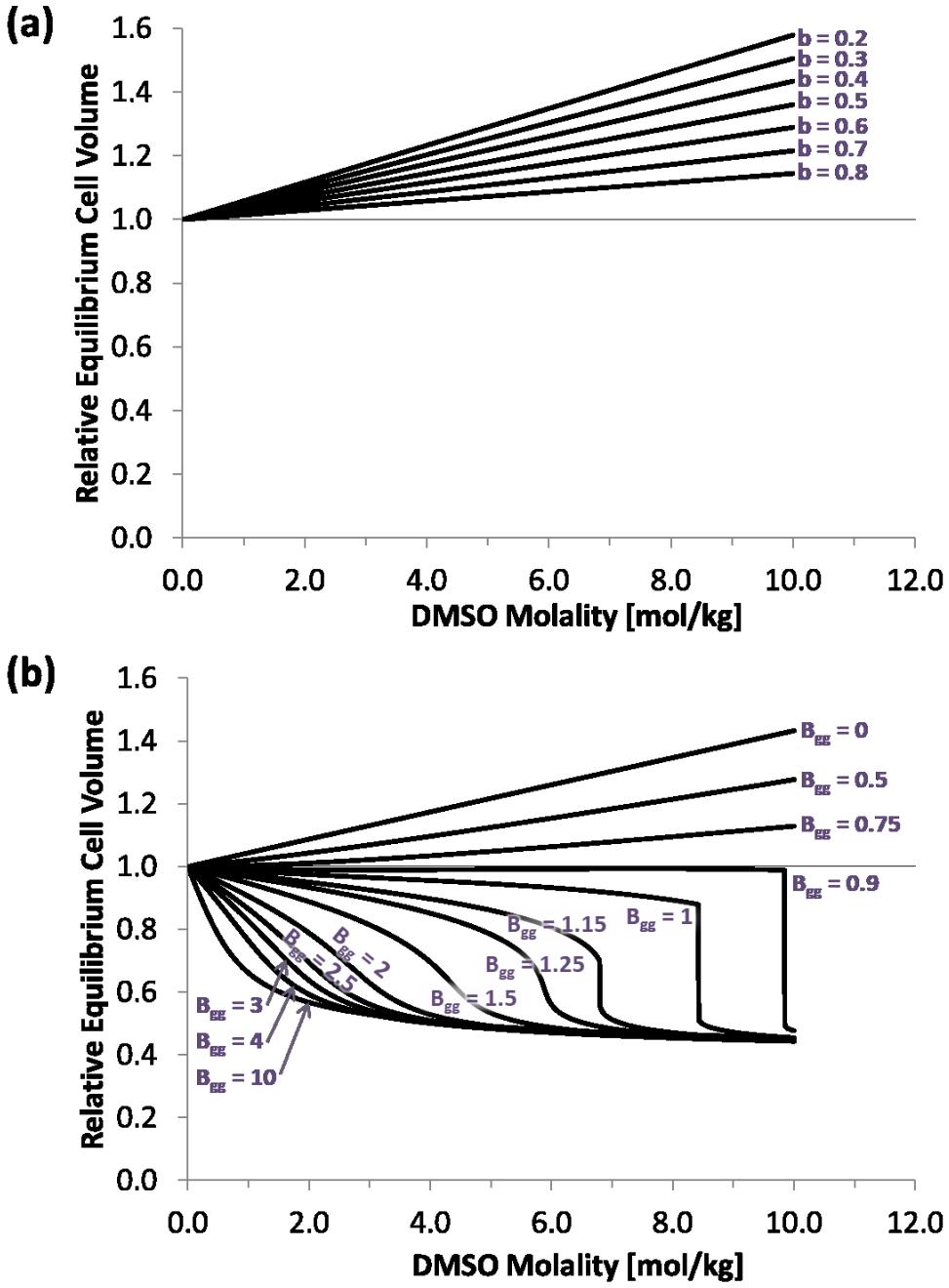


Figure 4.7. Model predictions of relative equilibrium cell volume for a cell placed into solutions containing a defined concentration of the permeating cryoprotectant DMSO. (a) For a range of values of $b$ with $B_{gg}$ and $C_{ggg}$ held constant at zero. (b) For a range of values of $B_{gg}$ (all in units of [moles of grouped solute/kg water]$^{-1}$) with $b$ and $C_{ggg}$ held constant at 0.4 and zero, respectively.

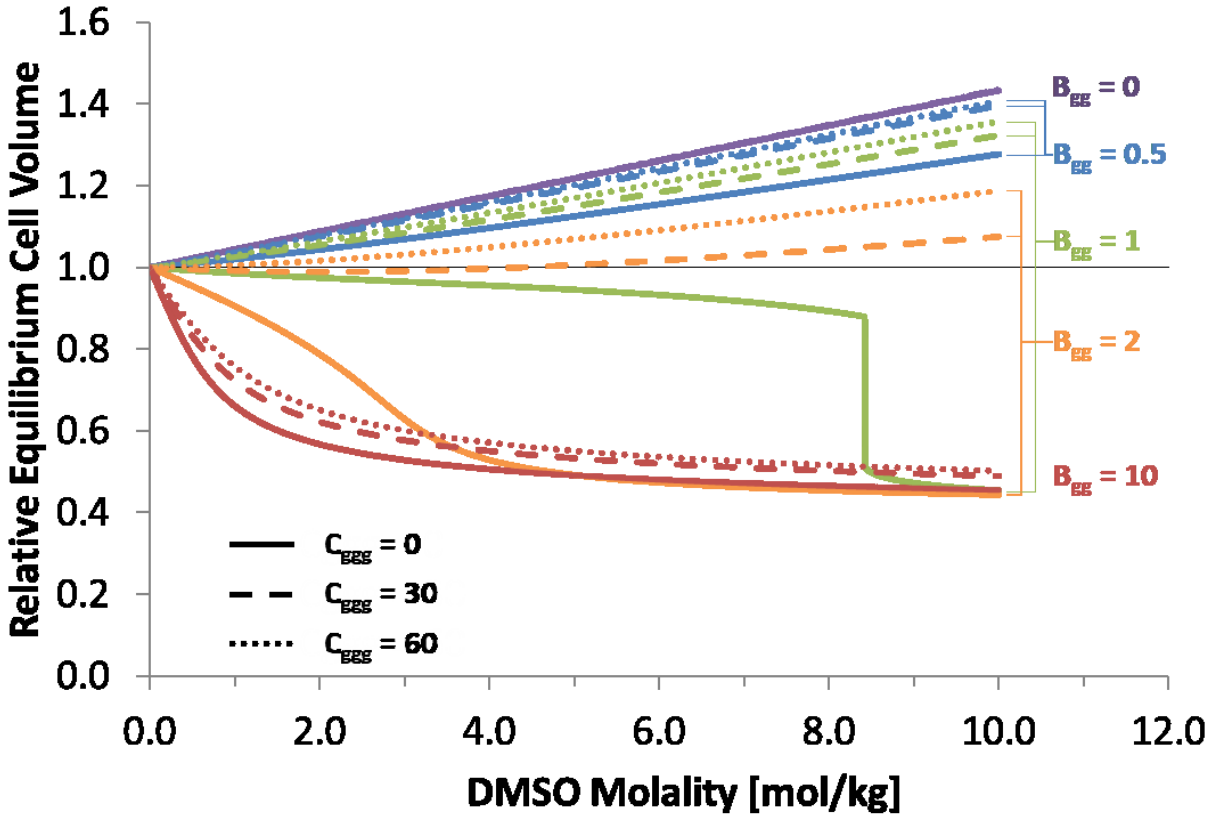


Figure 4.8. Model predictions of relative equilibrium cell volume for a cell placed into solutions containing a defined concentration of the permeating cryoprotectant DMSO, over a range of values of both $B_{gg}$ (all in units of [moles of grouped solute/kg water]$^{-1}$) and $C_{ggg}$ (all in units of [moles of grouped solute/kg water]$^{-2}$) with $b$ held constant at 0.4.

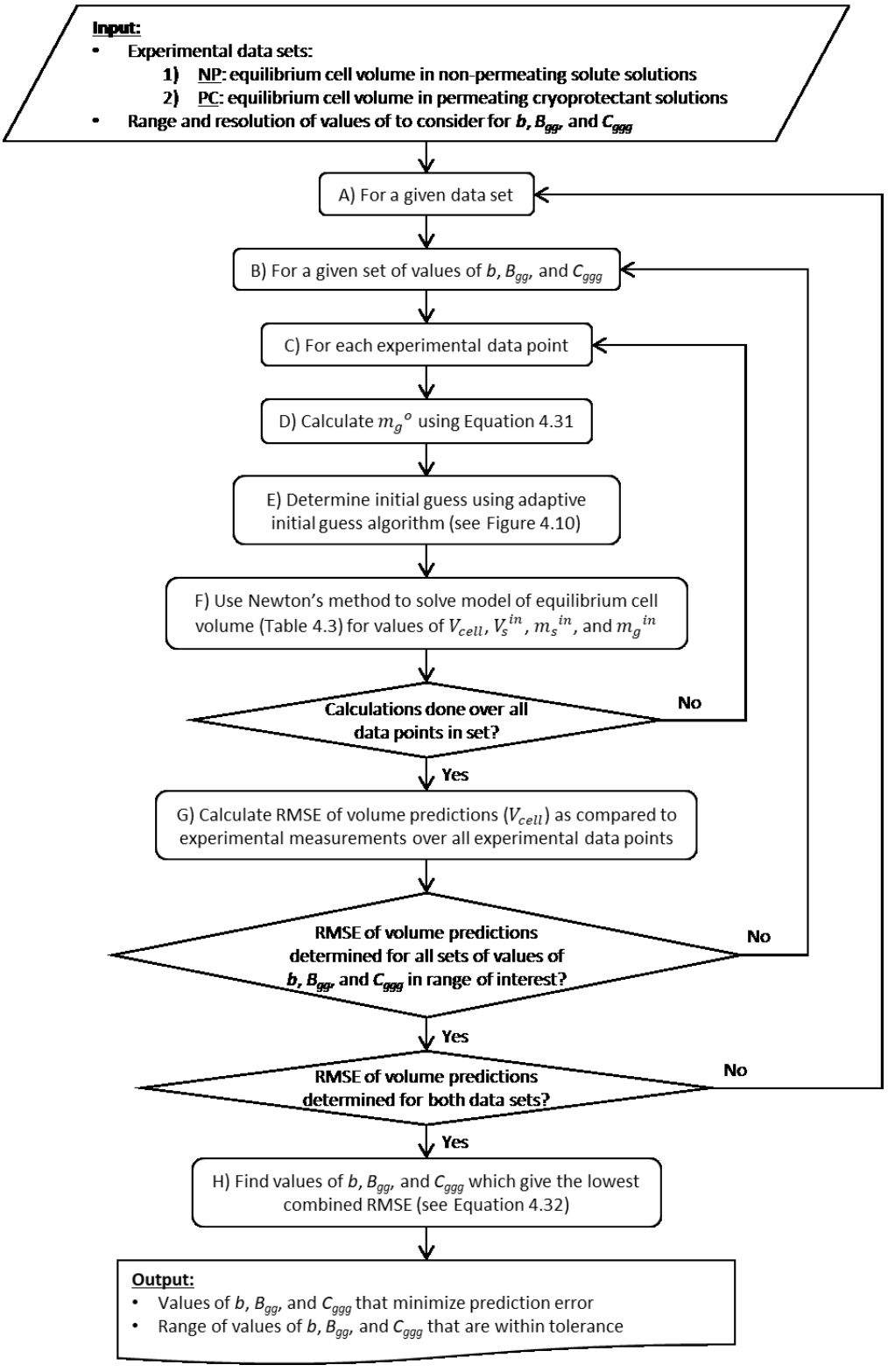


Figure 4.9. Overall fitting procedure used to obtain grouped intracellular solute osmotic virial coefficients from experimental measurements of equilibrium cell volume.

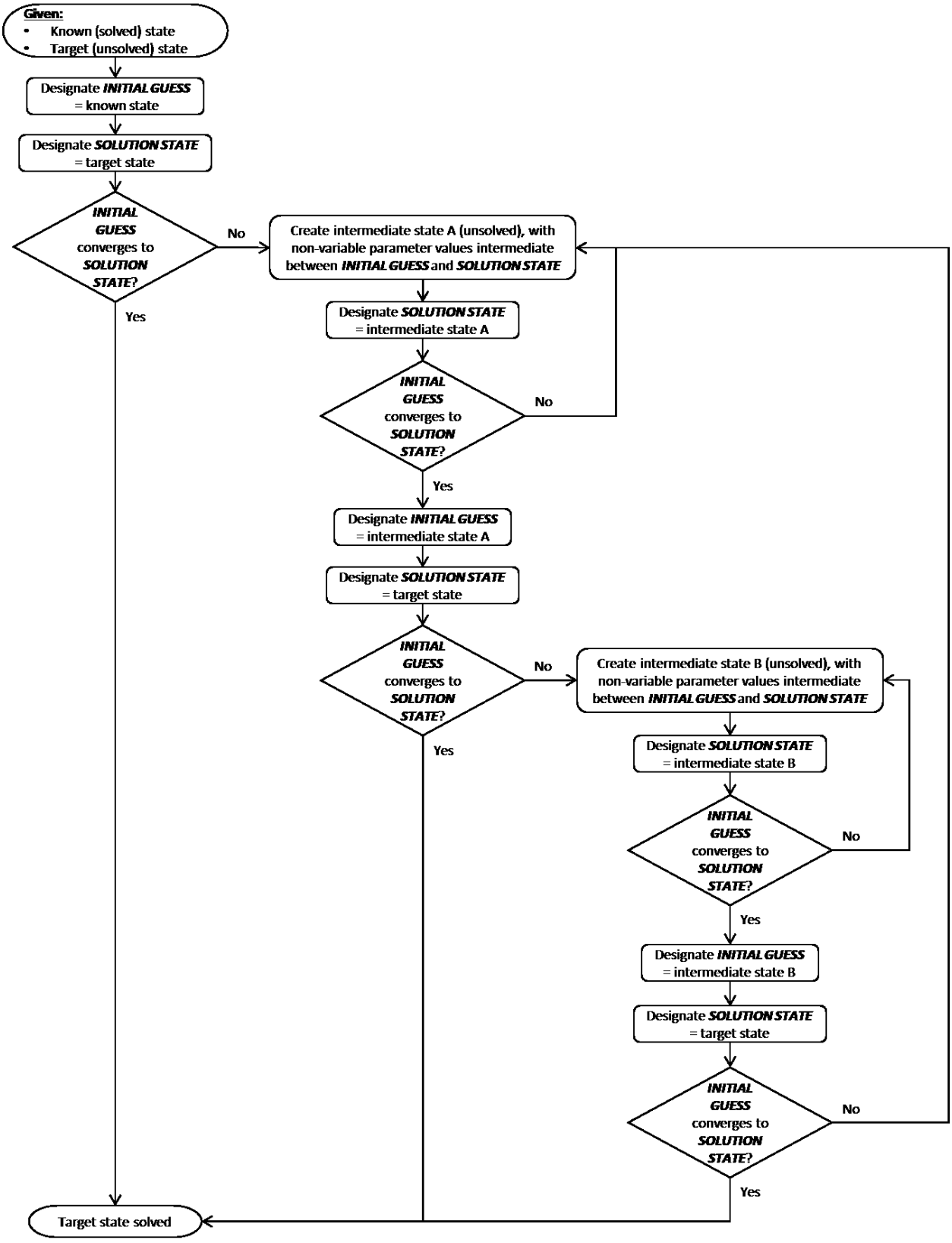


Figure 4.10. Adaptive initial guess algorithm.

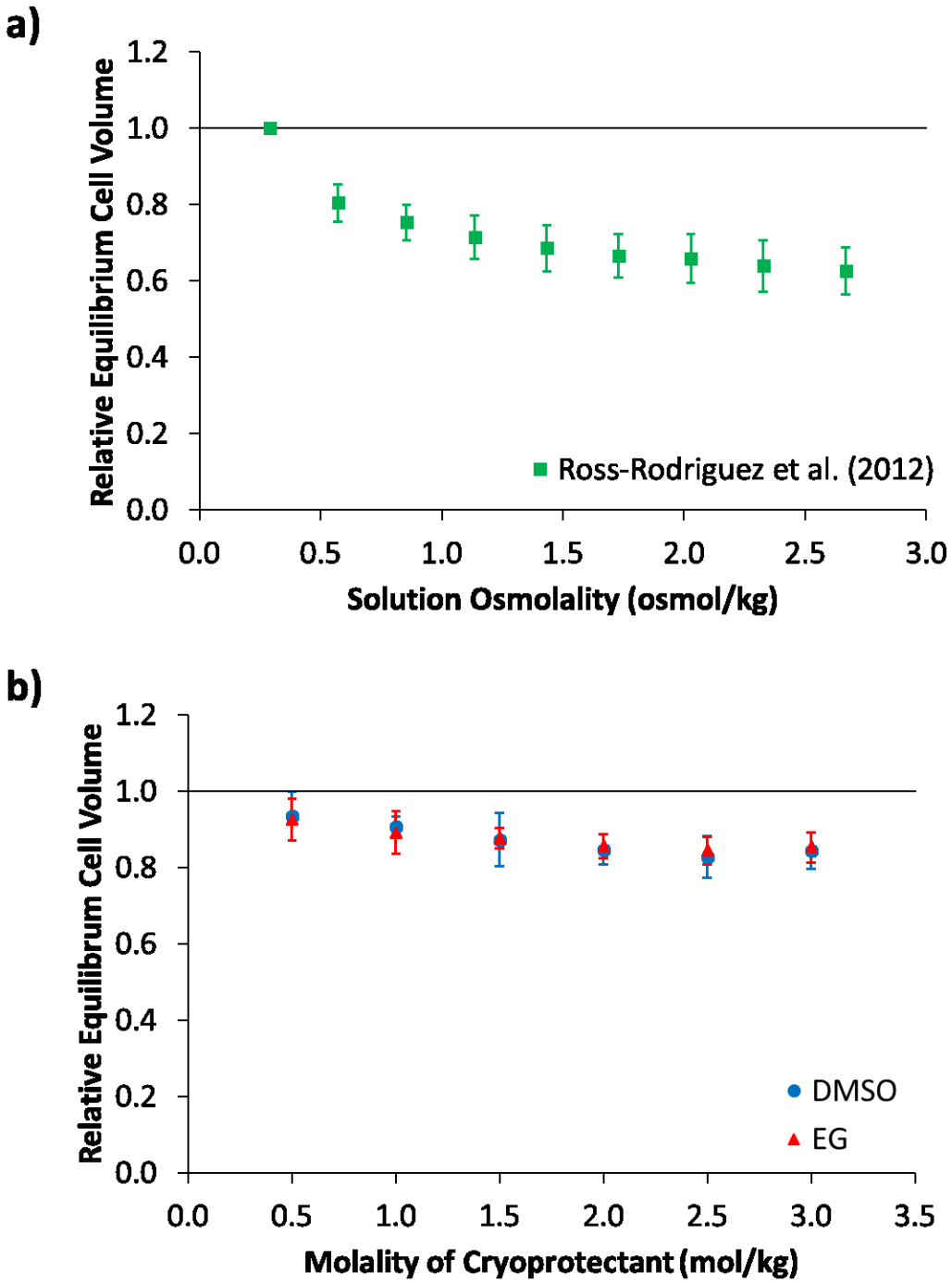


Figure 4.11. Experimental measurements of equilibrium HUVEC volume. (a) In solutions of only non-permeating solutes (data provided by Lisa Ross-Rodriguez [unpublished], with majority of data published in Ross-Rodriguez *et al*. [118]). (b) In solutions containing DMSO or EG. The error bars represent the standard deviation of the volume measurements.

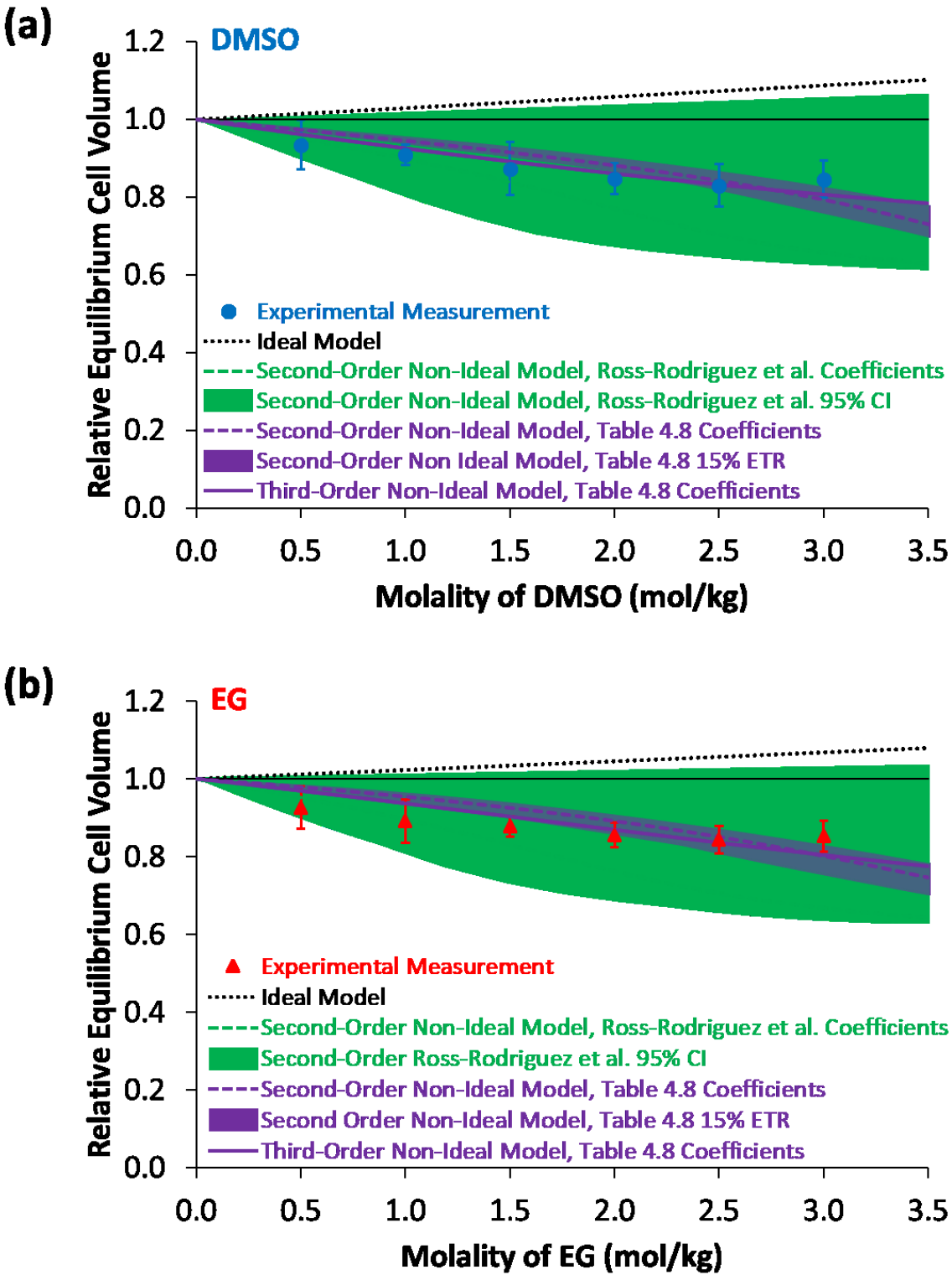


Figure 4.12. Second- and third-order non-ideal model fits to experimental equilibrium cell volume data (best-fit coefficient values in Table 4.8), along with model predictions of the data made using

the coefficient values obtained by Ross-Rodriguez *et al.* ($b = 0.524$ and $B_{gg} = 2.4$ [moles of grouped solute/kg water]$^{-1}$) [118] and an ideal dilute solution model ($b = 0.60$). The green shaded areas represent the model predictions that fall within the 95% confidence intervals (CIs) of the $B_{gg}$ value measured by Ross-Rodriguez *et al.* [118]. The purple shaded areas represent the model predictions that fall within the 15% error tolerance ranges (ETRs) for $B_{gg}$ measured in this work for a second-order fit. (a) For HUVEC in DMSO solutions. (b) For HUVEC in EG solutions.

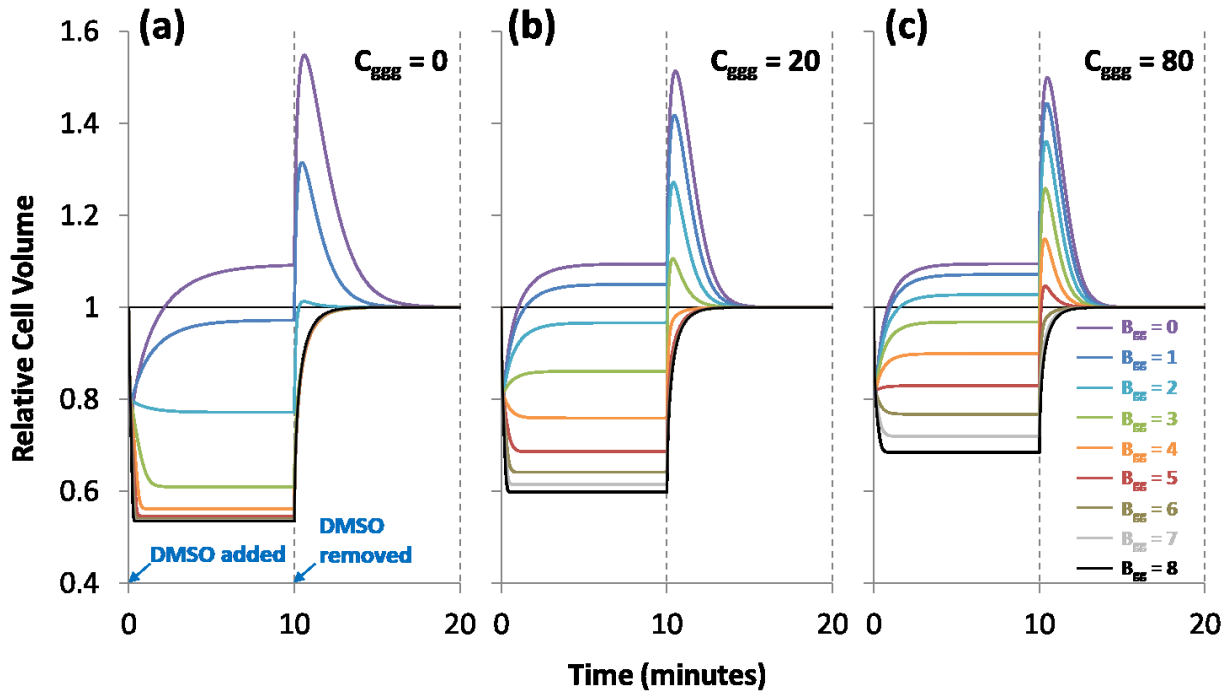


Figure 4.13. Model predictions of kinetic osmotic response for TF-1 exposed to 2 molal DMSO for 10 minutes and then returned to an isotonic solution for another 10 minutes, over a range of values of $B_{gg}$ (all in units of [moles of grouped solute/kg water]$^{-1}$). (a) For $C_{ggg} = 0$ [moles of grouped solute/kg water]$^{-2}$. (b) For $C_{ggg} = 20$ [moles of grouped solute/kg water]$^{-2}$. (c) For $C_{ggg} = 80$ [moles of grouped solute/kg water]$^{-2}$.

# Chapter 5. General discussion and conclusions

## 5.1. Summary of thesis

The current understanding of cellular cryoinjury and its prevention is still quite limited, as reflected in the relatively low number of cell types which can presently be successfully cryopreserved. Mathematical modeling offers a tool to help understand—and potentially predict—the complex processes that occur during cryopreservation. As such, it is a valuable part of the development of cryopreservation protocols which successfully avoid cryoinjury. A major area of focus for cryopreservation modeling is the simulation of the cellular osmotic response, which at its core depends on thermodynamic solution theories to calculate chemical potentials. However, to provide accurate predictions of chemical potential during cryopreservation, a solution theory must be able to account for the non-ideality of a typical cryobiological solution. Moreover, given the wide variety of solutes and thus possible solutions that are relevant in cryobiology, any non-ideal solution theory that is to be used in cryopreservation modeling should not be dependant on solution-specific thermodynamic parameters; rather, it should employ solute-specific parameters which can be experimentally measured once for that solute and then used in modeling any solution where that solute may be present. The primary focus of this thesis—the Elliott *et al.* form of the multi-solute osmotic virial equation—satisfies both of these conditions: it is a non-ideal solution theory that employs solute-specific osmotic virial coefficients to account for non-ideality. However, while this solution theory had been demonstrated to provide accurate predictions of chemical potential in cryobiologically-relevant solutions [24,105,106], there were at least two aspects of the model which required further work. First, the existing third-order molality-based water chemical potential equation had no corresponding thermodynamically consistent solute chemical potential equation, a requirement for modeling the osmotic response where permeating

cryoprotectants are present. Second, although the model could be used with a grouped intracellular solute approach in order to deal with the problem of unknown cytoplasm composition [118], it had never been shown that the use of this modeling approach did not affect model predictions of chemical potential—*i.e.*, that it was theoretically valid. Moreover, the existing method for measuring the osmotic virial coefficients of a grouped intracellular solute yielded results with low precision [118], which—in turn—could lead to highly imprecise predictions of cellular osmotic response. The overall goal of this thesis was to further develop the Elliott *et al.* model in order to address these issues and to incorporate the updated model into models of cellular osmotic response in order to advance understanding of cell behaviour during cryopreservation.

The first contribution of this thesis was a comprehensive comparison of the performance of the Elliott *et al.* form of the multi-solute osmotic virial equation (both molality- and mole fraction-based), the Kleinhans and Mazur freezing point summation model (another non-ideal solution theory that uses solute-specific parameters), and three forms of ideal dilute models. To perform this comparison, solute-specific thermodynamic coefficients were first obtained for the two non-ideal solution theories by curve-fitting to a single, consistent set of literature binary solution data. Then, the three types of models—incorporating the corresponding solute-specific coefficients as necessary—were used to predict water chemical potentials in a variety of cryobiologically-relevant multi-solute solutions for which experimental data were available in the literature. The model predictions were then compared to the experimental measurements in order to assess the accuracy of each model. The results of the comparison clearly indicated that the non-ideal solution theories provided similar prediction accuracy overall, and that both were considerably more accurate than the ideal model. Although this work was not directly related to the two issues described above, it provides general justification for the use of the Elliott *et al.*

model in cryobiological solution modeling (especially over an ideal dilute approach), and, furthermore, the coefficients obtained as part of the analysis were later also required when fitting for grouped intracellular solute osmotic virial coefficients (part of the second issue described above).

The second contribution of this thesis was the derivation of a novel solute chemical potential equation that is thermodynamically consistent with the existing third-order molality-based water chemical potential equation of the Elliott *et al*. model. Together, the solute and water chemical potential equations form a complete non-ideal molality-based solution theory that can be used to calculate all of the chemical potentials required to model the cellular osmotic response during cryopreservation.

The third contribution of this thesis was a thermodynamic proof that applied the now complete molality-based form of the Elliott *et al*. model to conclusively show that a grouped intracellular solute model of the cytoplasm can be used with this solution theory without affecting predictions of chemical potential—*i.e.*, this modeling approach is mathematically equivalent to treating the cytoplasm as if the concentrations of all non-permeating solutes inside the cell are known. This outcome means that non-ideal solution behaviour can be modeled inside of a cell using the molality-based Elliott *et al.* form of the multi-solute osmotic virial equation even where the cell's cytoplasmic composition is unknown without making any assumptions about the intracellular contents or sacrificing prediction accuracy in any way.

The final contribution of this thesis was the development of a novel technique for measuring grouped intracellular solute osmotic virial coefficients for the molality-based form of the Elliott *et al*. model with considerably greater precision that the previously-existing technique. This new method combines the updated thermodynamic theory developed in this work and a

mathematical model of equilibrium cell volume with experimental measurements of equilibrium cell volume in solutions containing only non-permeating solutes and in solutions containing a permeating solute. By fitting the theoretical model to the experimental measurements, one can obtain a set of cell-specific parameters—namely, osmotically inactive fraction and up to third order grouped intracellular solute osmotic virial coefficients—that completely characterize the non-ideal thermodynamic solution behaviour of the cell cytoplasm. As a practical demonstration of the new method, it was also employed to measure these parameters for human umbilical vein endothelial cells.

### 5.2. Implications of thesis

This thesis presents a complete solution thermodynamic model for cellular cryopreservation that can account for the non-ideality of cryobiological solutions and the generally unknown composition of the cell cytoplasm. It also provides methods for obtaining all of the thermodynamic coefficients required to apply the model in practice, along with the values of these coefficients for several cryobiologically-relevant solutes and for a cell type often used in cryopreservation studies: human umbilical vein endothelial cells [74,79,107,111,112,118,121, 135,148]. Overall, these contributions will allow for more accurate predictions of chemical potential in cryobiological solutions, both inside and outside the cell.

These advancements in cryobiological solution thermodynamics will in turn enable more accurate models of cellular osmotic behaviour, thus providing improved research tools for investigating the biophysical processes that occur during cryopreservation and, correspondingly, contributing towards the development of cryopreservation protocols that successfully minimize cryoinjury. For example, the thermodynamic model developed in this work can be integrated into

mathematical approaches for optimizing cryoprotectant addition and removal, such as the approach used by Davidson *et al.* for cells in suspension [12,13]. In their work, Davidson *et al.* combine models of cellular osmotic transport and cryoprotectant toxicity kinetics to design cell-specific cryoprotectant equilibration protocols that avoid excessive cell volume excursions while minimizing cell damage arising from cryoprotectant toxicity (the former occurs where the cryoprotectant is added/removed too quickly, whereas the latter increases with cryoprotectant exposure time and concentration) [12,13]. However, their approach employs an ideal dilute solution model to calculate the required chemical potentials, even up to very high solute concentrations (*i.e.*, those required for vitrification). As such, its effectiveness would likely be improved by replacing the ideal dilute assumption with a non-ideal thermodynamic model such as the one developed herein.

The thermodynamic model developed in this thesis can also be used to improve predictions of ice nucleation and growth inside of cells during cryopreservation. For example, the models of intracellular ice formation developed by Toner *et al.* [137] and Karlsson *et al.* [59–61] depend on instantaneous calculations of chemical potential inside and outside of the cell in order to keep track of intracellular water volume. However, these models assume an ideal dilute cytoplasm [59–61,137], despite modelling conditions—*i.e.*, low subfreezing temperatures—under which the cytoplasm may be quite concentrated, even at high cooling rates. Thus, these models would likely benefit from being able to instead calculate non-ideal chemical potentials inside the cell, as the contributions of this work allow.

Finally, while this work is predominantly focused on cellular cryopreservation, much of it is also applicable to larger and more complex biological materials such as tissues. The modeling of water and cryoprotectant transport in tissues during cryopreservation depends on the calculation

of chemical potentials just as it does for cells [1,2,26,56,94], and the solutions involved in tissue cryopreservation are generally no more ideal or dilute than those used in cellular cryopreservation. As such, the complete molality-based Elliott *et al*. form of the multi-solute osmotic virial equation offers the same benefits for models of tissue cryopreservation as it does for those of cellular cryopreservation. Furthermore, some models of tissue cryopreservation seek to predict not only transport throughout the bulk tissue, but also into and out of the individual cells comprising it [2,94]—for these models, all of the work in this thesis is relevant.

### 5.3. Limitations of thesis

Although this work provides a complete thermodynamic solution model for cellular cryopreservation, more information is required in order to accurately predict the cellular *kinetic* osmotic response, which reflects the actual time-dependent behaviour of a cell during cryopreservation. Specifically, kinetic modeling requires cell-specific permeability coefficients, which can only be obtained from experimental measurements of cell volume during the kinetic osmotic response.

It is important to note that the grouped intracellular solute approach, which was shown in Chapter 3 to be theoretically valid when used with the molality-based Elliott *et al*. form of the multi-solute osmotic virial equation, may not be likewise valid for other solution theories—*i.e.*, the proof in Chapter 3 is limited to that particular solution theory only. The appropriateness of using a grouped intracellular solute modeling approach for the cytoplasm with any other solution theory will have to be independently evaluated using a similar line of reasoning as that presented in Chapter 3.

## 5.4. Conclusions

Mathematical modeling is an important tool in the development of successful cryopreservation protocols. It helps us to understand—and allows us to predict—the processes that occur in cells (and tissues) during cryopreservation. Models of solution thermodynamics—*i.e.*, solution theories—lie at the core of most cryopreservation models. As such, it is essential that these models provide accurate predictions of chemical potential: any inaccuracies at this level will propagate to the higher-level models that simulate processes such as the osmotic response.

The insight gained in this thesis advances our ability to accurately model thermodynamic solution behaviour in cryobiologically-relevant solutions, including the cell cytoplasm. These advancements can be used to help propose and validate novel and superior cryopreservation protocols for cells and tissues.

## References


[1] A. Abazari, J.A.W. Elliott, G.K. Law, L.E. McGann, N.M. Jomha, A biomechanical triphasic approach to the transport of nondilute solutions in articular cartilage, Biophys. J. 97 (2009) 3054–3064.

[2] A. Abazari, R.B. Thompson, J.A.W. Elliott, L.E. McGann, Transport phenomena in articular cartilage cryopreservation as predicted by the modified triphasic model and the effect of natural inhomogeneities, Biophys. J. 102 (2012) 1284–1293.

[3] W. Afzal, A.H. Mohammadi, D. Richon, Volumetric properties of mono-, Di-, Tri-, and polyethylene glycol aqueous solutions from (273.15 to 363.15) K: Experimental measurements and correlations, J. Chem. Eng. Data. 54 (2009) 1254–1261.

[4] J.D. Benson, Stability analysis of several non-dilute multiple solute transport equations, J. Math. Chem. 49 (2011) 859–869.

[5] J.D. Benson, A. Bagchi, X. Han, J.K. Critser, E.J. Woods, Melting point equations for the ternary system water/sodium chloride/ethylene glycol revisited, Cryobiology. 61 (2010) 352–356.

[6] P.R. Bevington, D.K. Robinson, Data Reduction and Error Analysis for the Physical Sciences, McGraw-Hill, New York, NY, 2003.

[7] A.W. Bosse, J.F. Douglas, The osmotic virial formulation of the free energy of polymer mixing, J. Chem. Phys. 143 (2015) 104903.

[8] P. Boutron, A. Kaufmann, Stability of the amorphous state in the system water-glycerol-dimethylsulfoxide, Cryobiology. 15 (1978) 93–108.

[9] D. Castagne, M. Fillet, L. Delattre, B. Evrard, B. Nusgens, G. Piel, Study of the cholesterol extraction capacity of β-cyclodextrin and its derivatives, relationships with

their effects on endothelial cell viability and on membrane models, J. Incl. Phenom. Macrocycl. Chem. 63 (2009) 225–231.

[10] Y.A. Cengel, M.A. Boles, Thermodynamics: An Engineering Approach, 2nd ed., McGraw-Hill, 1994.

[11] J. Cheng, M. Gier, L.U. Ross-Rodriguez, V. Prasad, J.A.W. Elliott, A. Sputtek, Osmotic virial coefficients of hydroxyethyl starch from aqueous hydroxyethyl starch-sodium chloride vapor pressure osmometry, J. Phys. Chem. B. 117 (2013) 10231–10240.

[12] A.F. Davidson, J.D. Benson, A.Z. Higgins, Mathematically optimized cryoprotectant equilibration procedures for cryopreservation of human oocytes., Theor. Biol. Med. Model. 11 (2014) 13.

[13] A.F. Davidson, C. Glasscock, D.R. McClanahan, J.D. Benson, A.Z. Higgins, Toxicity Minimized Cryoprotectant Addition and Removal Procedures for Adherent Endothelial Cells, PLoS One. 10 (2015) 1–22.

[14] R. V Devireddy, Predicted permeability parameters of human ovarian tissue cells to various cryoprotectants and water, Mol. Reprod. Dev. 70 (2005) 333–343.

[15] R. V Devireddy, P.R. Barratt, K.B. Storey, J.C. Bischof, Liver Freezing Response of the Freeze-Tolerant Wood Frog, Rana sylvatica, in the Presence and Absence of Glucose, Cryobiology. 38 (1999) 327–338.

[16] R. V Devireddy, D.J. Swanlund, K.P. Roberts, J.C. Bischof, Subzero Water Permeability Parameters of Mouse Spermatozoa in the Presence of Extracellular Ice and Cryoprotective Agents, Biol. Reprod. 61 (1999) 764–775.

[17] D.A.T. Dick, Physical Bases of Circulatory Transport: Regulation and Exchange, W.B. Saunders Company, Philadelphia, PA, 1967.

[18] F. Döbert, A. Pfennig, M. Stumpf, Derivation of the consistent osmotic virial equation and its application to aqueous poly(ethylene glycol)-dextran two-phase systems, Macromolecules. 28 (1995) 7860–7868.

[19] S.L. Ebertz, L.E. McGann, Osmotic parameters of cells from a bioengineered human corneal equivalent and consequences for cryopreservation, Cryobiology. 45 (2002) 109–117.

[20] S.L. Ebertz, L.E. McGann, Cryoprotectant permeability parameters for cells used in a bioengineered human corneal equivalent and applications for cryopreservation, Cryobiology. 49 (2004) 169–180.

[21] E. Edmond, A.G. Ogston, An approach to the study of phase separation in ternary aqueous systems., Biochem. J. 109 (1968) 569–576.

[22] J.G. Eisenhauer, Regression through the origin, Teach. Stat. 25 (2003) 76–80.

[23] J.A.W. Elliott, H.Y. Elmoazzen, L.E. McGann, Method whereby onsager coefficients may be evaluated, J. Chem. Phys. 113 (2000) 6573–6578.

[24] J.A.W. Elliott, R.C. Prickett, H.Y. Elmoazzen, K.R. Porter, L.E. McGann, A multisolute osmotic virial equation for solutions of interest in biology, J. Phys. Chem. B. 111 (2007) 1775–1785.

[25] H.Y. Elmoazzen, Osmotic Transport in Cryobiology, PhD Thesis, University of Alberta, 2006.

[26] H.Y. Elmoazzen, J.A.W. Elliott, L.E. McGann, Cryoprotectant equilibration in tissues, Cryobiology. 51 (2005) 85–91.

[27] H.Y. Elmoazzen, J.A.W. Elliott, L.E. McGann, Osmotic transport across cell membranes in nondilute solutions: A new nondilute solute transport equation, Biophys. J. 96 (2009)

2559–2571.

[28] H.Y. Elmoazzen, A. Poovadan, G.K. Law, J.A.W. Elliott, L.E. McGann, N.M. Jomha, Dimethyl sulfoxide toxicity kinetics in intact articular cartilage, Cell Tissue Bank. 8 (2007) 125–133.

[29] F. Eslami, J.A.W. Elliott, Design of microdrop concentrating processes, J. Phys. Chem. B. 117 (2013) 2205–2214.

[30] F. Eslami, J.A.W. Elliott, Role of precipitating solute curvature on microdrops and nanodrops during concentrating processes: The nonideal Ostwald-Freundlich equation, J. Phys. Chem. B. 118 (2014) 14675–14686.

[31] F. Eslami, J.A.W. Elliott, Stability analysis of microdrops during concentrating processes., J. Phys. Chem. B. 118 (2014) 3630–3641.

[32] G.M. Fahy, Analysis of "solution effects" injury. Equations for calculating phase diagram information for the ternary systems NaCl-dimethylsulfoxide-water and NaCl-glycerol-water, Biophys. J. 32 (1980) 837–850.

[33] G.M. Fahy, The relevance of cryoprotectant "toxicity" to cryobiology, Cryobiology. 23 (1986) 1–13.

[34] G.M. Fahy, Cryoprotectant toxicity neutralization, Cryobiology. 60 (2010) S45–S53.

[35] G.M. Fahy, B. Wowk, J. Wu, J. Phan, C. Rasch, A. Chang, E. Zendejas, Cryopreservation of organs by vitrification: perspectives and recent advances, Cryobiology. 48 (2004) 157–178.

[36] J. Farrant, S.C. Knight, L.E. McGann, J. O'Brien, Optimal recovery of lymphocytes and tissue culture cells following rapid cooling, Nature. 249 (1974) 452–453.

[37] J. Farrant, C.A. Walter, H. Lee, L.E. McGann, Use of two-step cooling procedures to

examine factors influencing cell survival following freezing and thawing, Cryobiology. 14 (1977) 273–286.

[38] D.Y. Gao, Q. Chang, C. Liu, K. Farris, K. Harvey, L.E. McGann, D. English, J. Jansen, J.K. Critser, Fundamental cryobiology of human hematopoietic progenitor cells I: Osmotic characteristics and volume distribution, Cryobiology. 36 (1998) 40–48.

[39] D.Y. Gao, J. Liu, C. Liu, L.E. McGann, P.F. Watson, F.W. Kleinhans, P. Mazur, E.S. Critser, J.K. Critser, Prevention of osmotic injury to human spermatozoa during addition and removal of glycerol, Hum. Reprod. 10 (1995) 1109–1122.

[40] D.R. Gaskel, Phase Equilibrium in a One-Component System, in: Introd. to Thermodyn. Mater., 5th ed., New York, NY, 2008: pp. 149–176.

[41] D.R. Gaskel, The Behaviour of Solutions, in: Introd. to Thermodyn. Mater., 5th ed., Taylor & Francis Group, LLC, New York, New York, 2008: pp. 211–261.

[42] J. Gaube, A. Pfennig, M. Stumpf, Thermodynamics of Aqueous Poly(Ethylene Glycol)-Dextran Two-Phase Systems Using the Consistent Osmotic Virial Equation, Fluid Phase Equilib. 83 (1993) 365–373.

[43] F.W. Gayle, F.H. Cocks, M.L. Shepard, H2O-NaCl-Sucrose Phase Diagram and Applications in Cryobiology, J. Appl. Chem. Biotechnol. 27 (1977) 599–607.

[44] C.A. Glasbey, G.W. Horgan, Segmentation, in: Image Anal. Biol. Sci., Wiley, 1995: p. 93.

[45] H.A. Gordon, Errors in computer packages. Least-squares regression through the origin, Statistician. 30 (1981) 23–29.

[46] E.A. Guggenheim, Mixtures: the theory of the equilibrium properties of some simple classes of mixtures, solutions and alloys, Clarendon Press, Oxford, UK, 1952.

[47] X. Han, Y. Liu, J.K. Critser, Determination of the quaternary phase diagram of the water–

ethylene glycol–sucrose–NaCl system and a comparison between two theoretical methods for synthetic phase diagrams, Cryobiology. 61 (2010) 52–57.

[48] H. Hasse, H.-P. Kany, R. Tintinger, G. Maurer, Osmotic virial coefficients of aqueous poly(ethylene glycol) from laser-light scattering and isopiestic measurements, Macromolecules. 28 (1995) 3540–3552.

[49] J.R. Hauser, Solving Sets of Equations: Linear and Nonlinear, in: Numer. Methods Nonlinear Eng. Model., Springer, 2009: pp. 87–93.

[50] C.A. Haynes, R.A. Beynon, R.S. King, H.W. Blanch, J.M. Prausnitz, Thermodynamic properties of aqueous polymer solutions: poly(ethylene glycol)/dextran, J. Phys. Chem. 93 (1989) 5612–5617.

[51] W.H. Hildebrandt, Low temperature quantitative phase equilibria and glass formation in the water-sodium chloride-dimethyl sulfoxide system, PhD Thesis, Duke University, 1975.

[52] C.J. Hunt, S.E. Armitage, D.E. Pegg, Cryopreservation of umbilical cord blood: 1. Osmotically inactive volume, hydraulic conductivity and permeability of CD34+ cells to dimethyl sulphoxide, Cryobiology. 46 (2003) 61–75.

[53] M.H. Jacobs, The simultaneous measurement of cell permeability to water and to dissolved substances, J. Cell. Comp. Physiol. 2 (1933) 427–444.

[54] M.H. Jacobs, D.R. Stewart, A simple method for the quantitative measurement of cell permeability, J. Cell. Comp. Physiol. 1 (1932) 71–82.

[55] J.A. Johnson, T.A. Wilson, Osmotic volume changes induced by a permeable solute, J. Theor. Biol. 17 (1967) 304–311.

[56] N.M. Jomha, J.A.W. Elliott, G.K. Law, B. Maghdoori, J. Fraser Forbes, A. Abazari, A.B.

Adesida, L. Laouar, X. Zhou, L.E. McGann, Vitrification of intact human articular cartilage, Biomaterials. 33 (2012) 6061–6068.

[57] H.-P. Kany, H. Hasse, G. Maurer, Thermodynamic properties of aqueous dextran solutions from laser-light-scattering, membrane osmometry, and isopiestic measurements, J. Chem. Eng. Data. 44 (1999) 230–242.

[58] H.-P. Kany, H. Hasse, G. Maurer, Thermodynamic properties of aqueous poly(vinylpyrrolidone) solutions from laser-light-scattering, membrane osmometry, and isopiestic measurements, J. Chem. Eng. Data. 48 (2003) 689–698.

[59] J.O. Karlsson, E.G. Cravalho, I.H. Borel Rinkes, R.G. Tompkins, M.L. Yarmush, M. Toner, Nucleation and growth of ice crystals inside cultured hepatocytes during freezing in the presence of dimethyl sulfoxide., Biophys. J. 65 (1993) 2524–36.

[60] J.O.M. Karlsson, E.G. Cravalho, M. Toner, A model of diffusion-limited ice growth inside biological cells during freezing, J. Appl. Phys. 75 (1994) 4442–4455.

[61] J.O.M. Karlsson, A. Eroglu, T.L. Toth, E.G. Cravalho, M. Toner, Fertilization and development of mouse oocytes cryopreserved using a theoretically optimized protocol, Hum. Reprod. 11 (1996) 1296–1305.

[62] J.O.M. Karlsson, E.A. Szurek, A.Z. Higgins, S.R. Lee, A. Eroglu, Optimization of cryoprotectant loading into murine and human oocytes., Cryobiology. 68 (2014) 18–28.

[63] J.O.M. Karlsson, M. Toner, Long-term storage of tissues by cryopreservation: Critical issues, Biomaterials. 17 (1996) 243–256.

[64] J.O.M. Karlsson, A.I. Younis, A.W.S. Chan, K.G. Gould, A. Eroglu, Permeability of the rhesus monkey oocyte membrane to water and common cryoprotectants, Mol. Reprod. Dev. 76 (2009) 321–333.

[65] I.I. Katkov, A two-parameter model of cell membrane permeability for multisolute systems, Cryobiology. 40 (2000) 64–83.

[66] O. Kedem, A. Katchalsky, Thermodynamic analysis of the permeability of biological membranes to non-electrolytes, Biochim. Biophys. Acta. 27 (1958) 229–246.

[67] R.S. King, H.W. Blanch, J.M. Prausnitz, Molecular thermodynamics of aqueous two-phase systems for bioseparations, AIChE J. 34 (1988) 1585–1594.

[68] F.W. Kleinhans, Membrane permeability modeling: Kedem-Katchalsky vs a two-parameter formalism, Cryobiology. 37 (1998) 271–289.

[69] F.W. Kleinhans, P. Mazur, Comparison of actual vs. synthesized ternary phase diagrams for solutes of cryobiological interest, Cryobiology. 54 (2007) 212–222.

[70] J.M. Knox, G.S. Schwartz, K.R. Diller, Volumetric changes in cells during freezing and thawing, J. Biomech. Eng. 102 (1980) 91–97.

[71] M.H. Kutner, C.J. Nachtsheim, J. Neter, Applied Linear Regression Models, McGraw-Hill Irwin, New York, NY, 2004.

[72] T.O. Kvalseth, Cautionary Note about R2, Am. Stat. 39 (1985) 279–285.

[73] L.D. Landau, E.M. Lifshitz, Course of Theoretical Physics: Volume 5: Statistical Physics, Pergamon Press, Oxford, UK, 1980.

[74] K. Lehle, M. Hoenicka, V.R. Jacobs, F.X. Schmid, D.E. Birnbaum, Cryopreservation of human endothelial cells for vascular tissue engineering, Cryobiology. 50 (2005) 154–161.

[75] R.L. Levin, E.G. Cravalho, C.E. Huggins, Effect of solution non ideality on erythrocyte volume regulation, Biochim. Biophys. Acta. 465 (1977) 179–190.

[76] J.A. MacNeil, G.B. Ray, D.G. Leaist, Activity coefficients and free energies of nonionic mixed surfactant solutions from vapor-pressure and freezing-point osmometry, J. Phys.

Chem. B. 115 (2011) 5947–5957.

[77] J.A. MacNeil, G.B. Ray, P. Sharma, D.G. Leaist, Activity coefficients of aqueous mixed ionic surfactant solutions from osmometry, J. Solution Chem. 43 (2014) 93–108.

[78] S.A. Markarian, A.M. Asatryan, A.L. Zatikyan, Volumetric properties of aqueous solutions of diethylsulfoxide at temperatures from 298.15 K to 343.15 K, J. Chem. Thermodyn. 37 (2005) 768–777.

[79] L.A. Marquez-Curtis, A.B. Sultani, L.E. McGann, J.A.W. Elliott, Beyond membrane integrity: assessing the functionality of human umbilical vein endothelial cells after cryopreservation, Cryobiology. 72 (2016) 183–190.

[80] F.H. Martini, The Cellular Level of Organization, in: Fundam. Anat. Physiol., 7th ed., Benjamin Cummings, San Francisco, CA, 2006: pp. 62–105.

[81] P. Mazur, Kinetics of water loss from cells at subzero temperatures and the likelihood of intracellular freezing, J. Gen. Physiol. 47 (1963) 347–369.

[82] P. Mazur, Freezing of living cells: Mechanisms and implications, Am. J. Physiol. - Cell Physiol. 16 (1984) C125–C142.

[83] P. Mazur, S.P. Leibo, E.H.Y. Chu, A two-factor hypothesis of freezing injury. Evidence from Chinese hamster tissue-culture cells, Exp. Cell Res. 71 (1972) 345–355.

[84] P. Mazur, R.H. Miller, Permeability of the human erythrocyte to glycerol in 1 and 2 M solutions at 0 or 20°C1, Cryobiology. 13 (1976) 507–522.

[85] L.E. McGann, Differing actions of penetrating and nonpenetrating cryoprotective agents, Cryobiology. 15 (1978) 382–390.

[86] L.E. McGann, J. Farrant, Survival of tissue culture cells frozen by a two-step procedure to –196°C. I. Holding temperature and time, Cryobiology. 13 (1976) 261–268.

[87] W.G. McMillan Jr., J.E. Mayer, The statistical thermodynamics of multicomponent systems, J. Chem. Phys. 13 (1945) 276–305.

[88] P.M. Mehl, Nucleation and crystal growth in a vitrification solution tested for organ cryopreservation by vitrification, Cryobiology. 30 (1993) 509–518.

[89] A. Melinder, Thermophysical properties of aqueous solutions used as secondary working fluids, Kungliga Tekniska Hogskolan (Sweden), 2007.

[90] H.T. Meryman, Cryoprotective agents, Cryobiology. 8 (1971) 173–183.

[91] H.T. Meryman, Freezing injury and its prevention in living cells., Annu. Rev. Biophys. Bioeng. 3 (1974) 341–363.

[92] D.P. Miller, J.J. de Pablo, H. Corti, Thermophysical properties of trehalose and its concentrated aqueous solutions, Pharm. Res. 14 (1997) 578–590.

[93] D.C. Montgomery, G.C. Runger, Applied Statistics and Probability for Engineers, 4th ed., John Wiley & Sons, Inc., Hoboken, NJ, 2007.

[94] I.N. Mukherjee, Y. Li, Y.C. Song, R.C. Long Jr., A. Sambanis, Cryoprotectant transport through articular cartilage for long-term storage: experimental and modeling studies, Osteoarthr. Cartil. 16 (2008) 1379–1386.

[95] K. Muldrew, J.P. Acker, J.A.W. Elliott, L.E. McGann, The Water to Ice Transition: Implications for Living Cells, in: B.J. Fuller, N. Lane, E.E. Benson (Eds.), Life Frozen State, CRC Press, Boca Raton, Florida, 2004: p. 67.

[96] D.E. Pegg, Simple equations for obtaining melting points and eutectic temperatures for the ternary system glycerol/sodium chloride/water, Cryo-Letters. 4 (1983) 259–268.

[97] D.E. Pegg, Equations for obtaining melting points and eutectic temperatures for the ternary system dimethylsulfoxide/sodium chloride/water, Cryo-Letters. 7 (1986) 387–394.

[98] D.E. Pegg, The preservation of tissues for transplantation, Cell Tissue Bank. 7 (2006) 349–358.

[99] D.E. Pegg, The relevance of ice crystal formation for the cryopreservation of tissues and organs., Cryobiology. 60 (2010) S36-44.

[100] D.E. Pegg, F.G. Arnaud, Equations for obtaining melting points in the quaternary system propane-1,2-diol/glycerol/sodium chloride/water, Cryo-Letters. 9 (1988) 404–417.

[101] C. Polge, A.U. Smith, A.S. Parkes, Revival of spermatozoa after vitrification and dehydration at low temperatures [12], Nature. 164 (1949) 666.

[102] J.M. Prausnitz, R.N. Lichtenthaler, E.G. de Azevedo, Molecular Thermodynamics of Fluid-Phase Equilibria, 3rd ed., Prentice Hall PTR, Upper Saddle River, New Jersey, 1999.

[103] R.C. Prickett, The application of the multisolute osmotic virial equation to cryobiology, PhD Thesis, University of Alberta (Canada), 2010.

[104] R.C. Prickett, J.A.W. Elliott, S. Hakda, L.E. McGann, A non-ideal replacement for the Boyle van't Hoff equation, Cryobiology. 57 (2008) 130–136.

[105] R.C. Prickett, J.A.W. Elliott, L.E. McGann, Application of the osmotic virial equation in cryobiology, Cryobiology. 60 (2010) 30–42.

[106] R.C. Prickett, J.A.W. Elliott, L.E. McGann, Application of the multisolute osmotic virial equation to solutions containing electrolytes, J. Phys. Chem. B. 115 (2011) 14531–14543.

[107] R.C. Prickett, L.A. Marquez-Curtis, J.A.W. Elliott, L.E. McGann, Effect of supercooling and cell volume on intracellular ice formation, Cryobiology. 70 (2015) 156–163.

[108] V. Ragoonanan, A. Hubel, A. Aksan, Response of the cell membrane-cytoskeleton complex to osmotic and freeze/thaw stresses, Cryobiology. 61 (2010) 335–344.

[109] D.H. Rasmussen, A.P. Mackenzie, Phase diagram for system water-dimethylsulphoxide, Nature. 220 (1968) 1315–1317.

[110] S.J. Rathbone, C.A. Haynes, H.W. Blanch, J.M. Prausnitz, Thermodynamic properties of dilute aqueous polymer solutions from low-angle laser-light-scattering measurements, Macromolecules. 23 (1990) 3944–3947.

[111] A.J.F. Reardon, J.A.W. Elliott, L.E. McGann, Fluorescence as an alternative to light-scatter gating strategies to identify frozen-thawed cells with flow cytometry, Cryobiology. 69 (2014) 91–99.

[112] A.J.F. Reardon, J.A.W. Elliott, L.E. McGann, Investigating membrane and mitochondrial cryobiological responses of HUVEC using interrupted cooling protocols, Cryobiology. 71 (2015) 306–317.

[113] S. Rosłoniec, Methods for Numerical Solution of Nonlinear Equations, in: Fundam. Numer. Methods Electr. Eng., Springer, 2008: pp. 49–68.

[114] S. Rosłoniec, Methods for Numerical Integration of Ordinary Differential Equations, in: Fundam. Numer. Methods Electr. Eng., 2008: pp. 186–189.

[115] L.U. Ross-Rodriguez, J.A.W. Elliott, L.E. McGann, Investigating cryoinjury using simulations and experiments. 1: TF-1 cells during two-step freezing (rapid cooling interrupted with a hold time), Cryobiology. 61 (2010) 38–45.

[116] L.U. Ross-Rodriguez, J.A.W. Elliott, L.E. McGann, Investigating cryoinjury using simulations and experiments: 2. TF-1 cells during graded freezing (interrupted slow cooling without hold time), Cryobiology. 61 (2010) 46–51.

[117] L.U. Ross-Rodriguez, J.A.W. Elliott, L.E. McGann, Characterization of cryobiological responses in TF-1 cells using interrupted freezing procedures, Cryobiology. 60 (2010)

106–116.

[118] L.U. Ross-Rodriguez, J.A.W. Elliott, L.E. McGann, Non-ideal solution thermodynamics of cytoplasm, Biopreserv. Biobank. 10 (2012) 462–471.

[119] J.R. Rumble, ed., Physical Constants of Inorganic Compounds, in: CRC Handb. Chem. Phys. (Internet Version), 99th ed., CRC Press/Taylor & Francis, Boca Raton, Florida, 2018.

[120] J.R. Rumble, ed., Physical Constants of Organic Compounds, in: CRC Handb. Chem. Phys. (Internet Version), 99th ed., CRC Press/Taylor & Francis, Boca Raton, Florida, 2018.

[121] A.T. Schafer, C. Körber, M.W. Scheiwe, G. Rau, P. Franke, C. Mittermayer, Preliminary investigation of osmotic properties and freezing behavior of human endothelial cells, Cryo-Letters. 7 (1986) 55–67.

[122] M.W. Scheiwe, C. Körber, Basic investigations on the freezing of human lymphocytes., Cryobiology. 20 (1983) 257–73.

[123] M.W. Scheiwe, C. Körber, Thermally Defined Cryomicroscopy and Thermodynamic Analysis in Lymphocyte Freezing, Cryobiology. 21 (1984) 93–105.

[124] E.M. Schulson, The Structure and Mechanical Behavior of Ice, JOM. 51 (1999) 21–27.

[125] G.J. Schwartz, K.R. Diller, Osmotic Response of Individual Cells during Freezing. II. Membrane Permeability Analysis, Cryobiology. 20 (1983) 542–552.

[126] M. Shabana, J.J. McGrath, Cryomicroscope investigation and thermodynamic modeling of the freezing of unfertilized hamster ova, Cryobiology. 25 (1988) 338–354.

[127] N. Shardt, K.K. Al-Abbasi, H. Yu, N.M. Jomha, L.E. McGann, J.A.W. Elliott, Cryoprotectant kinetic analysis of a human articular cartilage vitrification protocol,

Cryobiology. (2016).

[128] M.L. Shepard, C.S. Goldston, F.H. Cocks, The H2O NaCl glycerol phase diagram and its application in cryobiology, Cryobiology. 13 (1976) 9–23.

[129] Z. Shu, S.M. Hughes, C. Fang, J. Huang, B. Fu, G. Zhao, M. Fialkow, G. Lentz, F. Hladik, D. Gao, A study of the osmotic characteristics, water permeability, and cryoprotectant permeability of human vaginal immune cells., Cryobiology. 72 (2016) 93–99.

[130] A.U. Smith, Prevention of hæmolysis during freezing and thawing of red blood cells, Orig. Publ. as Vol. 2, Issue 6644. 256 (1950) 910–911.

[131] G. Stacey, Fundamental Issues for Cell-Line Banks in Biotechnology and Regulatory Affairs, in: B.J. Fuller, N. Lane, E.E. Benson (Eds.), Life Frozen State, CRC Press, Boca Raton, Florida, 2004: p. 437.

[132] A.A. Steuter, A. Mozafar, J.R. Goodin, Water potential of aqueous polyethylene-glycol, Plant Physiol. 67 (1981) 64–67.

[133] P.J. Stiff, A.R. Koester, M.K. Weidner, K. Dvorak, R.I. Fisher, Autologous bone marrow transplantation using unfractionated cells cryopreserved in dimethylsulfoxide and hydroxyethyl starch without controlled-rate freezing, Blood. 70 (1987) 974–978.

[134] W. Strober, Appendix 3B - Trypan Blue Exclusion Test of Cell Viability, in: J.E. Coligan (Ed.), Curr. Protoc. Immunol., John Wiley & Sons, Inc., 1997.

[135] A.B. Sultani, L.A. Marquez-Curtis, J.A.W. Elliott, L.E. McGann, Improved Cryopreservation of Human Umbilical Vein Endothelial Cells: A Systematic Approach, Sci. Rep. 6 (2016) 34393.

[136] M. Toner, E.G. Cravalho, D.R. Armant, Water Transport and Estimated Transmembrane Potential during Freezing of Mouse Oocytes, J. Membr. Biol. 115 (1990) 261–272.

[137] M. Toner, E.G. Cravalho, M. Karel, Cellular response of mouse oocytes to freezing stress: Prediction of intracellular ice formation, J. Biomech. Eng. 115 (1993) 169–174.

[138] J.H. Van't Hoff, The role of osmotic pressure in the analogy between solutions and gases, J. Memb. Sci. 100 (1995) 39–44.

[139] A.M. Vian, A.Z. Higgins, Membrane permeability of the human granulocyte to water, dimethyl sulfoxide, glycerol, propylene glycol and ethylene glycol., Cryobiology. 68 (2014) 35–42.

[140] V.L. Vilker, C.K. Colton, K.A. Smith, The osmotic pressure of concentrated protein solutions: Effect of concentration and ph in saline solutions of bovine serum albumin, J. Colloid Interface Sci. 79 (1981) 548–566.

[141] H. Vink, Membrane equilibria in concentrated polymer solutions, Eur. Polym. J. 9 (1973) 887–894.

[142] R.C. Weast, M.J. Astle, Ed., CRC Handbook of Chemistry and Physics, CRC Press, Inc., Boca Raton, Florida, 1983.

[143] L. Weng, W. Li, J. Zuo, Kinetics of osmotic water flow across cell membranes in non-ideal solutions during freezing and thawing, Cryobiology. 61 (2010) 194–203.

[144] L. Weng, W. Li, J. Zuo, Two applications of the thermogram of the alcohol/water binary system with compositions of cryobiological interests, Cryobiology. 62 (2011) 210–217.

[145] L. Weng, W. Li, J. Zuo, DSC determination of partial ternary phase diagrams of methanol/sodium chloride/water and propylene glycol/sodium chloride/water and their applications for synthesized diagrams, Thermochim. Acta. 512 (2011) 225–232.

[146] E.J. Woods, M.A.J. Zieger, D.Y. Gao, J.K. Critser, Equations for obtaining melting points for the ternary system ethylene glycol/sodium chloride/water and their application to

cryopreservation, Cryobiology. 38 (1999) 403–407.

[147] M. Wusteman, C.J. Hunt, The Scientific Basis for Tissue Banking, in: B.J. Fuller, N. Lane, E.E. Benson (Eds.), Life Frozen State, CRC Press, Boca Raton, Florida, 2004: p. 541.

[148] G. Yang, A. Zhang, L.X. Xu, Experimental study of intracellular ice growth in human umbilical vein endothelial cells, Cryobiology. 58 (2009) 96–102.

[149] M.A. Yousef, R. Datta, V.G.J. Rodgers, Confirmation of free solvent model assumptions in predicting the osmotic pressure of concentrated globular proteins, J. Colloid Interface Sci. 243 (2001) 321–325.

[150] M.A. Yousef, R. Datta, V.G.J. Rodgers, Model of osmotic pressure for high concentrated binary protein solutions, AICHE J. 48 (2002) 913–917.

[151] L. Zargarzadeh, J.A.W. Elliott, Comparison of the osmotic virial equation with the Margules activity model and their application to solid–liquid equilibrium (to be submitted), (n.d.).

[152] T. Zhang, A. Isayeva, S.L. Adams, D.M. Rawson, Studies on membrane permeability of zebrafish (Danio rerio) oocytes in the presence of different cryoprotectants, Cryobiology. 50 (2005) 285–293.

[153] G. Zhao, H. Takamatsu, X. He, The effect of solution nonideality on modeling transmembrane water transport and diffusion-limited intracellular ice formation during cryopreservation, J. Appl. Phys. 115 (2014) 144701.

[154] M.W. Zielinski, L.E. McGann, J.A. Nychka, J.A.W. Elliott, Comparison of non-ideal solution theories for multi-solute solutions in cryobiology and tabulation of required coefficients, Cryobiology. 69 (2014) 305–317.

[155] M.W. Zielinski, L.E. McGann, J.A. Nychka, J.A.W. Elliott, Comment on “Determination of the quaternary phase diagram of the water–ethylene glycol–sucrose–NaCl system and a comparison between two theoretical methods for synthetic phase diagrams” Cryobiology 61 (2010) 52–57, Cryobiology. 70 (2015) 287–292.

[156] M.W. Zielinski, L.E. McGann, J.A. Nychka, J.A.W. Elliott, A Non-Ideal Solute Chemical Potential Equation and the Validity of the Grouped Solute Approach for Intracellular Solution Thermodynamics, J. Phys. Chem. B. 121 (2017) 10443–10456.

[157] The Wolfram Functions Site: General Identities, <http://functions.wolfram.com>, (2010).

## Appendix A. Matrix approach to multiple linear regression[5]

The solute-specific coefficients for the non-ideal models considered in this work were curve-fit using an analytical matrix approach to multiple linear regression. The general concept of this approach is briefly outlined here, along with details of the specific implementation for each non-ideal model.

Given "$n$" data points and "$p$" regressor variables (each of which has an associated regression coefficient), the general multiple linear regression model can be expressed as follows [93]

$$y_{(a)} = \beta_1 f_{1(a)} + \beta_2 f_{2(a)} + \cdots + \beta_p f_{p(a)} + \varepsilon_{(a)} \quad \text{for } a = 1, \ldots, n\,, \tag{A.1}$$

where $y$ is the dependent variable (sometimes called the regressand or observation), $\beta_1, \ldots, \beta_p$ are the regression coefficients, $f_1, \ldots, f_p$ are the regressor variables, and $\varepsilon$ is the error of the model prediction. The number in brackets (*i.e.* $a$) denotes the $a^{\text{th}}$ data point. The values of $y$ and $f_1, \ldots, f_p$ are known (obtained from experimental data), and the unknowns are the regression coefficients $\beta_1, \ldots, \beta_p$. Equation A.1 can be written in matrix notation as [93]

$$\vec{y} = \vec{\beta}\underline{F} + \vec{\varepsilon}\,, \tag{A.2}$$

where $\vec{y}$ is an ($n \times 1$) vector of the dependent variables (the regressand vector), $\vec{\beta}$ is a ($p \times 1$) vector of regression coefficients (the parameter vector), $\underline{F}$ is an ($n \times p$) matrix of regressors (the design matrix), and $\vec{\varepsilon}$ is an ($n \times 1$) vector of prediction errors. To obtain an estimate for the unknown values of $\vec{\beta}$, the method of ordinary least squares can be used. This method finds the values of $\vec{\beta}$

[5] This appendix, along with Chapter 2 and Appendix B, has been published as M.W. Zielinski, L.E. McGann, J.A. Nychka, J.A.W. Elliott, Comparison of non-ideal solution theories for multi-solute solutions in cryobiology and tabulation of required coefficients, Cryobiology 69 (2014) 305–317. This work is available at http://dx.doi.org/10.1016/j.cryobiol.2014.08.005.

that minimize the sum of the squared errors of the model predictions (*i.e.* minimize the sum of the squared residuals). In matrix notation, the ordinary least squares estimate of $\vec{\beta}$, $\hat{\vec{\beta}}$, is [93]

$$\hat{\vec{\beta}} = \left(\underline{F}^T \underline{F}\right)^{-1} \underline{F}^T \vec{y}\,. \tag{A.3}$$

A "hat" (^) above a value indicates that that value is an estimate from a fitted regression model. In this work, wherever used, the matrix approach was implemented using MATLAB R2010b (MathWorks, Natick, MA).

Using this matrix approach, the molality and mole-fraction based forms of the osmotic virial equation were fit to each of the binary (*i.e.* single-solute) solution data sets (written in terms of osmolality versus concentration) in order to obtain the corresponding osmotic virial coefficients (and, if applicable, the dissociation constant) for the solute of interest. Note that Equations 2.9 and 2.10 can be curve-fit as written; however, Equations 2.5 and 2.6 must be rewritten in order to avoid having regressors without coefficients, *i.e.*, respectively

$$\pi - m_i = B_{ii} {m_i}^2 + C_{iii} {m_i}^3 + \cdots, \tag{A.4}$$

and

$$\tilde{\pi} - x_i = B_{ii}{}^* {x_i}^2 + C_{iii}{}^* {x_i}^3 + \cdots. \tag{A.5}$$

The regressors in Equations 2.9, 2.10, A.4, and A.5 are the concentration powers, and the regression coefficients are the osmotic virial coefficients and/or the dissociation constants. For example, for Equation A.4, the first two regressors are $f_1 = {m_i}^2$ and $f_2 = {m_i}^3$, and the first two regression coefficients are $\beta_1 = B_{ii}$ and $\beta_2 = C_{iii}$. For each of Equations 2.9, 2.10, A.4, and A.5, the forms of $\vec{y}$, $\underline{F}$, and $\vec{\beta}$ are given in Table A.1.

The matrix approach was also used to curve-fit the freezing point summation model to the binary solution data (written in terms of freezing point depression versus concentration) to obtain

the corresponding solute-specific coefficients. The forms of $\vec{y}$, $\underline{F}$, and $\vec{\beta}$ for this model (Equation 2.20) are also given in Table A.1.

Table A.1. Forms of $\vec{y}$, $\underline{F}$, and $\vec{\beta}$ for the osmotic virial equation (OVE) and freezing point summation model.

| Applicable Model | $\vec{y}$ | $\vec{\beta}$ | $\underline{F}$ |
|---|---|---|---|
| **Molality-based, electrolyte OVE: Equation 2.9** | $\vec{\pi} = \begin{Bmatrix} \pi_{(1)} \\ \vdots \\ \pi_{(n)} \end{Bmatrix}$ | $\begin{Bmatrix} k_i \\ {k_i}^2 B_{ii} \\ {k_i}^3 C_{iii} \\ \vdots \end{Bmatrix}$ | $\begin{bmatrix} m_{i(1)} & {m_{i(1)}}^2 & {m_{i(1)}}^3 & \cdots \\ \vdots & \vdots & \vdots & \vdots \\ m_{i(n)} & {m_{i(n)}}^2 & {m_{i(n)}}^3 & \cdots \end{bmatrix}$ |
| **Mole fraction-based, electrolyte OVE: Equation 2.10** | $\vec{\tilde{\pi}} = \begin{Bmatrix} \tilde{\pi}_{(1)} \\ \vdots \\ \tilde{\pi}_{(n)} \end{Bmatrix}$ | $\begin{Bmatrix} k_i^* \\ {k_i^*}^2 {B_{ii}}^* \\ {k_i^*}^3 {C_{iii}}^* \\ \vdots \end{Bmatrix}$ | $\begin{bmatrix} x_{i(1)} & {x_{i(1)}}^2 & {x_{i(1)}}^3 & \cdots \\ \vdots & \vdots & \vdots & \vdots \\ x_{i(n)} & {x_{i(n)}}^2 & {x_{i(n)}}^3 & \cdots \end{bmatrix}$ |
| **Molality-based, non-electrolyte OVE: Equation A.4** | $\overrightarrow{(\pi - m_\iota)} = \begin{Bmatrix} \pi_{(1)} - m_{i(1)} \\ \vdots \\ \pi_{(n)} - m_{i(n)} \end{Bmatrix}$ | $\begin{Bmatrix} B_{ii} \\ C_{iii} \\ \vdots \end{Bmatrix}$ | $\begin{bmatrix} {m_{i(1)}}^2 & {m_{i(1)}}^3 & \cdots \\ \vdots & \vdots & \vdots \\ {m_{i(n)}}^2 & {m_{i(n)}}^3 & \cdots \end{bmatrix}$ |
| **Mole fraction-based, non-electrolyte OVE: Equation A.5** | $\overrightarrow{(\tilde{\pi} - x_\iota)} = \begin{Bmatrix} \tilde{\pi}_{(1)} - x_{i(1)} \\ \vdots \\ \tilde{\pi}_{(n)} - x_{i(n)} \end{Bmatrix}$ | $\begin{Bmatrix} {B_{ii}}^* \\ {C_{iii}}^* \\ \vdots \end{Bmatrix}$ | $\begin{bmatrix} {x_{i(1)}}^2 & {x_{i(1)}}^3 & \cdots \\ \vdots & \vdots & \vdots \\ {x_{i(n)}}^2 & {x_{i(n)}}^3 & \cdots \end{bmatrix}$ |
| **Freezing Point Summation Model: Equation 2.20** | $\overrightarrow{(-\Delta T_m)} = \begin{Bmatrix} -\Delta T_{m_{(1)}} \\ \vdots \\ -\Delta T_{m_{(n)}} \end{Bmatrix}$ | $\begin{Bmatrix} C_{1i} \\ C_{2i} \\ C_{3i} \end{Bmatrix}$ | $\begin{bmatrix} m_{i(1)} & {m_{i(1)}}^2 & {m_{i(1)}}^3 \\ \vdots & \vdots & \vdots \\ m_{i(n)} & {m_{i(n)}}^2 & {m_{i(n)}}^3 \end{bmatrix}$ |

## Appendix B. Adjusted $R^2$ and regression through the origin[6]

In this work, a criterion based on the coefficient of determination was used to determine the order of fit to single-solute solution data for the molality- and mole fraction-based forms of the osmotic virial equation. The coefficient of determination, $R^2$, can be defined as [22,93]

$$R^2 = 1 - \frac{ESS}{TSS}, \tag{B.1}$$

where ESS is the error sum of squares and TSS is the total sum of squares. The error sum of squares is defined as [22,93]

$$ESS = \sum_{a=1}^{n} \left(y_{(a)} - \hat{y}_{(a)}\right)^2, \tag{B.2}$$

with $n - p$ degrees of freedom, where $y_{(a)}$ is the value at the $a^{\text{th}}$ data point, $\hat{y}_{(a)}$ is the fitted model prediction of the $a^{\text{th}}$ data point, $n$ is the total number of data points, and $p$ is the number of parameters/coefficients in the model. The total sum of squares is commonly given as [22,93]

$$TSS = \sum_{a=1}^{n} \left(y_{(a)} - \bar{y}\right)^2, \tag{B.3}$$

with $n - 1$ degrees of freedom, where $\bar{y}$ is the mean value of all data points. The value of $R^2$ can range from 0, corresponding to a poor fit, to 1, corresponding to a good fit.

However, $R^2$ does not does not take into consideration the number of parameters used in the model and will always increase when a parameter is added [93]. Conversely, the adjusted $R^2$ statistic does take into account the number of parameters in the model, effectively applying a

[6] This appendix, along with Chapter 2 and Appendix A, has been published as M.W. Zielinski, L.E. McGann, J.A. Nychka, J.A.W. Elliott, Comparison of non-ideal solution theories for multi-solute solutions in cryobiology and tabulation of required coefficients, Cryobiology 69 (2014) 305–317. This work is available at http://dx.doi.org/10.1016/j.cryobiol.2014.08.005.

penalty for each additional parameter—as such, it can be used to evaluate the merit of increasing the order of fit (*i.e.* adding a coefficient). Adjusted $R^2$ can be defined as [93]

$$R^2_{adj} = 1 - \frac{ESS/DOF_{ESS}}{TSS/DOF_{TSS}}, \tag{B.4}$$

where $DOF_{ESS} = n - p$ is the degrees of freedom for the error sum of squares and $DOF_{TSS}$ is the degrees of freedom for the total sum of squares (for the above definition of the total sum of squares, $DOF_{TSS} = n - 1$).

It should be noted that the osmotic virial equation does not have an intercept; that is, it passes through the origin (by definition, the osmolality of pure water is zero). This is of consequence because in the above definitions of $R^2$ and adjusted $R^2$, the definition of the total sum of squares (Equation B.3) is obtained from the analysis of variance (ANOVA) identity [22,93]

$$\sum_{a=1}^{n} \left(y_{(a)} - \bar{y}\right)^2 = \sum_{a=1}^{n} \left(\hat{y}_{(a)} - \bar{y}\right)^2 + \sum_{a=1}^{n} \left(y_{(a)} - \hat{y}_{(a)}\right)^2, \tag{B.5}$$

which does not hold for regression through the origin [22]. A common alternative recommendation [22,71] is to use the following modified form of the analysis of variance identity for regression through the origin

$$\sum_{a=1}^{n} \left(y_{(a)}\right)^2 = \sum_{a=1}^{n} \left(\hat{y}_{(a)}\right)^2 + \sum_{a=1}^{n} \left(y_{(a)} - \hat{y}_{(a)}\right)^2, \tag{B.6}$$

in which case the definition for the total sum of squares becomes

$$TSS = \sum_{a=1}^{n} \left(y_{(a)}\right)^2, \tag{B.7}$$

with *n* degrees of freedom. Note that the definition of the error sum of squares remains unchanged. Although there has been some controversy [22,45,71,72] regarding the appropriate form of the total sum of squares to use in the definition of $R^2$ for regression through the origin, the argument

against using Equation B.7 (*i.e.* instead of Equation B.3) is essentially that the resulting value of $R^2$ is not directly comparable to a value computed the "usual" way (*i.e.* using Equation B.3) and cannot be interpreted in the same way [45,71,72], the primary consequence being that one cannot evaluate the benefit of adding/removing an intercept to/from the fitting model. In the case of the osmotic virial equation, this argument has no ramifications, as, by definition, we cannot consider a model with an intercept (the osmolality of pure water must be zero). Conversely, the argument against using Equation B.3 for regression through the origin is that it can result in an uninterpretable negative value of $R^2$ [22,71]. Thus, for choosing the order of fit for the osmotic virial equation in this work, the adjusted $R^2$ statistic that arises from using Equation B.7 as the definition of the total sum of squares was used, *i.e.*

$$R^2_{adj,\mathrm{RTO}} = 1 - \frac{\sum\left(y_{(a)} - \hat{y}_{(a)}\right)^2/(n-p)}{\sum\left(y_{(a)}\right)^2/(n)}. \tag{2.28}$$

This form of the adjusted $R^2$ is referred to as the regression-through-origin form in the main body of this work.

## Appendix C. Difference between Equation 3.7 and Guggenheim's "naïve assumption"[7]

Although there is no mathematical difference between the combining rule in Equation 3.7 and what Guggenheim called the "naïve assumption" [46,102] (see Equation C.3 below), the former does not suffer from the same problem as the latter due to the difference in the contexts in which the two equations are used—*i.e.,* liquid solutions for Equation 3.7 versus gas mixtures for the naïve assumption. This distinction and its impact are explained briefly in the following.

The thermodynamic behaviour of a gas mixture can generally be described by the gaseous virial equation of state [102],

$$\frac{Pv}{RT} = 1 + \frac{B^*_{mix}}{v} + \frac{C^*_{mix}}{v^2} + \cdots, \tag{C.1}$$

where $P$ is pressure, $v$ is molar volume, and $B^*_{mix}$ and $C^*_{mix}$ are the second and third gaseous virial coefficients of the mixture. For any given mixture, the gaseous virial coefficients can be obtained using mixing rules, which describe how a virial coefficient is related to composition. These rules are distinct from combining rules, which, as noted above, describe relationships between solute-specific single-solute coefficients and cross-coefficients. The second gaseous virial coefficient $B^*_{mix}$ can be obtained from the mixing rule [102]

$$B^*_{mix} = \sum_{i=1}^{r}\sum_{j=1}^{r} B^*_{ij} x_i x_j \,, \tag{C.2}$$

where $r$ is the total number of components in the mixture and $B^*_{ij}$ is the solute-specific gaseous virial coefficient for solutes *i* and *j*. Note that the $B^*_{ij}$ term includes both single-solute coefficients

[7] This appendix, along with Chapter 3 and Appendix D, has been published as M.W. Zielinski, L.E. McGann, J.A. Nychka, J.A.W. Elliott, A Non-Ideal Solute Chemical Potential Equation and the Validity of the Grouped Solute Approach for Intracellular Solution Thermodynamics, J. Phys. Chem. B. 121 (2017) 10443–10456. This work is available at http://pubs.acs.org/articlesonrequest/AOR-38xihDTThrSv82dTdyFp.

where $i = j$ and cross-coefficients where $i \neq j$. Much like the osmotic virial coefficients $B_{ij}$ or $B_{ij}^{+}$, the solute-specific gaseous virial coefficients $B_{ij}^{*}$, including the cross-coefficients, can be obtained empirically, from experimental measurements. The cross-coefficients can also be obtained from combining rules. One such combining rule, which is essentially Equation 3.7 rewritten for a gas mixture, is what Guggenheim referred to as the "naïve assumption" [46,102], *i.e.*,

$$B_{ij}^{*} = \frac{B_{ii}^{*} + B_{jj}^{*}}{2}. \tag{C.3}$$

The problem with this combining rule is that when it is substituted back into Equation C.2, it yields a mixing rule which inaccurately has a linear dependence on composition, as demonstrated below.

Substituting Equation C.3 into Equation C.2 yields

$$B_{mix}^{*} = \frac{1}{2}\sum_{i=1}^{r}\sum_{j=1}^{r}\left(B_{ii}^{*} + B_{jj}^{*}\right)x_i x_j\,, \tag{C.4}$$

which can be simplified to

$$B_{mix}^{*} = \frac{1}{2}\left[\sum_{i=1}^{r}\sum_{j=1}^{r}\left(B_{ii}^{*}x_i x_j\right) + \sum_{i=1}^{r}\sum_{j=1}^{r}\left(B_{jj}^{*}x_i x_j\right)\right]. \tag{C.5}$$

Note that

$$\sum_{i=1}^{r}\sum_{j=1}^{r}\left(B_{ii}^{*}x_i x_j\right) = \sum_{i=1}^{r}\sum_{j=1}^{r}\left(B_{jj}^{*}x_i x_j\right), \tag{C.6}$$

meaning that Equation C.5 can be further simplified to

$$B_{mix}^{*} = \sum_{i=1}^{r}\sum_{j=1}^{r}\left(B_{ii}^{*}x_i x_j\right). \tag{C.7}$$

Applying the second-order general multiplication rule for finite sums (see Equation D.1 in Appendix D), Equation C.7 becomes

$$B^*_{mix} = \left(\sum_{i=1}^{r} B^*_{ii} x_i\right)\left(\sum_{j=1}^{r} x_j\right). \tag{C.8}$$

Finally, applying the definition of mole fraction, *i.e.*, $\sum_{i=1}^{r} x_i = 1$, we ultimately obtain

$$B^*_{mix} = \sum_{i=1}^{r} B^*_{ii} x_i \,, \tag{C.9}$$

in which the gaseous virial coefficient of the mixture has a linear dependence on composition. Such a linear dependence is not in agreement with experimental measurements of gas mixtures [46,102].

The problem with Equation C.3, highlighted in Equation C.9 above, does not apply to Equation 3.7. This is because unlike the *gaseous* virial equation—*i.e.,* the model in which Equation C.3 is used, the *osmotic* virial equation—*i.e.*, the model in which Equation 3.7 is used—does not provide coefficients to account for solvent interactions. As a consequence, the "mixing rule" for the (mole fraction-based) second osmotic virial coefficient of a solution, $B^+_{sol}$, is

$$B^+_{sol} = \sum_{i=2}^{r}\sum_{j=2}^{r} B^+_{ij} x_i x_j \,, \tag{C.10}$$

where $r$ still represents the total number of components in the solution, but in this case means the solvent (subscript index 1) plus $r - 1$ solutes. When Equation 3.7 is substituted into Equation C.10 and a similar procedure is undertaken to that carried out for Equations C.2 and C.3 above, the ultimate result is

$$B_{sol}^{+} = \left(\sum_{i=2}^{r} B_{ii}^{+} x_i\right)\left(\sum_{j=2}^{r} x_j\right) = (1 - x_1)\left(\sum_{i=2}^{r} B_{ii}^{+} x_i\right). \tag{C.11}$$

Equation C.11 will always be quadratic in composition for any multi-component system. Thus, the combining rule in Equation 3.7 is not the "naïve assumption" in Equation C.3, and, unlike the latter, will result in a mixing rule that has a quadratic dependence on composition.

## Appendix D. Multiplication rule for finite sums[8]

The second and third-order multiplication rules for finite sums are [157]

$$\left(\sum_{i=i_o}^{i_f} a_i\right)\left(\sum_{j=j_o}^{j_f} b_j\right) = \sum_{i=i_o}^{i_f}\sum_{j=j_o}^{j_f} a_i b_j \tag{D.1}$$

and

$$\left(\sum_{i=i_o}^{i_f} a_i\right)\left(\sum_{j=j_o}^{j_f} b_j\right)\left(\sum_{k=k_o}^{k_f} c_k\right) = \sum_{i=i_o}^{i_f}\sum_{j=j_o}^{j_f}\sum_{k=k_o}^{k_f} a_i b_j c_k\,, \tag{D.2}$$

where the $a_i$ depend solely on $i$, the $b_j$ depend solely on $j$, the $c_k$ depend solely on $k$, and $i_o$, $i_f$, $j_o$, $j_f$, $k_o$, and $k_f$ are all finite positive integers. Equation D.2 can be shown to be true as follows (a similar procedure can be used to show that Equation D.1 is true).

We start by considering the right-hand side of the Equation D.2, *i.e.,*

$$\sum_{i=i_o}^{i_f}\sum_{j=j_o}^{j_f}\sum_{k=k_o}^{k_f} a_i b_j c_k\,. \tag{D.3}$$

As neither $a_i$ nor $b_j$ depend on $k$ (*i.e.,* they are constants with respect to $k$), they can be divided out of the innermost sum, *i.e.,*

$$\sum_{i=i_o}^{i_f}\sum_{j=j_o}^{j_f}\sum_{k=k_o}^{k_f} a_i b_j c_k = \sum_{i=i_o}^{i_f}\sum_{j=j_o}^{j_f}\left(a_i b_j \sum_{k=k_o}^{k_f} c_k\right). \tag{D.4}$$

Likewise, neither $a_i$ nor $\sum_{k=k_o}^{k_f} c_k$ depend on $j$, so these terms can be taken out of the middle sum as follows

[8] This appendix, along with Chapter 3 and Appendix C, has been published as M.W. Zielinski, L.E. McGann, J.A. Nychka, J.A.W. Elliott, A Non-Ideal Solute Chemical Potential Equation and the Validity of the Grouped Solute Approach for Intracellular Solution Thermodynamics, J. Phys. Chem. B. 121 (2017) 10443–10456. This work is available at http://pubs.acs.org/articlesonrequest/AOR-38xihDTThrSv82dTdyFp.

$$\sum_{i=i_o}^{i_f}\sum_{j=j_o}^{j_f}\sum_{k=k_o}^{k_f} a_i b_j c_k = \sum_{i=i_o}^{i_f}\left[(a_i)\left(\sum_{k=k_o}^{k_f} c_k\right)\left(\sum_{j=j_o}^{j_f} b_j\right)\right]. \quad \text{(D.5)}$$

Finally, neither $\sum_{j=j_o}^{j_f} b_j$ nor $\sum_{k=k_o}^{k_f} c_k$ depend on $i$, so they can be divided out of the outermost sum, giving back Equation D.2, as required.

## Appendix E. Measurement of cell equilibration kinetics

To determine the amount of time required for cryoprotectant equilibration—*i.e.*, the cryoprotectant exposure time—a modified form of the procedure used in the equilibrium cell volume measurements was applied. In this case, the aim was to measure the time-dependant changes in cell volume—*i.e.*, the kinetic osmotic response—following the addition of a defined concentration of a permeating cryoprotectant.

Cell suspensions were prepared in the same way as for the equilibrium volume measurements, albeit with a lower minimum cell concentration of $4\times10^6$ cells/mL. As before, the cell suspensions were then kept in an ice–water bath until used in the experiment. For the measurements, the cell suspension was subdivided into twelve experimental samples. Three such samples were used with each of the experimental cryoprotectant concentrations considered: 0 (control), 1, 2, and 3 molal.

As for the equilibrium volume measurements, cell volumes were measured using bright-field optical microscopy and image analysis. (Note that trypan blue staining was not used in these experiments.) Unlike the equilibrium volume measurements, the cryoprotectant was added directly to the experimental sample all at once (*i.e.*, not dropwise or incrementally) in the amount required to give the desired cryoprotectant concentration in the cell suspension. This was followed by a very brief period of pipette mixing. As soon as the cryoprotectant was added and mixed in to the suspension, the timer was started and a small volume (10 μL) of the cell suspension was placed onto a haemocytometer positioned under a 40× objective lens in an optical microscope. As with the equilibrium volume measurements, the haemocytometer grid was used to focus the image such that the top edges of the grid were in focus. Once the image was focussed, a region on the haemocytometer with approximately 10 to 20 cells was located and the field of view was set to

this region and left unchanged for the duration of the measurements. Photos of the cells were then taken at set intervals.

The first photo was taken at 30 seconds post-cryoprotectant addition. Given the amount of time required to inject the cell sample into the haemocytometer, focus the image, and locate an appropriate region for measurements, earlier photos could not be reliably acquired. For the purposes of this work, this limitation was not a problem, as we were only interested in the final stages of the cellular osmotic response—*i.e.*, where the cell reaches its equilibrium volume—and not in the initial shrink-swell response (see Figure 4.13 for a representative cellular osmotic response). After the initial photo, photos were taken at 10 second intervals up until 1 minute post-cryoprotectant addition, then at 20 second intervals until 3 minutes post-cryoprotectant addition, and then at 30 second intervals up to the end of the experiment at 10 minutes post-cryoprotectant addition. Finally, after all the cell photos had been acquired, a photo was taken in the central portion of the haemocytometer grid for scale calibration purposes. The cell photos were then analyzed using a custom ImageJ macro script, described briefly below (see Appendix F for the script itself).

In the early stages, the macro script for the kinetic measurements (see "Measure HUVEC Kinetic Osmotic Volume Changes" in Appendix F) is fundamentally similar to the one described above for the equilibrium volume measurements. It uses a calibration image to account for uneven lighting in the same way, and then applies the same identifyCells function to locate the cells in all of the images. However, at this point, the macros diverge. Once the cells have been located in each of the images for a given experimental sample, the kinetic measurements macro tracks each individual cell through all of the images such that a cell-specific measurement of cross-sectional area—and thus volume—as a function of time can be obtained for all of the cells. Briefly, an

identified cell is tracked through the images by finding the cell in the next image whose central coordinates are within the area of the identified cell in the current image and whose area is within 20% of that of the identified cell in the current image (for further details, see Appendix F below). With the time-dependant volumetric behaviour of each cell measured, it is then possible to establish the point at which the cell stops changing volume—*i.e.*, when it has equilibrated.

This procedure to determine the cryoprotectant exposure time was carried out with HUVEC in the presence of each of DMSO and EG. For both cryoprotectants and at all concentrations examined (*i.e.*, 1, 2, and 3 molal), the cells were found to have equilibrated by no later than 7 minutes post-cryoprotectant addition. As such, 7 minutes was used as the cryoprotectant exposure time in all of the equilibrium volume measurements.

# Appendix F. Custom ImageJ macro script for measuring cell volume and membrane integrity

```
//GLOBAL VALUES/VARIABLES

//this value represents the number of times cell ROIs will be eroded to find their
centres
var paintErodeIter = 4;

//this value is used to determine which pixels belong to the haemocytometer grid -
i.e. very bright pixels ("very bright" = mean pixel value + gridMultiplier*[standard
deviation])
var gridMultiplier = 2;

//this value is used to enhance the image after finding the edges of cells (every
pixel in the image is multiplied by this value)
var imageMultiplier = 1.5;

//this value is used to find unusually light pixels (usually belonging to cell
"halos")
var standardMultiplier = 0.25;

//this value is used to find dark pixels close to unusually light pixels (i.e. cells
with "halos")
var diffThreshold = 10;

//this is the value by which dark pixels next to halos are dropped/decreased in value
var edgeDropValue = 20;

//this is the minimum required average pixel value for an ROI to be considered to
contain a cell (used to determine whether or not to "paint in" a potential cell's
centre)
var minMeanROI = 20;

//above this average pixel value, a ROI containing a cell will have the cell centre
"painted in" to a lesser extent than normal (paintErodeIter will be applied twice to
these centres)
var maxMeanROI = 175;

//this value is the minimum required cell circularity for equilibrium measurements
var equilibriumCirc = 0.6;

//this value is the minimum required cell circularity for kinetic measurements
var kineticCirc = 0.7;

//this value is used in determining whether a cell is membrane-compromised (blue) or
intact - the lower this value is, the more likely a cell is to be considered
membrane-compromised
var intactThresholdMultiplier = 0.98;

//this value represents the maximum allowed area change between images for a given
cell when tracking cells from image to image for kinetic measurements
```

```
var allowedDifference = 0.2;

//this value represents the maximum number of times the kinetic volume change
algorithm will try to find a "lost" cell before giving up
var lostCellMax = 5;

//this value represents the minimum number of data points required for a cell to be
considered in kinetic measurements
var minDataPoints = 10;


macro "Measure HUVEC Equilibrium Volume and Membrane Integrity" {

	//load calibration image (i.e. haemocytometer master image)
	run("Set Measurements...", "area mean feret's display redirect=None
decimal=5");
	showMessageWithCancel("Image Calibration", "Please load haemocytometer master
calibration image before continuing (a file selection dialogue will open after you
press OK)");
	run("Open...");
	hcMasterTitle = getTitle();
	hcMasterDir = File.directory;
	selectWindow(hcMasterTitle);
	close();

	//load images to be analyzed
	dir = getDirectory("Choose Folder Containing Images to Analyze");
	list = getFileList(dir);
	calList = newArray(list.length);
	setBatchMode(false);

	//calibrate images and identify locations of cells
	for (i=0; i<list.length; i++) {
		open(dir+list[i]);
		open(hcMasterDir+hcMasterTitle);
		imageCalculator("Subtract create",list[i],hcMasterTitle);
		saveAs("jpeg",dir+list[i]+" Calibrated");
		calList[i] = getTitle();
		selectWindow(calList[i]);
		run("Close");
		selectWindow(list[i]);
		run("Close");
		selectWindow(hcMasterTitle);
		run("Close");
		identifyCells(dir+calList[i], equilibriumCirc);
	}

	//measure cell size
	for (i=0; i<list.length; i++) {
		open(dir+calList[i]);
		open(dir+calList[i]+"_ALL.zip");
		roiManager("Measure");
		roiManager("Reset");
		selectWindow(calList[i]);
		run("Close");
```

```
}

selectWindow("ROI Manager");
run("Close");

saveAs("Results",dir+"Measurements Summary, All Cells.xls");
selectWindow("Results");
run("Close");

//identify which cells are intact
for (i=0; i<list.length; i++) {
	open(dir+calList[i]);
	open(dir+calList[i]+"_ALL.zip");

	numCells = roiManager("count");
	run("Split Channels");

	selectWindow(calList[i]+" (red)");
	run("Select All");
	getStatistics(area, redMean);
	run("Select None");

	selectWindow(calList[i]+" (green)");
	run("Select All");
	getStatistics(area, greenMean);
	run("Select None");

	selectWindow(calList[i]+" (blue)");
	run("Select All");
	getStatistics(area, blueMean);
	run("Select None");

	meanBORratio = blueMean/redMean;
	meanBOGratio = blueMean/greenMean;

	j = 0;
	while(j < numCells) {
		selectWindow(calList[i]+" (red)");
		roiManager("select", j);
		getStatistics(area, redCell);
		roiManager("deselect");
		run("Select None");

		selectWindow(calList[i]+" (green)");
		roiManager("select", j);
		getStatistics(area, greenCell);
		roiManager("deselect");
		run("Select None");

		selectWindow(calList[i]+" (blue)");
		roiManager("select", j);
		getStatistics(area, blueCell);
		roiManager("deselect");
		run("Select None");
```

```
                cellBORratio = blueCell/redCell;
                cellBOGratio = blueCell/greenCell;

                if((cellBORratio > (intactThresholdMultiplier*meanBORratio)) ||
(cellBOGratio > (intactThresholdMultiplier*meanBOGratio))){
                        roiManager("select", j);
                        roiManager("delete");
                        numCells = roiManager("count");
                } else {
                        j++;
                }
        }

        if(numCells > 0){
                roiManager("Save",dir+calList[i]+"_INTACT.zip");
        }
        roiManager("Reset");

        open(dir+calList[i]+"_ALL.zip");
        numCells = roiManager("count");

        j = 0;
        while(j < numCells) {
                selectWindow(calList[i]+" (red)");
                roiManager("select", j);
                getStatistics(area, redCell);
                roiManager("deselect");
                run("Select None");

                selectWindow(calList[i]+" (green)");
                roiManager("select", j);
                getStatistics(area, greenCell);
                roiManager("deselect");
                run("Select None");

                selectWindow(calList[i]+" (blue)");
                roiManager("select", j);
                getStatistics(area, blueCell);
                roiManager("deselect");
                run("Select None");

                cellBORratio = blueCell/redCell;
                cellBOGratio = blueCell/greenCell;

                if((cellBORratio <= (intactThresholdMultiplier*meanBORratio)) &&
(cellBOGratio <= (intactThresholdMultiplier*meanBOGratio))){
                        roiManager("select", j);
                        roiManager("delete");
                        numCells = roiManager("count");
                } else {
                        j++;
                }
        }

        if(numCells > 0){
```

```
			roiManager("Save",dir+calList[i]+"_DEAD.zip");
		}
		roiManager("Reset");

		selectWindow(calList[i]+" (red)");
		run("Close");
		selectWindow(calList[i]+" (green)");
		run("Close");
		selectWindow(calList[i]+" (blue)");
		run("Close");
		run("Close All");
}

//measure cell membrane integrity
processedList = getFileList(dir);
intactCellsPresent = false;
deadCellsPresent = false;

for (i=0; i<list.length; i++) {
		open(dir+calList[i]);
		for (j=0; j<processedList.length; j++){
			if(processedList[j] == calList[i]+"_INTACT.zip"){
				intactCellsPresent = true;
				open(dir+calList[i]+"_INTACT.zip");
			}
		}
		roiManager("Measure");
		roiManager("Reset");
		selectWindow(calList[i]);
		run("Close");
}

selectWindow("ROI Manager");
run("Close");

if(intactCellsPresent){
		saveAs("Results",dir+"Measurements Summary, Intact Cells Only.xls");
		selectWindow("Results");
		run("Close");
}

for (i=0; i<list.length; i++) {
		open(dir+calList[i]);
		for (j=0; j<processedList.length; j++){
			if(processedList[j] == calList[i]+"_DEAD.zip"){
				deadCellsPresent = true;
				open(dir+calList[i]+"_DEAD.zip");
			}
		}
		roiManager("Measure");
		roiManager("Reset");
		selectWindow(calList[i]);
		run("Close");
}
```

```
	selectWindow("ROI Manager");
	run("Close");

	if(deadCellsPresent){
		saveAs("Results",dir+"Measurements Summary, Dead Cells Only.xls");
		selectWindow("Results");
		run("Close");
	}
}


macro "Measure HUVEC Equilibrium Volume" {

	//load calibration image (i.e. haemocytometer master image)
	run("Set Measurements...", "area mean feret's display redirect=None
decimal=5");
	showMessageWithCancel("Image Calibration", "Please load haemocytometer master
calibration image before continuing (a file selection dialogue will open after you
press OK)");
	run("Open...");
	hcMasterTitle = getTitle();
	hcMasterDir = File.directory;
	selectWindow(hcMasterTitle);
	close();

	//load images to be analyzed
	dir = getDirectory("Choose Folder Containing Images to Analyze");
	list = getFileList(dir);
	calList = newArray(list.length);
	setBatchMode(false);

	//calibrate images and identify locations of cells
	for (i=0; i<list.length; i++) {
		open(dir+list[i]);
		open(hcMasterDir+hcMasterTitle);
		imageCalculator("Subtract create",list[i],hcMasterTitle);
		saveAs("jpeg",dir+list[i]+" Calibrated");
		calList[i] = getTitle();
		selectWindow(calList[i]);
		run("Close");
		selectWindow(list[i]);
		run("Close");
		selectWindow(hcMasterTitle);
		run("Close");
		identifyCells(dir+calList[i], equilibriumCirc);
	}

	//measure cell size
	for (i=0; i<list.length; i++) {
		open(dir+calList[i]);
		open(dir+calList[i]+"_ALL.zip");
		roiManager("Measure");
		roiManager("Reset");
		selectWindow(calList[i]);
		run("Close");
```

```
	}

	selectWindow("ROI Manager");
	run("Close");

	saveAs("Results",dir+"Measurements Summary, All Cells.xls");
	selectWindow("Results");
	run("Close");
}


macro "Measure HUVEC Kinetic Osmotic Volume Changes" {

	//load calibration image (i.e. haemocytometer master image)
	run("Set Measurements...", "area mean feret's display redirect=None
decimal=5");
	showMessageWithCancel("Image Calibration", "Please load haemocytometer master
calibration image before continuing (a file selection dialogue will open after you
press OK)");
	run("Open...");
	hcMasterTitle = getTitle();
	hcMasterDir = File.directory;
	selectWindow(hcMasterTitle);
	close();

	//load images to be analyzed
	dir = getDirectory("Choose Folder Containing Images to Analyze");
	list = getFileList(dir);
	calList = newArray(list.length);
	setBatchMode(false);

	//calibrate images and identify locations of cells
	for (i=0; i<list.length; i++) {
		open(dir+list[i]);
		open(hcMasterDir+hcMasterTitle);
		imageCalculator("Subtract create",list[i],hcMasterTitle);
		saveAs("jpeg",dir+list[i]+" Calibrated");
		calList[i] = getTitle();
		selectWindow(calList[i]);
		run("Close");
		selectWindow(list[i]);
		run("Close");
		selectWindow(hcMasterTitle);
		run("Close");
		identifyCells(dir+calList[i], kineticCirc);
	}

	//setup for cell tracking
	open(dir+calList[0]);
	open(dir+calList[0]+"_ALL.zip");
	numFirstCells = roiManager("count");
	selectWindow(calList[0]);
	run("Close");
	selectWindow("ROI Manager");
	run("Close");
```

```
	//track each individual cell from first image in series to last (or as far as
possible)
	for(j=0; j<numFirstCells; j++){
		open(dir+calList[0]);
		open(dir+calList[0]+"_ALL.zip");
		roiManager("select", j);
		roiManager("Measure");
		getSelectionBounds(xCURRENT, yCURRENT, wCURRENT, hCURRENT);
		xCentreCURRENT = round(xCURRENT+0.5*wCURRENT);
		yCentreCURRENT = round(yCURRENT+0.5*hCURRENT);
		areaCURRENT = wCURRENT*hCURRENT;
		roiManager("Reset");
		selectWindow(calList[0]);
		run("Close");

		lostCellCounter = 0;
		foundCellCounter = 1;
		for(i=1; (i<list.length)&&(lostCellCounter<3); i++){
			open(dir+calList[i]);
			open(dir+calList[i]+"_ALL.zip");
			numNextCells = roiManager("count");

			foundCell = false;
			cellIndex = 0;
			for(k=0; (k<numNextCells)&&!(foundCell); k++){
				roiManager("select", k);
				getSelectionBounds(xTEST, yTEST, wTEST, hTEST);
				xCentreTEST = round(xTEST+0.5*wTEST);
				yCentreTEST = round(yTEST+0.5*hTEST);
				areaTEST = wTEST*hTEST;

	if((xCentreTEST>xCURRENT)&&(xCentreTEST<(xCURRENT+wCURRENT))&&(yCentreTEST>yCU
RRENT)&&(yCentreTEST<(yCURRENT+hCURRENT))){

	if((xCentreCURRENT>xTEST)&&(xCentreCURRENT<(xTEST+wTEST))&&(yCentreCURRENT>yTE
ST)&&(yCentreCURRENT<(yTEST+hTEST))){
                                        if((abs(areaCURRENT-
areaTEST)/areaCURRENT)<allowedDifference){
                                                foundCell = true;
                                                cellIndex = k;
                                        }
                                }
                        }
                }

                if(foundCell){
                        roiManager("select", cellIndex);
                        getSelectionBounds(xCURRENT, yCURRENT, wCURRENT,
hCURRENT);
                        xCentreCURRENT = round(xCURRENT+0.5*wCURRENT);
                        yCentreCURRENT = round(yCURRENT+0.5*hCURRENT);
                        areaCURRENT = wCURRENT*hCURRENT;
                        roiManager("Measure");
                        foundCellCounter++;
```

```
                        lostCellCounter = 0;
                } else {
                        lostCellCounter++;
                }

                roiManager("Reset");
                selectWindow(calList[i]);
                run("Close");
        }

        if(foundCellCounter > minDataPoints){
                saveAs("Results",dir+"Measurements Summary, Cell "+(j+1)+".xls");
        }
        selectWindow("Results");
        run("Close");
    }

    selectWindow("ROI Manager");
    run("Close");
}


function identifyCells(path, circValue){

    //initial setup
    open(path);
    title = getTitle();
    run("Options...", "iterations=1 count=1 black pad edm=Overwrite");
    h = getHeight();
    w = getWidth();
    setColor(0);

    //preliminary operations
    run("Find Edges");
    run("Multiply...", "value=3.50000");

    //binarize image
    run("8-bit");
    setAutoThreshold("Default dark");
    setOption("BlackBackground", true);
    run("Convert to Mask");

    //binary operations to identify possible ROIs
    run("Close-");
    run("Fill Holes");
    run("Dilate");
    run("Close-");
    run("Fill Holes");
    run("Dilate");
    run("Close-");
    run("Fill Holes");
    run("Erode");
    run("Erode");
    run("Erode");
    run("Watershed");
```

```
	run("Watershed");
	run("Erode");
	run("Erode");
	run("Erode");
	run("Erode");
	run("Gaussian Blur...", "sigma=10");
	setAutoThreshold("Default dark");
	setOption("BlackBackground", true);
	run("Convert to Mask");
	run("Dilate");
	run("Close-");
	run("Dilate");
	run("Close-");

	//create two temporary clone images for painted overlay (cell centres)
	run("Select All");
	run("Copy");
	temp1Title = title+"TEMP1";
	newImage(temp1Title, "8-bit black", w, h, 1);
	selectImage(temp1Title);
	run("Paste");
	setAutoThreshold("Default dark");
	setOption("BlackBackground", true);
	run("Convert to Mask");
	run("Watershed");
	run("Watershed");
	run("Options...", "iterations="+paintErodeIter+" count=1 black pad
edm=Overwrite");
	run("Erode");
	run("Options...", "iterations=1 count=1 black pad edm=Overwrite");

	run("Select All");
	run("Copy");
	temp2Title = title+"TEMP2";
	newImage(temp2Title, "8-bit black", w, h, 1);
	selectImage(temp2Title);
	run("Paste");
	setAutoThreshold("Default dark");
	setOption("BlackBackground", true);
	run("Convert to Mask");
	run("Options...", "iterations="+paintErodeIter+" count=1 black pad
edm=Overwrite");
	run("Erode");
	run("Options...", "iterations=1 count=1 black pad edm=Overwrite");

	//capture ROI coordinates of original image and revert
	selectImage(title);
	run("Select None");
	run("Dilate");
	run("Analyze Particles...", "size=0-Infinity pixel circularity=0.00-1.00
show=Nothing clear include add");
	run("Revert");

	//preliminary operations part 2
	run("8-bit");
```

```
	getStatistics(area, mean, min, max, std);
	for(x=0; x<w; x++){
		for(y=0; y<h; y++){
			value = getPixel(x,y);
			if(value>(mean+gridMultiplier*std)){
				setPixel(x,y,(mean+gridMultiplier*std));
			}
		}
	}
	getStatistics(area, mean, min, max, std);
	for(x=1; x<(w-1); x++){
		for(y=1; y<(h-1); y++){
			value = getPixel(x,y);
			valueNN = getPixel(x-1,y-1);
			valueON = getPixel(x,y-1);
			valuePN = getPixel(x+1,y-1);
			valueNO = getPixel(x-1,y);
			valuePO = getPixel(x+1,y);
			valueNP = getPixel(x-1,y+1);
			valueOP = getPixel(x,y+1);
			valuePP = getPixel(x+1,y+1);

			if(value<mean){
				if((valueNN>(mean+standardMultiplier*std))&&((valueNN-
value)>diffThreshold)){
					setPixel(x,y,(value-edgeDropValue));
				} else
if((valueON>(mean+standardMultiplier*std))&&((valueON-value)>diffThreshold)){
					setPixel(x,y,(value-edgeDropValue));
				} else
if((valuePN>(mean+standardMultiplier*std))&&((valuePN-value)>diffThreshold)){
					setPixel(x,y,(value-edgeDropValue));
				} else
if((valueNO>(mean+standardMultiplier*std))&&((valueNO-value)>diffThreshold)){
					setPixel(x,y,(value-edgeDropValue));
				} else
if((valuePO>(mean+standardMultiplier*std))&&((valuePO-value)>diffThreshold)){
					setPixel(x,y,(value-edgeDropValue));
				} else
if((valueNP>(mean+standardMultiplier*std))&&((valueNP-value)>diffThreshold)){
					setPixel(x,y,(value-edgeDropValue));
				} else
if((valueOP>(mean+standardMultiplier*std))&&((valueOP-value)>diffThreshold)){
					setPixel(x,y,(value-edgeDropValue));
				} else
if((valuePP>(mean+standardMultiplier*std))&&((valuePP-value)>diffThreshold)){
					setPixel(x,y,(value-edgeDropValue));
				}
			}
		}
	}
	for(x=0; x<w; x++){
		for(y=0; y<h; y++){
			value = getPixel(x,y);
			if(value>(mean+standardMultiplier*std)){
```

```
                        setPixel(x,y,mean);
                }
        }
}
run("Find Edges");
run("Multiply...", "value="+imageMultiplier);
getStatistics(area, mean, min, max, std);

//using a third cloned image, deal with each ROI seperately to look for cells
numROIs = roiManager("count");
temp3Title = title+"TEMP3";
newImage(temp3Title, "8-bit black", w, h, 1);
j = 0;
while(j < numROIs) {
        selectImage(title);
        roiManager("select", j);
        run("Copy");
        selectImage(temp3Title);
        roiManager("select", j);
        run("Paste");
        roiManager("deselect");
        run("Select None");
        j++;
}
run("Max...", "value="+(mean+standardMultiplier*std));
run("Despeckle");
roiManager("Reset");

//initial binary operations
selectImage(temp3Title);
setAutoThreshold("Default dark");
setOption("BlackBackground", true);
run("Convert to Mask");
run("Close-");
run("Fill Holes");

//use first two cloned images to paint cell centres onto third cloned image
(if there appears to be a cell at the location of interest)
selectImage(temp1Title);
run("Select None");
run("Analyze Particles...", "size=0-Infinity pixel circularity=0.00-1.00
show=Nothing clear exclude include add");
numROIs = roiManager("count");
j = 0;
while(j < numROIs) {
        selectImage(temp3Title);
        roiManager("select", j);
        getStatistics(tempArea, tempMean);
        if(tempMean > minMeanROI){
                if(tempMean <= maxMeanROI){
                        selectImage(temp1Title);
                        roiManager("select", j);
                        run("Copy");
                        selectImage(temp3Title);
                        roiManager("select", j);
```

```
                        run("Paste");
                }
        } else {
                fill();
        }
        roiManager("deselect");
        run("Select None");
        j++;
}
selectImage(temp1Title);
close();
roiManager("Reset");

selectImage(temp2Title);
run("Select None");
run("Analyze Particles...", "size=0-Infinity pixel circularity=0.00-1.00
show=Nothing clear exclude include add");
numROIs = roiManager("count");
j = 0;
while(j < numROIs) {
        selectImage(temp3Title);
        roiManager("select", j);
        getStatistics(tempArea, tempMean);
        if(tempMean > minMeanROI){
                selectImage(temp2Title);
                roiManager("select", j);
                run("Copy");
                selectImage(temp3Title);
                roiManager("select", j);
                run("Paste");
        }
        roiManager("deselect");
        run("Select None");
        j++;
}
selectImage(temp2Title);
close();
roiManager("Reset");

//final binary operations
selectImage(temp3Title);
run("Close-");
run("Fill Holes");
run("Dilate");
run("Close-");
run("Fill Holes");
run("Erode");
run("Watershed");
run("Options...", "iterations=2000 count=5 black pad edm=Overwrite");
run("Erode");
run("Options...", "iterations=2 count=4 black pad edm=Overwrite");
run("Erode");
run("Options...", "iterations=2000 count=5 black pad edm=Overwrite");
run("Erode");
run("Options...", "iterations=1 count=1 black pad edm=Overwrite");
```

```
	run("Watershed");
	run("Analyze Particles...", "size=10-Infinity pixel circularity="+circValue+"-
1.00 show=Nothing exclude include add");
	run("Select None");
	close();

	selectImage(title);
	run("Revert");
	roiManager("Save",path+"_ALL.zip");
	roiManager("Reset");
	selectWindow(title);
	run("Close");
}
```